2008

Investigation of tribological properties of biobased polymers and polymeric composites

Satyam Kumar Bhuyan
Iowa State University

Investigation of tribological properties of biobased polymers and polymeric composites

by

Satyam Kumar Bhuyan

A dissertation submitted to the graduate faculty

in partial fulfillment of the requirements for the degree of

DOCTOR OF PHILOSOPHY

Major: Mechanical Engineering

Program of Study Committee:
Sriram Sundararajan, Major Professor
Pranav Shrotriya
Robert C Brown
Leonard S Chumbley
Tong Wang

Iowa State University

Ames, Iowa

2008

TABLE OF CONTENTS

ACKNOWLEDGEMENTS

I would like to take this opportunity to express my gratitude to all those who have helped me with the various fundamentals my PHD research which have been explicitly reported this thesis. First and foremost, I would like to thank my advisor, Professor Sriram Sundararajan for his guidance and constant support and the unshakable faith he had in me throughout my graduate career. It was through him that I learnt how to be persistent and consistent in order to accomplish any goal. Although it is not possible to express such gratitude in few lines, I will be ever grateful for all the knowledge that I have gained over the years which has set the foundation for all my upcoming accomplishments.

I would also like to extend my sincere thanks to all my committee members for serving on my Program of Study (POS) committee and providing me with all the valuable inputs and suggestions for my research. Apart from my advisor, the list includes Professor Pranav Shrotriya (Mechanical Engineering), Professor Robert Brown (Mechanical Engineering), Professor Scott Chumbley (Material Science and Engineering) and Professor Tong Wang (Food Science and Human Nutrition).

I would also like to thank all the collaborators at Iowa State University with whom I have worked in the various research projects. For the biolubricant project (not included in this thesis), I am thankful to Professor Earl Hammond and his student Linxing Yao of Food Science and Human Nutrition along with Professor Tong Wang. For the biopolymer project, I express my sincere gratitude to Professor Richard Larock of Chemistry and his team of workers which includes Dejan Andjelkovic, Daniel Pfister and Dr. Yongshang Lu. In

addition, I would also like to mention the names of Jerry Amenson of Materials Analysis and Research Laboratory (MARL) and Richard Egger of Chemistry Machine Shop for their cooperation and assistance. The contributions of Dr. Xiaodong Li and Zhi-Hui Xu from University of South Carolina were of immense help for most part of my research.

I would like to express my gratitude to my former and current colleagues in the Multiscale Surface Engineering and Tribology Laboratory – KS Kanaga Karuppiah, Yilei Zhang, Sam Holden, Jason Check, Angela Bruck and Chris Tourek. In addition, my thankfulness goes to my colleagues and all of Professor Shrotriya's students in Advance Sensors and Nanoscale Mechanics Lab – Jae-Joong Ryu, Andrew Mitchell, Kyungho Kang, Dinesh Kalyanasundaram and Janice Marquardt. They have been a source of entertainment and support with whom I have shared all my professional ups and downs and the mutual encouragement we boosted upon each other. And, special thanks to Jason and Andrew for writing out codes in LabView and Matlab respectively which I have used during my research.

Finally, I owe a lot to all my friends in and around Ames who have been very understanding and encouraging at every step of these past six years. I share a lot of pleasant and unforgettable memories with them. This acknowledgment would not be complete without the mention of my parents, Bijoy and Oley Bhuyan. Without their unconditional love and support, I simply could not have accomplished whatever I have till now.

Financial support for this study was provided by the Plant Science Institute at Iowa State University.

ABSTRACT

Worldwide potential demands for replacing petroleum derived raw materials with renewable plant-based ones in the production of valuable polymeric materials and composites are quite significant from the social and environmental standpoints. Therefore, using low-cost renewable resources has deeply drawn the attention of many researchers. Among them, natural oils are expected to be ideal alternative feedstock since oils, derived from plant and animal sources, are found in profusion in the world. The important feature of these types of materials is that they can be designed and tailored to meet different requirements. The real challenge lies in finding applications which would use sufficiently large quantities of these materials allowing biodegradable polymers to compete economically in the market. Lack of material and tribological characterizations have created an awareness to fulfill this essential objective.

In order to understand the viability of biobased polymers in structural applications, this thesis work elucidates the study of friction and wear characteristics of polymers and polymeric composites made out of natural oil available profusely in plants and animals. The natural oils used in this study were soybean and tung oil. Various monomeric components like styrene, divinely benzene etc. were used in the synthesis of biobased polymers through Rh-catalyzed isomerization techniques. For the different polymeric composites, spent germ, a byproduct of ethanol production, is used as the filler and an organoclay called montmorillonite is used as the reinforcing agent in the polymer matrix. The effect of crosslinker concentration, filler composition and reinforcement agent concentration was studied under dry sliding. A ball-on-flat tribometer with a probe made out of steel, silicon

nitride or diamond was used for most of the experimental work to measure friction and generate wear. The wear tracks were quantified with an atomic force microscope and a contact profilometer. The wear morphologies were studied with a scanning electron microscope. Thermosetting epoxy resin was used as a benchmark material to compare the tribological characteristics of the biobased polymers. Synthetic polymeric materials made out of norbornene monomers were also subjected to friction and wear tests. An empirical relationship between wear behavior and crosslinking was established.

CHAPTER 1. INTRODUCTION

1.1 Biorenewables

Biorenewable resources, commonly known as biomass, are defined as organic materials of recent biological origin[1]. Nature processes biogenic material (i.e. those derived from living organisms) which can be classified as biomass. A concrete example of a biomass is the waste generated from a recently cultivated farmland. Biorenewable resources are by definition are sustainable and occurring in nature. They are sustainable because if, properly, renewed at a sustainable rate, they will be available by future generations. Biorenewable resources can be converted in to biobased products.

Biobased products include transportation fuels, chemicals and natural fibers which are derived from biorenewable resources. Liquid fuels like biodiesel, ethanol etc. are examples of transportation fuels because they posses enough bioenergy to convert in to mechanical power, like vehicle propulsion. Chemicals may include pharmaceuticals and other fine chemicals which can produce high demands for biorenewables. More emphasis on bioproducts from fine chemicals will be done later in the chapter. Natural fibers are bundles of long and thin plant cells with walls that are durable and occur naturally on plant tissues.

The total biomass potential in United States is in excess of 1 billion tons or more precisely, 21 x 10^9 GJ. It is reasonable to estimate that such an enormous prospective will meet 21% of U.S. energy demands or 66% of U.S. transportation fuels. Figure 1 shows the distribution (in million tons) of the total biomass potential amongst the various available biorenewable resources. It can be clearly seen that significantly large amounts of predicted

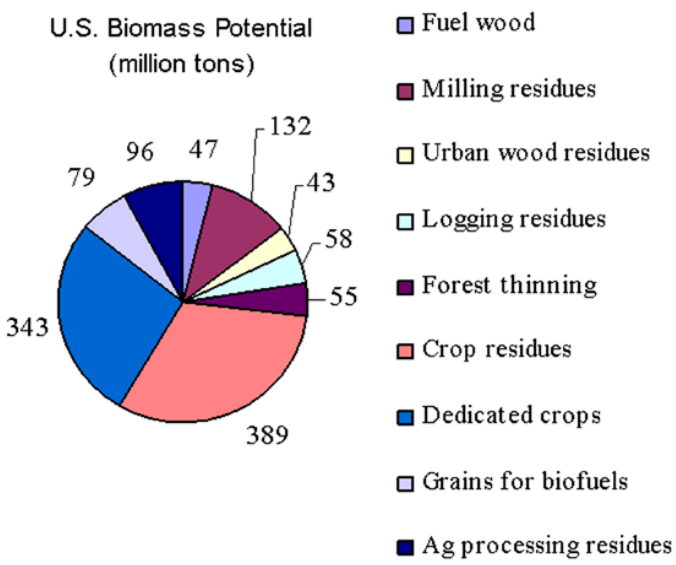

Figure 1. Distribution of the total potential of biomass in United States (Source: Office of the Biorenewables Program, Iowa State University)

biomass production comes from crop residues and dedicated crops. This indicates that the biobased feedstock has the potential to replace the existing petroleum based feedstock.

Currently, the demand for petroleum-based products is at large. However, biorenewable resources are favored over fossil resources due to several different reasons. Some of these factors include the desire to improve environmental quality, the excess agricultural production, the potential for rural development and the concern on national security over the dependence on foreign oil. Utilization of fossil fuels can produce lot of local, regional and global impact. For example, combustion of coal or petroleum-based motor fuels produces carbon monoxide and smog as local pollution problems. On the other hand global impacts are like ozone depletion due to chlorofluorocarbons and nitrogen oxides; greenhouse effects due to release of carbon dioxide during combustion and global climate

change. The vast agricultural lands in United States which are normally used for growing domestic crops can be utilized for production of feedstock for biobased products with no immediate threat to rising food prices and feeding developing countries of the world. This will significantly lead to the development of rural economy and lifestyle. The rural communities are on the lookout for opportunities for boosting income and economic development. Developing crops for new markets would provide plethora of opportunity for rural development. Finally, the Energy Crisis of the seventies caused a severe threat to the national security when United States and some other nations reduced their dependence on imported oil by switching over to domestic energy sources like coal, natural gas and petroleum. One of the many lessons learned from the Energy Crisis was that the dependence on foreign sources can be made inevitable if biorenewable resources are properly built up.

1.2 Tribology

Tribology is study of friction, lubrication and wear of interacting surfaces in relative motion. It has been found that about $100 billion are lost each year due to friction and wear of machine components (not including savings due to properly engineered surfaces). Figure 2 shows a distribution of the total expenditure for a machine when it is in operating condition[2]. It is quite clear that a large proportion of the costs involved are due to breakdown and maintenance. In a tribological interface, surface interactions are highly complex and their understanding requires knowledge of various disciplines.

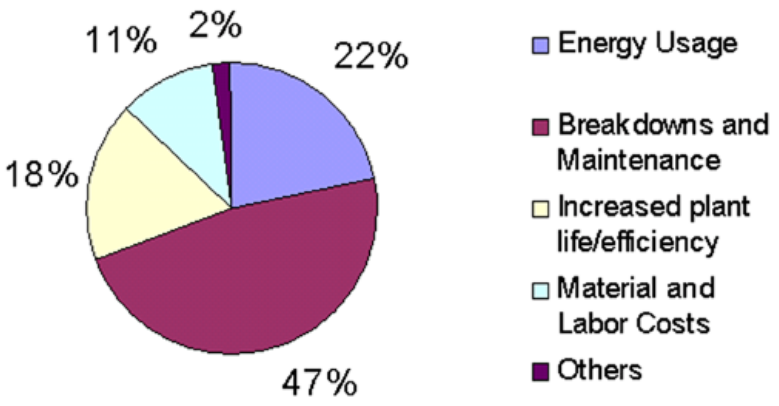

Figure 2. Distribution of costs associated with the operation of a machinery (Source: Handbook of Micro/Nanotribology, B. Bhushan, 1999, CRC-Press, Boca Raton,FL)

1.2.1 Friction

When two surfaces come in contact they impart resistance to their relative motion which, in scientific term, is called friction. The friction force is a tangential force which acts in a direction directly opposite to the direction of motion. The coefficient of friction is a study of how much a surface can resist to the perpetuated motion under the application of normal load. It is defined by the ratio of the friction force and the normal load. Friction is not a material property, but, it is often dependent on the surfaces that are in contact, i.e. it is a response of the system. There are two main types of friction that are commonly encountered – dry friction and fluid friction. In case of dry friction, the two solid surfaces are clean and dry and are in relative motion to one another. Fluid friction or lubrication represents movement between two contact surfaces in the presence of a liquid or gas whose adjacent layers are moving at different velocities relative to one another. Friction between two dry, clean surfaces is generally high which can be lowered when they are lubricated and hence,

this is the essence of studying lubrication and the lubricative properties of various available lubricants. Friction forces are generally good or bad. Without friction it is impossible to walk or even drive. On the other hand in machines, where sliding and rotating components are present especially in bearings and seals, friction is undesired. Over a prolongated period of time machine parts will wear out and become redundant. Hence, friction needs to be minimized in such applications.

Sliding friction is governed by two fundamental intrinsic laws. These laws are referred to as Amontons' law after the French physicist Guillaume Amonton who discovered them in 1699[3]. The first law states that the friction force (F) is directly proportional to the applied normal load (W). Mathematically, it is written as,

$$F = \mu W \tag{1}$$

where μ is the co-efficient of friction. Depending on the mating system, the coefficient of dry friction can range from a very small value of 0.05 to values as large as 10 [4]. The second law state that the friction force (or coefficient of friction) is independent of the apparent area of contact between the contacting bodies. This means that two bodies, regardless of their sizes, have the same value of friction coefficient. A third law due to Coulomb states that the friction force (or coefficient of friction) is independent of the sliding velocity.

1.2.2 Wear

Wear is defined as the damage done to a surface by the removal of material due to two solid bodies in any motion relative to one another. Wear could occur in either or both the bodies. Any engineering surface has an apparent area of contact and roughness associated with it at all length scales. Hence, when two engineering surfaces come into contact, the

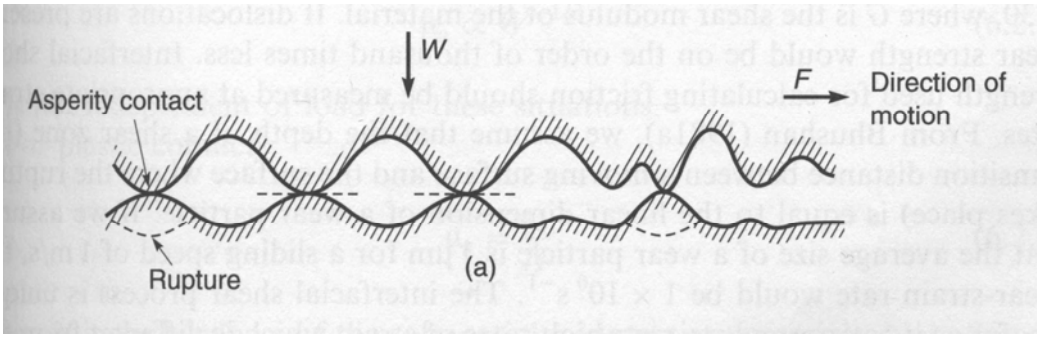

Figure 3. Two engineering surfaces come into contact at discrete points called asperities (Source: B. Bhushan, Principles and Applications of Tribology, 1999, John Wiley & Sons, NY)

contact occurs at discrete points called asperities[4] as shown in Figure 3. In some cases, when a hard material comes in contact with a soft material, the soft material gets worn out due to particles getting displaced from the surface in the form of loose debris. Very often it is not unusual to see the soft material getting transferred to the harder body. Wear is a property that is characteristics of the material. It is generally said that hard surface exhibit less wear than soft surfaces. During wear if particles are abraded from the surface, then wear can be quantified as mass loss. In addition, if it leaves a distinct groove on the surface then wear depth and wear volume can also be measured. Just like friction, wear can be good or bad. Wear is good when it is applied for machining or polishing; generally for fine finish textures. On the other hand in machinery parts involving motion, wear should be minimized to avoid damage and breakdown.

Wear can occur in several different ways[4]. Six different principles of wear mechanism are: 1) adhesive, 2) abrasive, 3) fatigue, 4) impact by erosion and percussion, 5) chemical or corrosive and 6) electrical-erc-induced. According to study, two-thirds of all

wear encountered in industrial applications occur through adhesive and abrasive wear mechanisms. If wear is a repetitive process, then the machine part can result in failure. Researchers often study failure analysis to determine the mechanisms of wear. There are several different microscopic and surface analysis techniques that can be used to study failure.

Different materials respond differently to friction and wear. Our focus of attention for this thesis work is on polymers. The presence of weak bonding forces such as van der Walls force and hydrogen bonding in polymers gives rise to adhesive friction. They have low co-efficient of friction compared to metals and ceramics. Polymers are very compliant as compared to metals and ceramics with lower values of modulus of elasticity and strength. They are often used in sliding applications against hard mating surfaces. Polymers which are rubbers and elastomers are used in bearings and seal applications. Composites that are made out of polymers provide a balance between material strength and low friction and wear. Polymers that are sliding against a hard material often results in a transfer of softer material on to the harder one. The formation and behavior of transfer films are important factors in friction and wear of these materials [5, 6]. The transfer film which could be up to micrometers thick contains molecular chains oriented parallel to the sliding direction. For polymers with smooth surfaces the deformations of asperities or hills (present on surfaces) are primarily elastic. This is mainly because of the low Young's modulus to hardness ratio of polymers compared to metals and ceramics.

Polymers exhibit moderate wear. The dominant mechanisms of wear in polymers are adhesive, abrasive and fatigue. By definition, adhesive wear occurs when two nominally flat solid bodies are in sliding contact. The asperities or hills present in the soft polymer surface

are sheared by sliding which results in formation of transfer films or loose debris scattered around the wear track. Some are fractured by fatigue process due to repeated loading and unloading. The laws of adhesive wear are governed by the equation due to Archard [7]

$$v = \frac{kWx}{H} \tag{2}$$

where k is the nondimentional wear coefficient, W is the applied load, x is the sliding distance and H is the hardness. Abrasive wear occurs when asperities of a rough, hard surface, slide on a softer surface and cause damage to the interface by plastic deformation or fatigue. In most cases of abrasive wear scratching of the softer surface is observe as a series of grooves parallel to the direction of sliding. One of the common modes of plastic deformation is ploughing. In case of ploughing the material gets displaced from a groove to the sides without any removal. A characteristic feature of ploughing is the ridge formation along the sides of the ploughed grooves. Archard's equation of wear is also applicable for abrasive wear but the adhesive wear coefficient is replaced by the abrasive wear coefficient k_{abr}. Repeated rolling or sliding on surfaces results in subsurface and surface cracks which propagate throughout the material causing subsurface and surface fatigue. This generally happens after a critical number of cycles. Prior to this critical point, insignificant wear takes place which is similar to wear caused by adhesive or abrasive mechanism. Wear particles are generated through the propagation and intersection of cracks. The fatigue mechanism is important for harder polymers especially in thermosets sliding against smooth surfaces.

1.3 Materials from biorenewable sources for tribological applications

As discussed before biorenewable resources can be transformed in to a wide variety of products like transportation fuels, chemicals and natural fibers. For the purpose of the thesis, we will restrict our discussion to chemicals and to some extent fibers. Chemicals that are referred as commodity chemicals find applications in the manufacture of a wide variety of commodities like absorbent, adhesives, solvents, lubricants, inks, pesticides, coatings, films and polymers. A wide variety of naturally occurring polymers derived from renewable resources are available for material application. The benefits of using these types of polymers for material applications are many. For example, due to lack of environmental burden the environmental compatibility will improve. The agriculture industry in Unites States produces sufficient supplies of agricultural products that could be used as renewable sources for polymer feedstock either through direct use or indirectly through carbon sources. Biodegradability and biocompatibility are two additional benefits of renewable sources of polymers. Any polymer synthesizes through a biological system is inherently biodegradable. However, it is important to control the environment in which these polymers are in use in order to prevent premature biodegradation. Although this is a challenging task but it can be accomplished through a control of moisture, nutrients, microorganisms etc[8].

The viability of biobased polymers can be achieved by understanding the growing interface between molecular biology and polymer chemistry. By controlling the polymer structure and its functional attributes new and useful applications of these polymers can be studied. Initial application for these types of bioengineered materials can be on a small scale.

With time, as the tools of molecular biology gets optimized, high volume applications will come in to picture as production costs get reduced in contrast with the expected increase in the cost for synthetic petroleum-based polymers. A wide variety on polymers and polymeric composites derivable from naturally occurring resources is discussed in this thesis all of which are in the experimental stages of investigation.

1.3.1 Biobased polymers from naturally occurring oil

Scientist and researchers have found that promising new materials can be developed from functionalized, low molecular weight natural substances by utilizing polymerization techniques similar to the ones use for procession petroleum-based polymers. One of the most promising renewable resources for such type of processing techniques is natural oil[9]. Typically natural oil by nature possesses a triglyceride structure with fatty acid side chains acquiring varying degrees of unsaturation[10-12]. The presence of carbon-carbon double bonds makes these biological oils ideal monomers of natural origin for the preparation of biopolymers. Soybean oil is available abundantly accounting for about 30% of vegetable oil supply in the world[13]. Besides, its low cost, high purity, the possibility of genetically engineering the number of C=C bonds present in the oil[10], its significantly higher molecular weight when compared to other conventional alkene monomers (~880 g/mol), makes it advantageous to use for polymerization compared to other types of vegetable oils. These advantages make soybean oil ideal starting materials for biopolymer synthesis.

Considerable recent efforts have been aimed at the conversion of soybean oil and other types of vegetable oil into solid polymeric materials[14-16]. More recently, Larock and coworkers have developed a variety of novel polymeric materials ranging from elastomers to

tough, rigid plastics prepared by the cationic copolymerization of regular soybean oil, tung oil, corn oil and fish oil[17-33]. The advantages of these polymer materials are their low cost, availability from a renewable natural source, and their possible biodegradability. These oil-based polymers generally possess viable mechanical properties with moduli ranging from 400 MPa to 1 GPa and thus show promise as structural materials in a variety of applications[34]. It has been found that the original C=C bonds of the soybean oil side chains participate in this free-radical copolymerization. A schematic[9] of such type of cationic copolymerization reaction is shown in Figure 4.

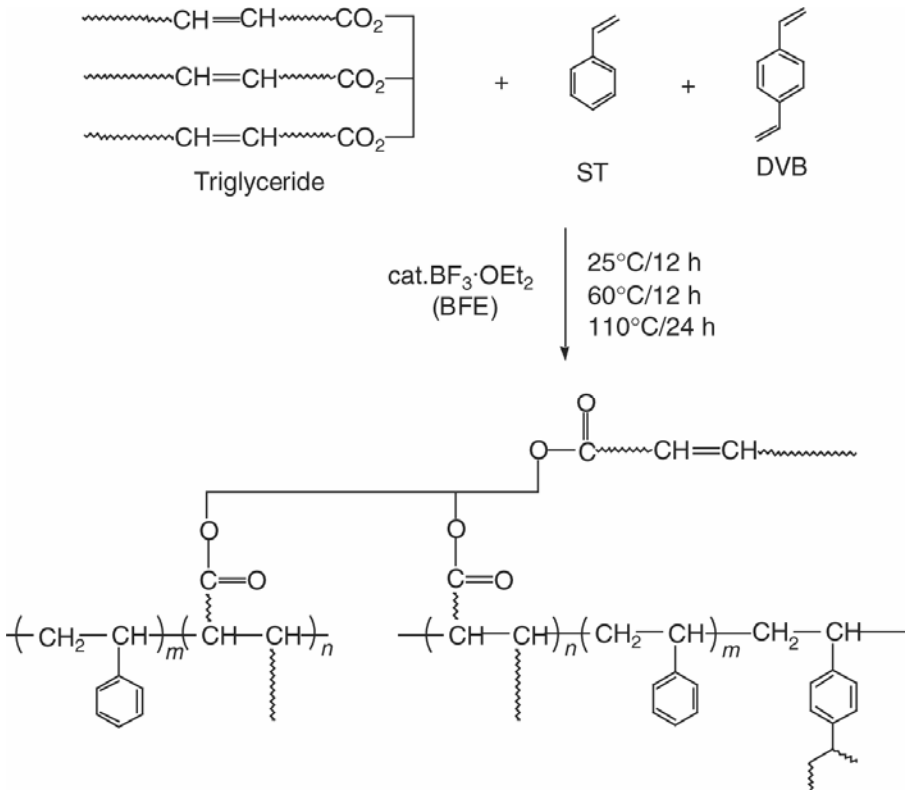

Figure 2. Copolymerization of soybean oil triglyceride with styrene and divinyl benzene (Source: D.D. Andjelkovic *etal*, in *Feedstocks for the Future: Renewables for the Production of Chemicals and Materials*, J.J. Bozell and M. Patel, 2006, ACS: Washington DC, p. 67-81)

1.3.2 Biobased lubricants from vegetable oils.

There is a budding interest in the development and usage vegetable oil based lubricants and fluids for industrial applications[35]. Recent concerns about the environmental and diminution of world fossil fuel reserves have forced researchers to look at substitutes for mineral oils with biodegradable fluids like vegetable-based oil. Biobased esters which are generally derived from plants and vegetable oils exhibit better performance at lower costs compared to synthetic esters[36]. Vegetable oils by their chemical nature are long-chained fatty acid tri-esters of glycerol and provide most of the desired lubricant properties such as good boundary lubrication, high viscosity index, high flash point and low volatility[37]. The nontoxic and biodegradability of vegetable oil pose less danger to environment, flora and fauna in case of accidental spillage during disposal. In some cases biodegradable greases are important, like, for example, in open lubrication system where the lubricant is in direct contact with the environment, as well as in other cases like total loss system where there is immediate contact with the environment. Data on field tests on the commercially available vegetable oil are lacking. One has to rely upon several factors to rationalize whether vegetable oils have any practical applications and whether they can match the competitive performance of petroleum-based engine oils[38].

From a review of available literature, it has been found that significant amount of work has been done on biobased lubricants. For example, Erhan and Asadauskas[39] have found out that chemical modification of triglycerides is necessary for better oxidative stability and improved low temperature behavior. According to Yao and Hammond[40], branched chain esters have lower melting point than straight chained ones indicating that the straight chain esters tends to form a better bond amongst themselves. Study of boundary

lubrication behavior of lipid-based compounds by Bhuyan etal[41] have shown that branched chained compound can reduced friction by 20% compared to their straight chained counterparts.

1.4 Motivation and Research Objectives

It is quite clear that polymers made out of biorenewable resources can be generously utilized for structural applications. Characterization of relevant properties (mechanical behavior, thermal, tribology etc) of biobased materials is needed to evaluate their potential before considering them for viable applications. Much of the work did in the past have been on studying the material strength of biobased polymers and their possible feasibility in many applications. However, study on tribology of these materials is lacking. The main objective of this thesis work is to look at the tribological properties of biobased polymers and polymeric composites and establish relations between processing parameters and tribological response. One such processing parameters is the crosslinking density which is defined as the density of chains or segments that connect two infinite parts of polymer network[42]. The crosslinking density is affected by the functionality of the crosslinker molecule. Keeping this in mind, the research objectives of this thesis work are as follows:

1. Investigate the effect of crosslinking density on friction and wear of soybean and tung oil-based polymers.
2. Investigate the effect of clay concentration on friction and wear behavior of polymer-clay nanocomposites.

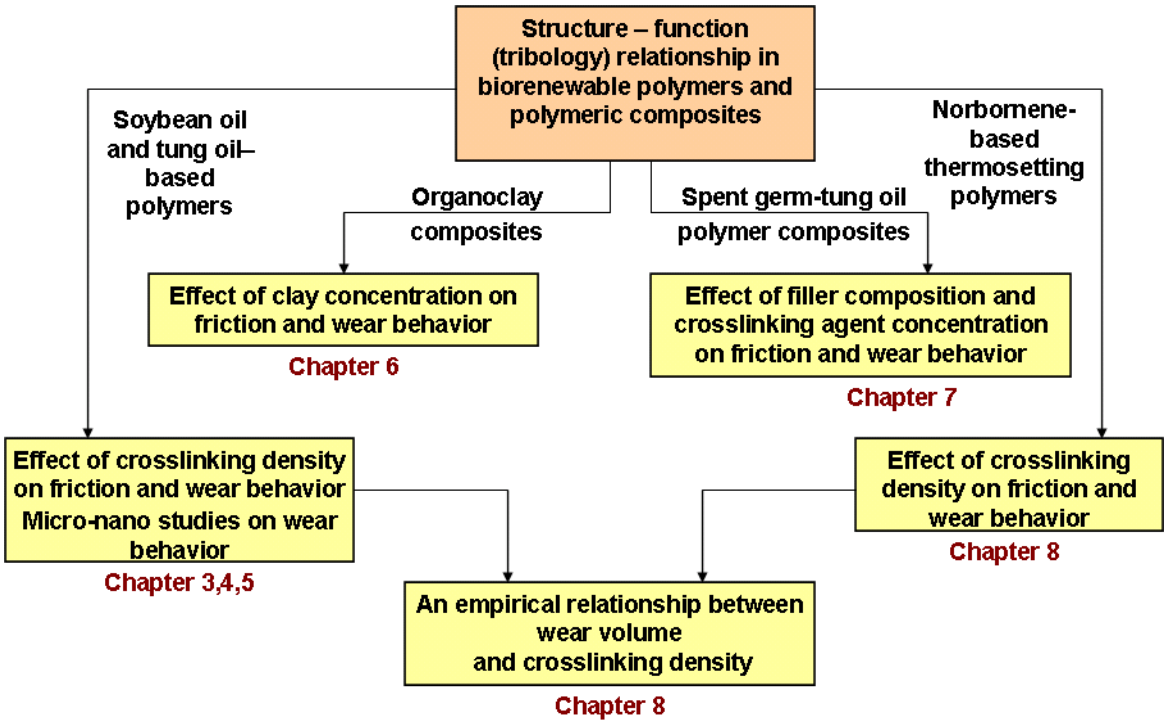

Figure 3. Outline of research objectives

3. Investigate the effect of filler composition and crosslinking agent concentration on friction and wear behavior of polymeric composites made out of a tung-oil based resin and spent germ particles.
4. Investigate the influence of crosslinking density on the friction and wear behavior of norbornene-based polymers.
5. Develop an empirical relationship between wear volume and crosslinking density.

1.5 Thesis Organization

Figure 5 shows a flowchart of the research objectives and the chapters in which they are organized in this dissertation. Following this introductory chapter, chapter 2 discusses the major experimental techniques used in this research. In chapter 3, the effect of crosslinking

density on the friction and wear behavior of soybean oil-based polymers are reported. Chapter 4 compares the microscale and nanoscale tribological response of soybean oil-based polymers of different crosslinking densities. Chapter 5 elucidates the effect of crosslinking on the tribological behavior of tung oil-based polymers. In chapter 6, the effect of clay concentration on the friction and wear behavior of polymer-clay nanocomposites is discussed. Chapter 7 includes the investigation of friction and wear behavior polymeric composites made out of a tung oil-based resin and spent germ particles as a function of the filler composition and crosslinker concentration. Chapter 8 reports the friction and wear data on norbornene-based ROMP (Ring-Opening Metathesis Polymerized) thermosetting polymers and an empirical relationship between the wear volume and crosslinking density has been established. In the Chapter 9, conclusions from different chapters are listed.

1.6 References

1. R.C. Brown, *Biorenewable Resources: Engineering New Products from Agriculture*. 1st ed. 2003, Ames: Iowa State Press.
2. B. Bhushan, *Handbook of Micro/Nanotribology*. 1999, Boca Raton, FL: CRC-Press.
3. G. Amontons, *De la resistance causee dans les Machines.* Memoires de l'Academie Royale A, 1699: p. 257-282.
4. B. Bhushan, *Principles and Application of Tribology*. 1999, New York: John Wiley & Sons, Inc.
5. B. Bhushan and D.F. Wilcock, *Frictional behavior of Polymeric Compositions in Dry Sliding*, in *Prodeedings of the Seventh Leeds-Lyon Symphosium of Tribology*, D. Dawson, et al., Editors. 1981, IPC Business Press: Guildford, UK. p. 103-113.

6. B. Bhushan and F. Dashnaw, *Material Study for Advanced Stern-Tube Beaarings and Face Seals.* ASLE Transactions, 1981. **24**: p. 398-409.

7. J.F. Archard, *Contact and Rubbing of Flat Surfaces.* Journal of Applied Physics, 1953. **24**: p. 981-988.

8. D.L. Kaplan, *Biopolymers from Renewable Resources*. 1998, Berlin, Heidelberg: Springer-Verlag.

9. D.D. Andjelkovic, F. Li, and R.C. Larock, *Novel Polymeric Materials from Soybean Oils - Synthesis, Properties and Potential Applications*, in *Feedstocks for the Future: Renewables for the Production of Chemicals and Materials*, J.J. Bozell and M. Patel, Editors. 2006, American Chemical Society: Washington DC. p. 67-81.

10. R.D. O'Brien, *Fats and Oils – Formulating and Processing for Applications*. 2nd ed. 2004, Boca Raton, FL: CRC Press LLC.

11. E.W. Eckey, *Vegetable Fats and Oils*, in *The ACS Monograph Series*. 1954, Reinhold Publishing Co.,: New York.

12. D.K. Salunkhe, et al., *World Oilseeds: Chemistry, Technology and Utilization*. 1991, New York: Van Nostrand Reinhold.

13. W.R. Fehr, in *Oil Crops of the World: Their Breeding and Utilization*, G. Robbelen, R.K. Downey, and A. Ashri, Editors. 1989, McGraw-Hill: New York.

14. E. Can, S. Küsefoglu, and R.P. Wool, *Rigid, thermosetting liquid molding resins from renewable resources. I. Synthesis and polymerization of soy oil monoglyceride maleates.* Journal of Applied Polymer Science, 2001. **81**(1): p. 69-77.

15. S.N. Khot, et al., *Development and application of triglyceride-based polymers and composites.* Journal of Applied Polymer Science, 2001. **82**(3): p. 703-723.

16. E. Can, S. Küsefoglu, and R.P. Wool, *Rigid thermosetting liquid molding resins from renewable resources. II. Copolymers of soybean oil monoglyceride maleates with neopentyl glycol and bisphenol A maleates.* Journal of Applied Polymer Science, 2002. **83**(5): p. 972-980.

17. R.C. Larock and F.K. Li, *Novel polymeric materials from biological oils.* Abstracts of Papers of the American Chemical Society, 2004. **227**: p. U290-U290.

18. F. Li, M.V. Hanson, and R.C. Larock, *Soybean oil-divinylbenzene thermosetting polymers: synthesis, structure, properties and their relationships.* Polymer, 2001. **42**(4): p. 1567-1579.

19. F. Li, R.C. Larock, and J.U. Otaigbe, *Fish oil thermosetting polymers: creep and recovery behavior.* Polymer, 2000. **41**(13): p. 4849-4862.

20. F. Li, et al., *Fish oil thermosetting polymers: synthesis, structure, properties and their relationships.* Polymer, 2000. **41**(22): p. 7925-7939.

21. F.K. Li, J. Hasjim, and R.C. Larock, *Synthesis, structure, and thermophysical and mechanical properties of new polymers prepared by the cationic copolymerization of corn oil, styrene, and divinylbenzene.* Journal of Applied Polymer Science, 2003. **90**(7): p. 1830-1838.

22. F.K. Li and R. Larock, *Novel polymeric materials from biological oils.* Abstracts of Papers of the American Chemical Society, 2002. **223**: p. D95-D95.

23. F.K. Li and R.C. Larock, *New soybean oil-styrene-divinylbenzene thermosetting copolymers. II. Dynamic mechanical properties.* Journal of Polymer Science Part B-Polymer Physics, 2000. **38**(21): p. 2721-2738.

24. F.K. Li and R.C. Larock, *Thermosetting polymers from cationic copolymerization of tung oil: Synthesis and characterization.* Journal of Applied Polymer Science, 2000. **78**(5): p. 1044-1056.

25. F.K. Li and R.C. Larock, *New soybean oil-styrene-divinylbenzene thermosetting copolymers. I. Synthesis and characterization.* Journal of Applied Polymer Science, 2001. **80**(4): p. 658-670.

26. F.K. Li and R.C. Larock, *New soybean oil-styrene-divinylbenzene thermosetting copolymers. III. Tensile stress-strain behavior.* Journal of Polymer Science Part B-Polymer Physics, 2001. **39**(1): p. 60-77.

27. F.K. Li and R.C. Larock, *Novel polymeric materials from biological oils.* Journal of Polymers and the Environment, 2002. **10**(1-2): p. 59-67.

28. F.K. Li and R.C. Larock, *New soybean oil-styrene-divinylbenzene thermosetting copolymers - IV. Good damping properties.* Polymers for Advanced Technologies, 2002. **13**(6): p. 436-449.

29. F.K. Li and R.C. Larock, *New soybean oil-styrene-divinylbenzene thermosetting copolymers. v. shape memory effect.* Journal of Applied Polymer Science, 2002. **84**(8): p. 1533-1543.

30. F.K. Li and R.C. Larock, *Synthesis, structure and properties of new tung oil-styrene-divinylbenzene copolymers prepared by thermal polymerization.* Biomacromolecules, 2003. **4**(4): p. 1018-1025.

31. F.K. Li and R.C. Larock, *New soybean oil-styrene-divinylbenzene thermosetting copolymers. VI. Time-temperature-transformation cure diagram and the effect of*

curing conditions on the thermoset properties. Polymer International, 2003. **52**(1): p. 126-132.

32. F.K. Li, A. Perrenoud, and R.C. Larock, *Thermophysical and mechanical properties of novel polymers prepared by the cationic copolymerization of fish oils, styrene and divinylbenzene.* Polymer, 2001. **42**(26): p. 10133-10145.

33. D.W. Marks, et al., *Synthesis of thermoset plastics by Lewis acid initiated copolymerization of fish oil ethyl esters and alkenes.* Journal of Applied Polymer Science, 2001. **81**(8): p. 2001-2012.

34. F. Li and R.C. Larock, *Thermosetting polymers from soybean oil.* Polymer, 2001. **42**: p. 1567-1579.

35. W. Bartz, *Lubricants and the Environment.* Tribology International, 1998. **31**(1-3): p. 35-47.

36. D.R. Kodali, *High performance ester lubricants from natural oils.* Industrial Lubrication and Tribology, 2002. **54**(4): p. 165-170.

37. A. Adhvaryu, S.Z. Erhan, and J.M. Perez, *Tribological studies of thermally and chemically modified vegetable oils for use as environmentally friendly lubricants.* Wear, 2004. **257**(3-4): p. 359-367.

38. S.Z. Erhan, *Industrial Usage of Vegetable oils*. 2005, Champaign, IL: American Oil Chemists Society Press.

39. S.Z. Erhan and S. Asadauskas, *Lubricant basestocks from vegetable oils* Industrial Crops and Products, 2000. **11**: p. 277–282.

40. L. Yao and E. Hammond, *Saturated methyl-branched fatty acids and their derivatives as biolubricants.* Journal of American Oil Chemists Society, 2006. **83**(6): p. 547-552.

41. S. Bhuyan, et al., *Boundary lubrication properties of lipid-based compounds evaluated using microtribological methods.* Tribology Letters, 2006. **22**(2): p. 167-172.

42. J.L. Scala and R. Wool, *Property analysis of triglyceride-based thermosets.* Polymer, 2005. **46**: p. 61-69.

CHAPTER 2. INSTRUMENTS AND METHODS

In order to evaluate the friction and wear response of the materials, tribological characterization studies were performed primarily at the microscale level and some at the macroscale and nanoscale level. At microscale, a ball-on-flat microtribometer was used to stimulate multiple asperity contact whereas at nanoscale an atomic force microscope (AFM) was used. A pin-on-disc tribometer was employed to test wear at the macroscale level. Post tests characterization of the wear track was done with the AFM, scanning electron microscope (SEM) and a contact profilometer. The instruments and associated measurement techniques are described in the sections below.

2.1 Microtribometer

To study the friction and wear of material interfaces at the microscale, a microtribometer was used in all our studies[1]. The instrument used was a custom-built reciprocating microtribometer with a sub-millinewton resolution. A probe (silicon nitride or steel ball of radius ~ 1.2 mm, conical diamond probe of radius ~ 100 μm and 90^0 cone angle) is placed at the end of crossed I-beam structure as shown in Figure 1. The normal and frictional (lateral) forces are monitored with the use of semiconductor strain gages mounted on the cantilevers. Friction forces can be resolved to approximately ±5 μN and normal forces to approximately ±15 μN. The sample is placed on a spacer block and it can be moved in a reciprocating manner with a two-axis stage controller. The vertical stage moves with the crossed I-beam structure onto the sample by which it applies different normal loads on the sample. The signals from the stain gages mounted on the cantilevers are amplified using a

signal conditioning amplifier. The signal is then sent to a desktop computer through a Data Acquisition (DAQ) card. The load and lateral stage are fully motorized and can be controlled through a program and a stage controller by the desktop PC with a standard RS-232 serial port. The motion and data acquisition are controlled by a software interface written in LabView 5.1 (Appendix A). A picture and a schematic of the microtribometer setup are shown in Figures 1 and 2.

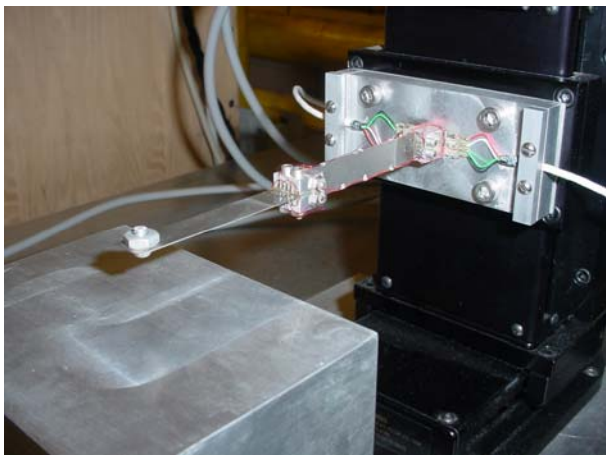

Figure 1. Crossed I-beam structure with the two cantilevers (normal and lateral) and strain

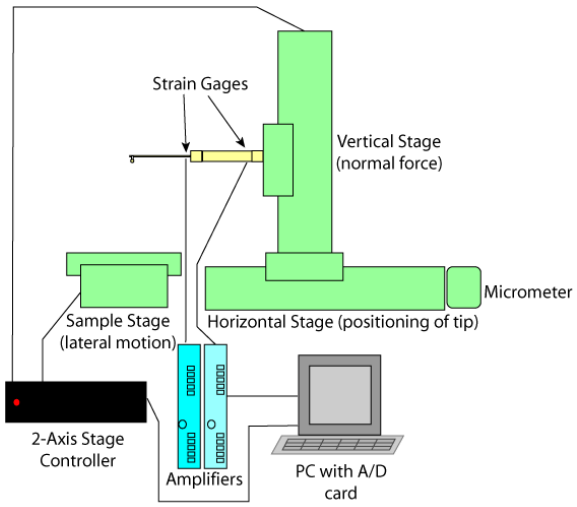

Figure 2. Schematic of a microtribometer

The tribometer was calibrated once every six months to check for any inconsistency in the strain gages as well as with the signal conditioning amplifier over time. The system was calibrated for a maximum load of 1 N for both the normal and the lateral cantilever. This is near the limit of linear response of the material of the cantilever which is grade 5 (6Al-4V) titanium. This was achieved by placing masses on the end of the cantilever and recording the resulting voltage output. It can be seen in Figure 3 that the response of the tribometer is extremely linear within the operating range.

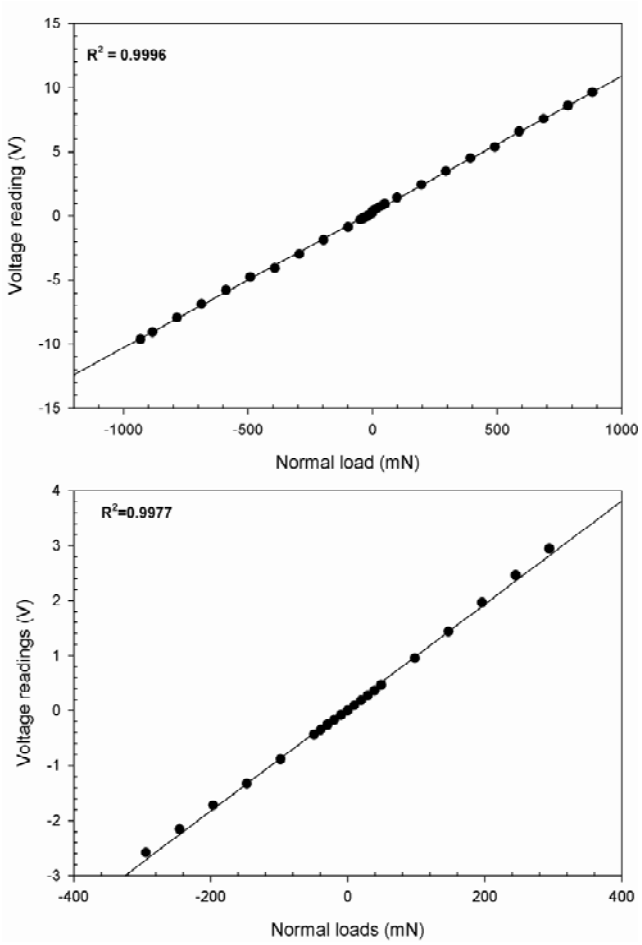

Figure 3. Graph of amplifier voltage output vs. applied load during calibration of the normal (top) and lateral (bottom) cantilever, including linear fit and regression analysis.

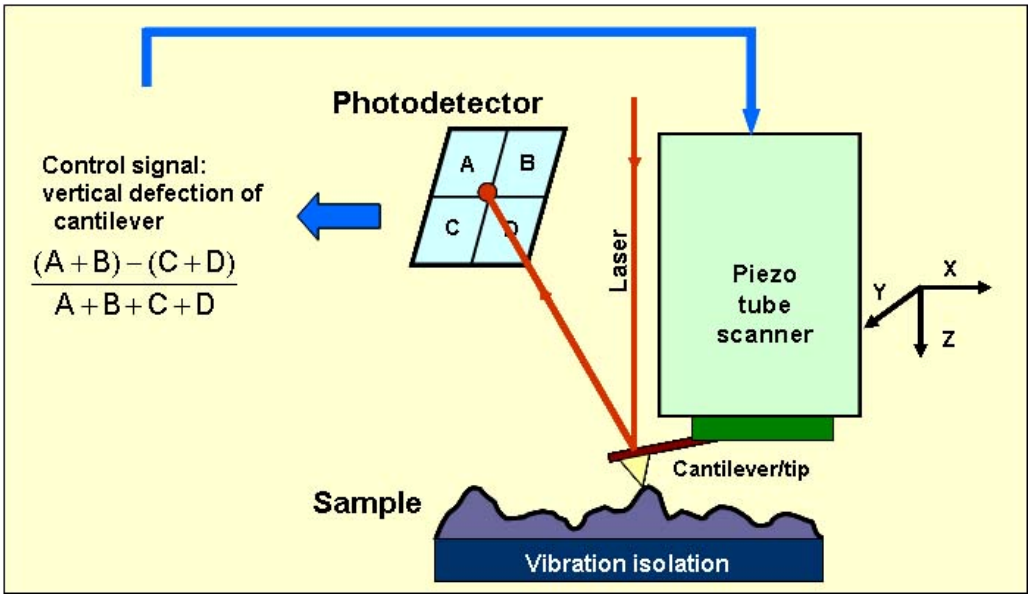

Figure 4. Operating principle of an atomic force microscope (AFM)

For experimental purposes, the normal load for the friction tests was ramped from 0.2 to 1 N while the lateral force was monitored simultaneously. For the reciprocating wear test, the normal load was kept constant at a desired value depending upon the surface damage (if any) observed from the friction tests. The sliding velocities were adjusted accordingly from 0-10 mm/s as the probe was moved across a stroke distance of 30 to 50 mm.

2.2 Atomic Force Microscope

To study the wear in polymers at a nanoscale level, we used an atomic force microscope (AFM). The AFM can measure very small forces between the probe and the surfaces with subnanometer resolution. The operating principle behind an AFM is shown in Figure 4. A sharp cantilever/tip assembly is placed at the end of a piezo tube. The probe is scanned over the surface in a raster pattern. A laser beam is focused on the end of the cantilever during raster-scanning (Figure 5) and is reflected onto a quadrant photodiode.

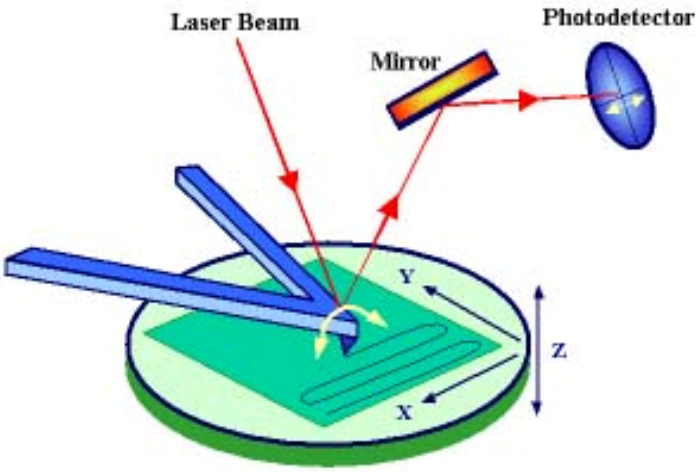

Figure 5. Raster-scanning of the AFM cantilever tip

A constant force on the sample is maintained by a feedback loop control system to compensate for the topographical features of the surface. This results in a three-dimensional map of the sample. The deflection signal for achieving topographical map is calculated as laser spot intensity for quadrants (A+B) – (C+D) as shown in Figure 4.

V-shaped triangular silicon probes doped with antimony (n) and coated with DLC (from Veeco) with calibrated force constant of 41.1 N/m and measured tip radius of 200 nm were used for nanoscale wear measurements. The spring constant of the cantilever used were calibrated using the technique described by Sader[2]. The radius of the tip was characterized before and after the experiments using commercially available calibration samples (TGT01 from MikroMasch USA, Portland, OR). Tip contamination was monitored using a standard tipcheck sample (Tipcheck from Aurora Nanodevices). Tipcheck has a Ti thin film coated on a Si surface and TGT01 has sharp spiked silicon features. Both these samples exploit the reverse imaging to provide a fast and simple way of assessing tips. The sample's sharp features, when imaged using the AFM, result in height maps that contain information

regarding the tip shape[3]. Deconvolution of these images using blind reconstruction methods results in a fairly accurate estimate of the tip shape and radius. A typical image of a probe is shown in Figure 6 and the parabolic fit to the probe is shown in Figure 7 which was generated by a custom written MATLAB code (see Appendix B). The adhesive forces between the probe and the sample were measured from force-displacement curves after each test. For scratch tests the probe was moved back and forth at a constant normal load by disabling the slow scan axis which allowed it to scratch the sample along a line. Normal forces were varied from 0 to 10 μN as the wear depth was monitored after 10 cycles of scratching.

2.3 Pin-on-disc tribometer

A pin-on-disc wear tester was used for wear experiments in which the stationary alumina pin was in contact with a rotating polymeric disk. Rectangular pins of size 6 mm X 6 mm in cross-section and 16 mm long were machined for use as the specimens for wear tests. The disc used was 8 mm in diameter and 5 mm in thickness with a RMS surface roughness of 102 ± 21 mm at 15 X 15 μm scale. Dry sliding at ambient condition with a normal load of 15 N and a sliding speed of 0.123 m/s was performed in a track of 7 mm in diameter giving rise

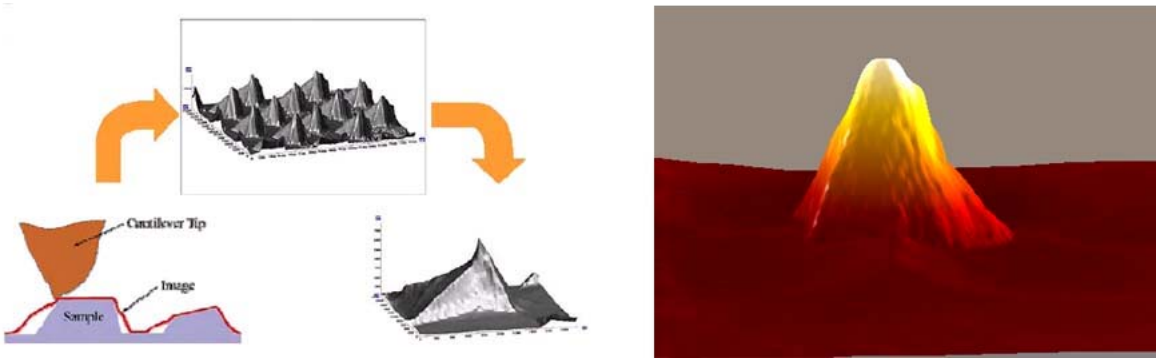

Figure 6. Schematic of reverse imaging of the probe when it scans over the silicon spiked

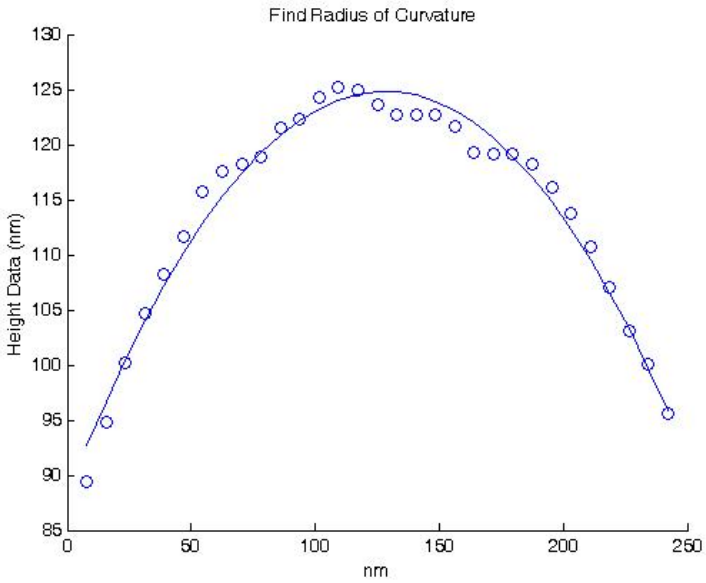

Figure 7. Parabolic fit to an AFM probe

to a total sliding distance of 200 m. Before testing, the pins were abraded against a 600 grade SiC paper to ensure good contact between the sliding pin surface and the counterface during a sliding experiment. The surface of both the pin and disc were cleaned with a soft paper soaked in ethyl alcohol and thoroughly dried. The specimens were weighed both before and after the tests to an accuracy of 0.0001 g in a precision balance. Frictional force was recorded from the output of strain gauges mounted on the arm holding of the pin.

2.4 References

1. J. Check, *Design and construction of a microtribometer and its use in the study of the micro/nanotribological behavior of ultra-high molecular weight polyethylene (UHMWPE)*, in *Masters Thesis*. 2004, Iowa State University: Ames, IA.

2. J.E. Sader, J.W.M. Chon, and P. Mulvaney, *Calibration of rectangular atomic force microscope cantilevers.* Review of Scientific Instruments, 1999. **70**: p. 3967-3969.

3. J. Check, K.S.K. Karuppiah, and S. Sundararajan, *Comparison of the effect of surface roughness on the micro/nanotribological behavior of ultra-high-molecularweight polyethylene (UHMWPE) in air and bovine serum solution.* Journal of Biomedical Materials Research Part A, 2005. **74A**(4): p. 687-695.

CHAPTER 3. EFFECT OF CROSSLINKING ON THE FRICTION AND WEAR BEHAVIOR OF SOYBEAN OIL-BASED POLYMERIC MATERIALS

Modified from a paper published in *Wear*

Satyam Bhuyan, Sam Holden, Sriram Sundararajan, Dejan Andjelkovic and Richard Larock

3.1 Abstract

In this study, the friction and wear behavior of soybean oil-based polymers prepared by cationic polymerization of low saturated soybean oil (LSS) with divinyl benzene and polystyrene are evaluated as a function of crosslink density. Tribological measurements were performed on samples of three crosslinking densities (10%, 15% and 20% of crosslinking agent concentration by weight) using a ball-on-flat reciprocating microtribometer with normal loads ranging from 0 – 800 mN. Friction and wear behavior during dry sliding was evaluated using a spherical (1.2 mm radius) silicon nitride probe as well as a conical (100 micron radius, 90° cone angle) diamond probe. Friction behavior was evaluated from single strokes at ramped normal loads, whereas wear experiments were evaluated from 10 to 500 reciprocating cycles at fixed normal loads. All samples showed comparable coefficients of friction. In general a higher crosslinking density resulted in lower adhesive wear. Increased abrasive wear was observed for the lowest and highest crosslinking densities. Atomic force microscopy and scanning electron microscopy of wear tracks were used to elucidate

deformation mechanisms in the various samples. These results provide some insight into the friction and wear behavior of soybean oil-based polymers.

3.2 Introduction

In the past two decades the awareness and concern over the usage of petroleum-based products and their impact on the environment has created an opportunity and thrust to produce environmentally acceptable materials from agricultural feedstock. The benefits of environmentally acceptable products include lower pollution, minimal health and safety risks and easier disposal due to their facile biodegradability. The benefits of using agricultural feedstock as sources for engineering materials includes taking advantage of excess agricultural production, the potential for rural development and minimizing the nation's dependency on petroleum [1]. Research is being conducted on developing a variety of bio-based products including transportation fuels [2], lubricants [3-5] and polymers [6, 7].

Soybean oil is biodegradable oil which is readily available in bulk from a renewable natural resource. The polyunsaturation of soybean oil and low-saturation soybean oil with still higher polyunsaturated fatty acid content makes it possible to polymerize or copolymerize these natural oils into useful new materials [8]. Larock and coworkers have developed a variety of novel polymeric materials ranging from elastomers to tough, rigid plastics prepared by the cationic copolymerization of regular soybean oil, low-saturation soybean oil, and conjugated low-saturation soybean oil [6]. These thermosets exhibit thermophysical and mechanical properties that are competitive with those of their petroleum based counterparts. The advantages of these polymer materials are their low cost, availability from a renewable natural source, and their possible biodegradability. Extensive

characterization of mechanical and interfacial properties of these materials are needed to evaluate their potential in replacing existing petroleum-based products for engineering applications. In this paper, the tribological (friction and wear) properties of these soybean oil-based polymeric materials are evaluated as a function of the crosslink density of the polymers. Crosslinking increases the tightness of the polymer network and reduces the molecular mobility of chains between the junctions. As a result, the number of conformations that a polymer can adopt decreases as the crosslink density increases [9]. Thus, crosslinking increases the stiffness of the polymers, which should in turn affect the tribological properties. Wear mechanisms and correlations between material composition and wear behavior are identified and discussed.

3.3 Materials

The natural oil used to prepare the materials in this study was food-grade low-saturation (LSS) soybean oil commercially available in the supermarkets. The oil was used without further purification. The materials synthesis procedure is briefly described here and can be found in extensive detail elsewhere [6]. The LSS was subjected to cationic copolymerization with styrene (ST) and divinyl benzene (DVB) initiated by boron triflouride diethyl etherate ($BF_3.OEt_2$) and modified with Norway fish oil ethyl ester (NFO). This process yields viable polymers ranging from soft rubbers to hard, tough, or brittle plastics by varying oil content, crosslinking density and other parameters [6]. For this study, three materials were prepared with 45% (w/w) oil content and crosslinking agent (divinyl benzene) concentration of 10%, 15% and 20% by weight as listed in Table 1. The table also lists basic material properties and surface roughness data. Throughout the manuscript, these materials

Table 1: Mechanical Properties of the test samples

Samples	Crosslinking Density[a] (moles/m^3)	Young's Modulus[a] (MPa)	Ultimate Tensile Strength[a] (MPa)	Elongat-ion at break[a] (%)	Toughness[a,b] (MPa)	RMS Roughness[c] (nm)
LSS45-ST37-DVB10-(NFO5-BFE3)	2.0 x 10^2	20	2.7	96	1.64	99 ± 11
LSS45-ST32-DVB15-(NFO5-BFE3)	5.3 x 10^2	90	6.0	64	2.86	102 ±9
LSS45-ST27-DVB20-(NFO5-BFE3)	9.0 x 10^2	116	7.6	20	1.09	80 ± 1
Epoxy (EP) resin		1698	21.3	2.4		111 ± 19
UHMWPE		1075	94	330		58 ± 5

[a] Values for LSS samples taken from Ref. [9].
[b] Toughness is defined as the fracture energy per unit volume (area under the tensile stress-strain curve).
[c] Measured using AFM, 15 μm X 15 μm scan size

will be referred to as DVB 10, DVB 15 and DVB 20. DVB 10 is an elastomeric material whereas DVB 20 is hard and brittle. This is reflected by the elastic modulus and elongation at break data from Table 1. Epoxy (EP) resin and Ultra-high molecular weight polyethylene (UHMWPE) were used as benchmark polymeric materials for comparison. Prior to surface

topography and tribological measurements, all samples were polished (Allied High Tech Inc., Rancho Dominguez, California) to remove topography steps generated from the curing process. The polishing conditions were kept identical for each sample; i.e. 207 kPa (30 psi) pressure, 300 rpm and three cycles of 2 minutes each, which resulted in comparable RMS roughness data for the three samples (Table 1). After polishing, all samples were cleaned with de-ionized water in an ultrasonic bath for 10 minutes and dried using dry air prior to tests. FT-IR absorption spectroscopy of the samples before and after cleaning revealed that the samples were not affected chemically by the cleansing treatment.

3.4 Methods

3.4.1 Microscale Friction and Wear Tests

For the experiments described in this paper, a custom-built reciprocating ball-on-flat microtribometer that can produce a microscale (apparent area ~1000 square microns) multi-asperity contact [10] was used. A schematic of its major components is shown in Figure 1. A spherical probe is placed at the end of a crossed I-beam structure which is lowered using a linear stage to apply a desired normal load to the sample. The normal and friction (lateral) forces are measured using semiconductor strain gages on the cantilevers. Friction forces can be resolved to approximately ±5 μN and normal forces to approximately ±15 μN. The signal from the normal load is monitored and used in a simple proportional-integral (PI) feedback loop to maintain the desired normal force regardless of any slope or waviness in the surface of the sample. The desired sample is affixed to another stage set perpendicular to the beam, which provides linear motion.

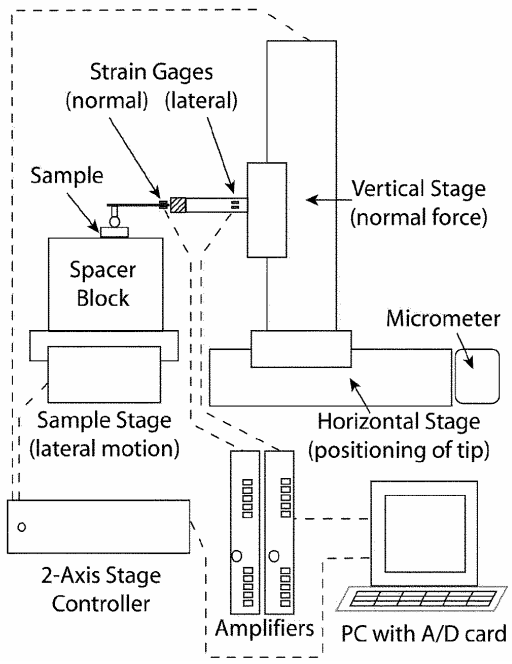

Figure 1. Schematic of a microtribometer setup.

To obtain the coefficient of friction, ramped load tests were performed in which the normal load between a silicon nitride (Si_3N_4) ball (radius - 1.2 mm, RMS roughness - 4 nm, scan size 15 μm X 15 μm) and the sample was increased linearly with the sliding distance while the friction force was monitored. . The load was increased from 0.2 to 800 mN as the probe was moved across a stroke distance of 35 mm at 10 mm/s. Preliminary tests showed that, for our load conditions, sliding speed had negligible effect on friction and wear relative to other factors.

A 500 cycle reciprocating sliding wear test was performed against the Si_3N_4 probe at a constant load of 800 mN and a stroke speed of 5 mm/s for a total sliding distance of 30 m. A preliminary scratch response study of the materials was performed in order to evaluate normal loads to be used for sliding wear tests using a conical (100 micron radius, 90° cone

angle) diamond probe. A 10 cycle reciprocating test with the diamond probe was then carried out at 700 mN at 5mm/s. All tests were performed at 24 °C and 30% relative humidity. Wear track profiling was carried out using a contact profilometer (Dektak II) and contact mode atomic force microscopy or AFM (Dimension 3100, Nanoscope IV, Veeco Instruments, Santa Barbara, California). High resolution images of the wear tracks as well as the transfer films on the probes were obtained using a JOEL JSM-6060LV Scanning Electron Microscope (SEM).

3.5 Results and Discussion

3.5.1 Friction

Figure 2 shows representative friction data for the samples tested under elastic conditions. Friction force increased with an increase in normal load for all the samples. DVB10 exhibited stick-slip behavior sometimes associated with dry sliding. Coefficient of friction values obtained from linear fits of the data are shown in Table 2. The DVB 10 showed higher friction compared to DVB 15 and DVB 20. The high values observed for DVB 10 are consistent with high values observed for rubbery elastomers [11, 12] . This is because rubber friction theory predicts that the adhesion component of friction can be very high when in contact with smooth surfaces, especially in the absence of lubricant [13]. No discernable grooves were observed on the surface after the tests, which is not surprising since the tests were under elastic contact conditions. Coefficient of friction values for the soybean oil-based polymers were comparable to that of the epoxy (EP) resin and higher than that of UHMWPE (Table 2). This suggests that the materials are not well-suited as low-friction materials under unlubricated conditions.

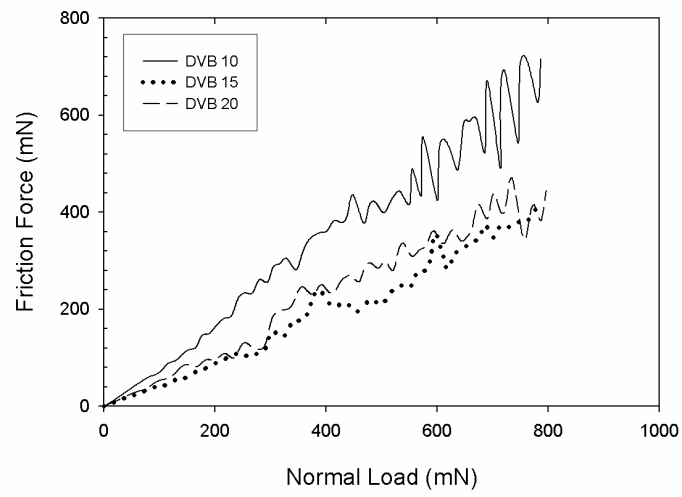

Figure 2. Representative friction force vs. normal load plots obtained from friction tests for DVB 10, DVB 15 and DVB 20 using a spherical Si_3N_4 probe.

3.5.2 Wear against Si_3N_4 ball

Figure 3 shows the friction force on the samples as a function of the sliding distance during wear tests against Si_3N_4 probe at constant load. It can be clearly seen that DVB 10 shows a higher friction force than DVB 15 and DVB 20, which is consistent with the friction data. The DVB 15 showed a unique trend of a sudden increase in friction force which usually corresponds to the onset of damage on the sample. SEM images of the sample (Fig. 4) displayed clear wear tracks on DVB 10 and DVB 15 but none on DVB 20. This indicates that DVB 20 did not undergo any wear even after 500 cycles. Upon examining the wear track closely at higher magnification, it was observed that DVB 10 displays some material buildup and debris scattered along the track, whereas DVB 15 did not exhibit any significant features. The generation of wear particles and debris in DVB 15 may account for the larger variation in friction forces seen for this sample (Fig. 3). AFM images obtained across the wear-track boundary (Fig. 5) indicate that a very shallow groove has been formed (~100-150

nm) on both samples. These AFM data were used to estimate average wear depths. Average wear depth for DVB 10 was 157 nm which is slightly greater than DVB 15 with an average of 127 nm. Upon examining the Si_3N_4 probe under the SEM (Fig. 6) transfer films on both the probes for DVB 10 and DVB 15 were seen. This suggests that the adhesive wear was the dominant mechanism for these samples. No transfer film was observed on the probe that was run against DVB 20. The observed area of transfer film due to DVB 10 probe is larger (~300 μm) than that due to DVB 15 (~150 μm). This suggests that DVB 10 transfers more material compared to DVB 15. High magnification SEM images of the transfer film revealed distinct striations along the direction of stroke in both samples. These data indicate that the soybean oil-based polymers exhibit a decrease in adhesive wear depth with an increase in crosslinking density. The wear behaviors of DVB 10 and DVB 15 were significantly better than that of epoxy (EP) resin and UHMWPE (Table 2) whereas DVB 20 exhibited no wear track at all.

Table 2: Summary of test results. The averages and standard deviation values have been reported from four data sets.

Samples	Coeff. of friction against Si_3N_4[a]	Coeff. of friction against diamond[b]	Wear depth with Si_3N_4 probe[c] (nm)	Wear depth with diamond probe[d] (μm)
DVB 10	0.826 ± 0.021	0.686 ± 0.058	157 ± 14.76	27 ± 1.19
DVB 15	0.522 ± 0.024	0.413 ± 0.015	127 ± 13.08	7.68 ± 0.44
DVB 20	0.550 ± 0.019	0.423 ± 0.043	---	9.92 ± 0.42
Epoxy (EP) resin	0.701 ± 0.039	0.830 ± 0.033	2234 ± 1221	9.28 ± 5.96
UHMWPE	0.216 ± 0.012	0.297 ± 0.030	281 ± 32.67	66 ± 4.23

[a] For normal load range of 0.2-800 mN
[b] For normal load range of 0.2-100 mN
[c] After 500 cycles at 800 mN normal load
[d] After 10 cycles at 700 mN normal load.

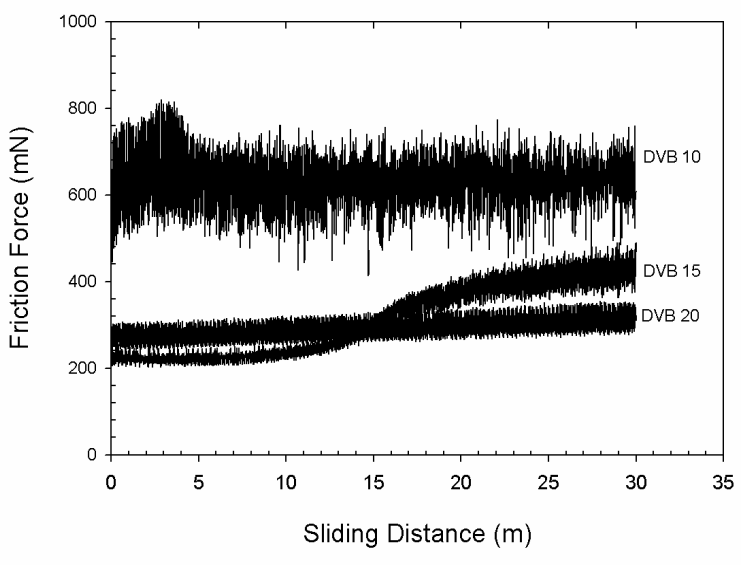

Figure 3. Representative friction force vs. sliding distance for all samples at 800 mN normal load obtained during the sliding wear test against a spherical Si_3N_4 probe.

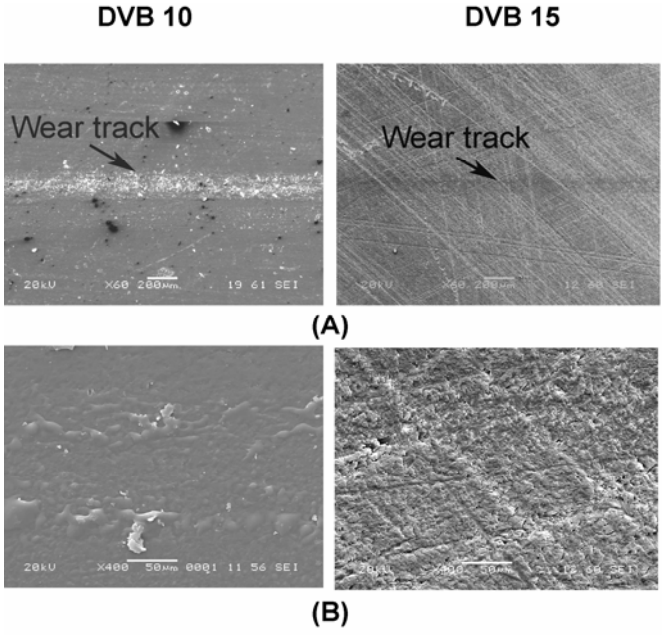

Figure 4. Scanning electron microscopy images of the wear tracks of DVB 10 and DVB 15 against the Si_3N_4 probe at lower (A) and higher (B) magnifications. DVB 20 exhibited no discernable wear track.

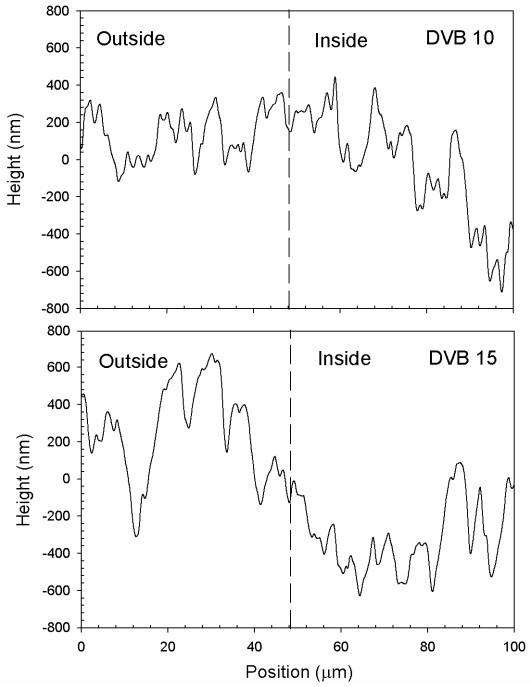

Figure 5. Representative profiles of the wear track periphery for DVB 10 and DVB 15 obtained from sliding wear tests against the Si_3N_4 probe using atomic force microscopy. The average wear depths were quantified using such profiles (listed in Table 2).

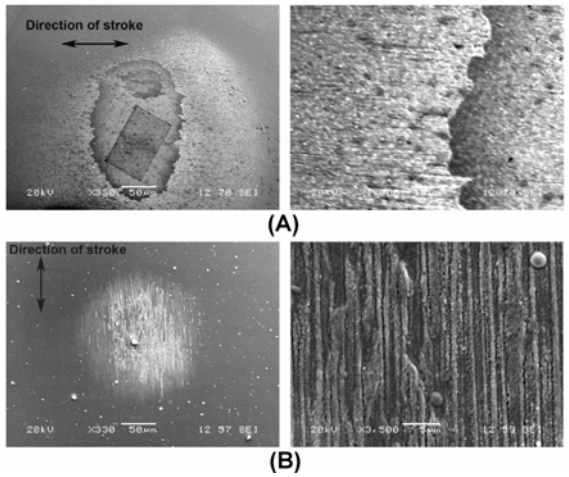

Figure 6. Scanning electron microscopy images of the transfer film formed during sliding wear tests on the Si_3N_4 probe due to DVB 10 (A) and DVB 15 (B). The high magnification images (right) of the films reveal distinct striations parallel to the direction of stroke.

3.5.3 Scratch tests.

The results from the scratch tests using the conical diamond probe are shown in Figs. 7, 8 and 9. The figures show the friction force as a function of increasing normal load as well as the sliding distance, along with optical micrographs of representative regions (A,B and C) from the final scratches. In all the samples, there was no damage generated at lower loads, leading to an almost linear increase in friction force with normal load (regions A). At intermediate loads (regions B); DVB 10 exhibited some cracks on the surface (Fig. 7), which suggest that microcracking plays a strong role in the wear process. This region of damage was accompanied with an increase in slope of the friction vs. normal load data, which can be expected due to the increase in dissipative energy necessary for material damage. Both DVB 15 and DVB 20 did not exhibit any marked material damage at intermediate loads. However they exhibited significant variation in friction force (regions B, Figs. 8 and 9) due to stick slip behavior that was observed during the experiments. Observations of the scratches on DVB 15 and DVB 20 immediately after the tests revealed some grooving at regions corresponding to intermediate loads. However these grooves did not appear during the optical measurements performed later (within 24 hrs). This suggests that these materials exhibit some form of scratch recovery, which may be elastic in nature and warrants further investigation.

At high loads (regions C) all samples exhibited some form of damage. DVB 10 exhibited larger and more cracks (Fig. 7), whereas DVB 15 and 20 exhibited a plastic groove (Figs. 8 and 9). Based on these data, subsequent sliding wear tests were conducted at 800 mN, which would allow us to observe and quantify material damage on all three samples.

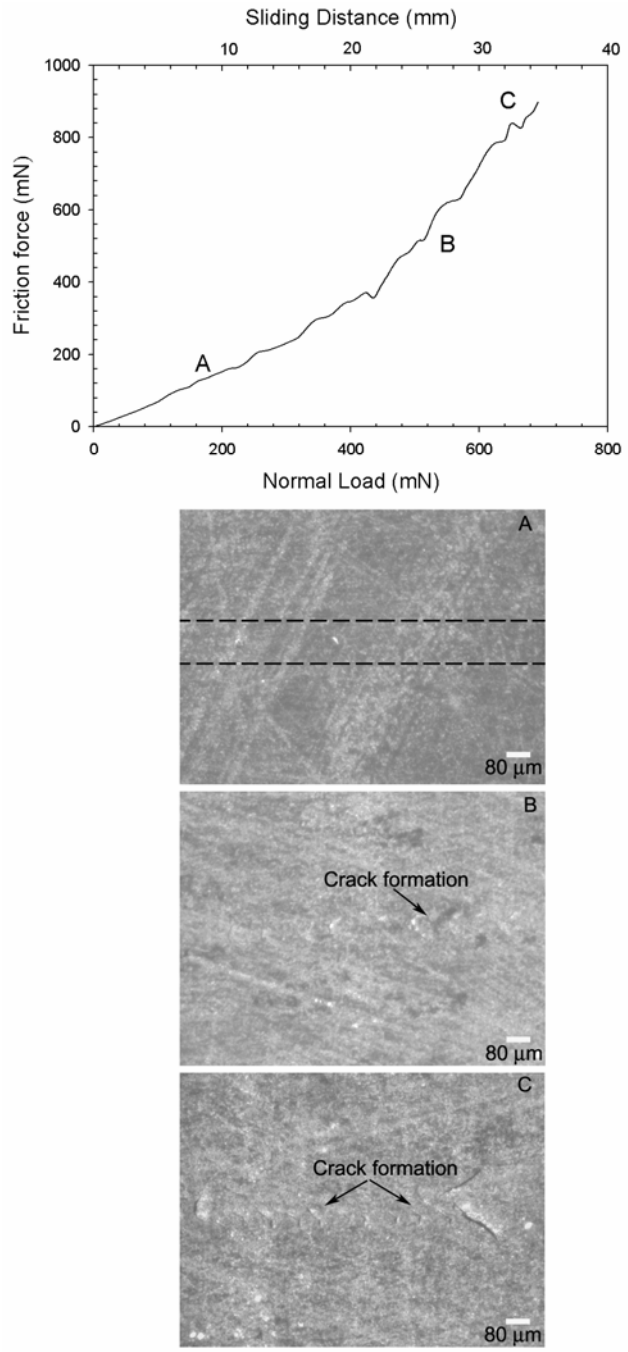

Figure 7. Representative friction force vs. normal load plots obtained from a scratch test using a conical diamond probe (for DVB 10). The optical micrographs represent three different regions from the friction trace indicated by A, B and C. The dashed lines in A are guides for the eye enclosing the region where the probe slid over the surface

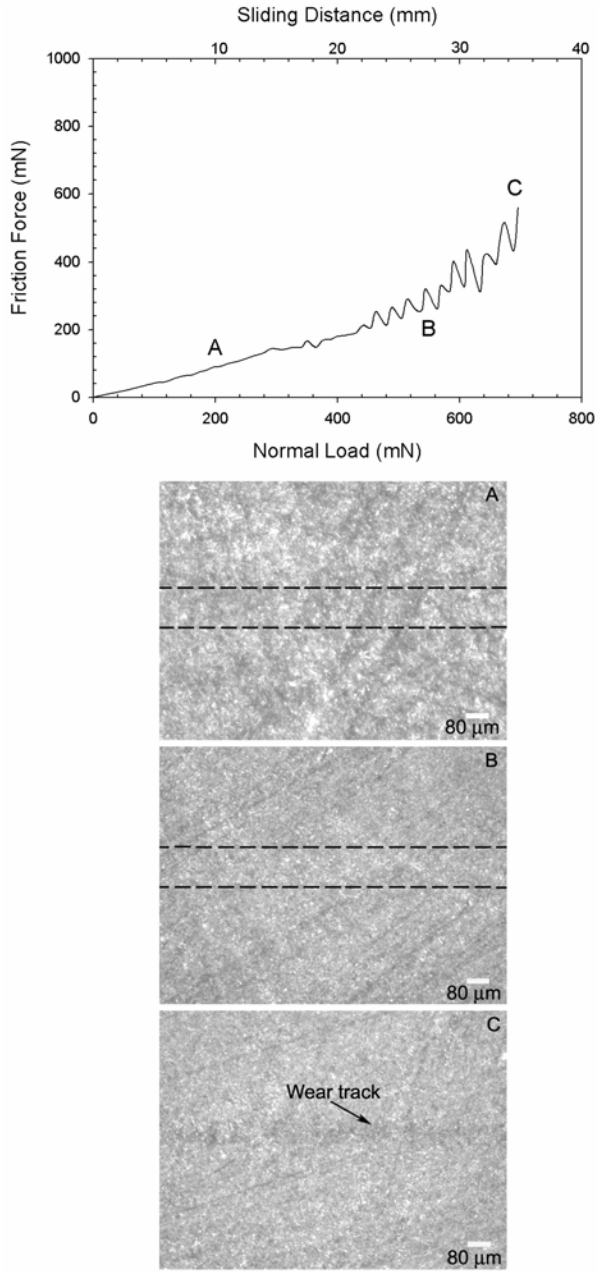

Figure 8. Representative friction force vs. normal load plots obtained from a scratch test using a conical diamond probe (for DVB 15). The optical micrographs represent three different regions from the friction trace indicated by A, B and C. The dashed lines in A and B are guides for the eye enclosing the region where the probe slid over the surface

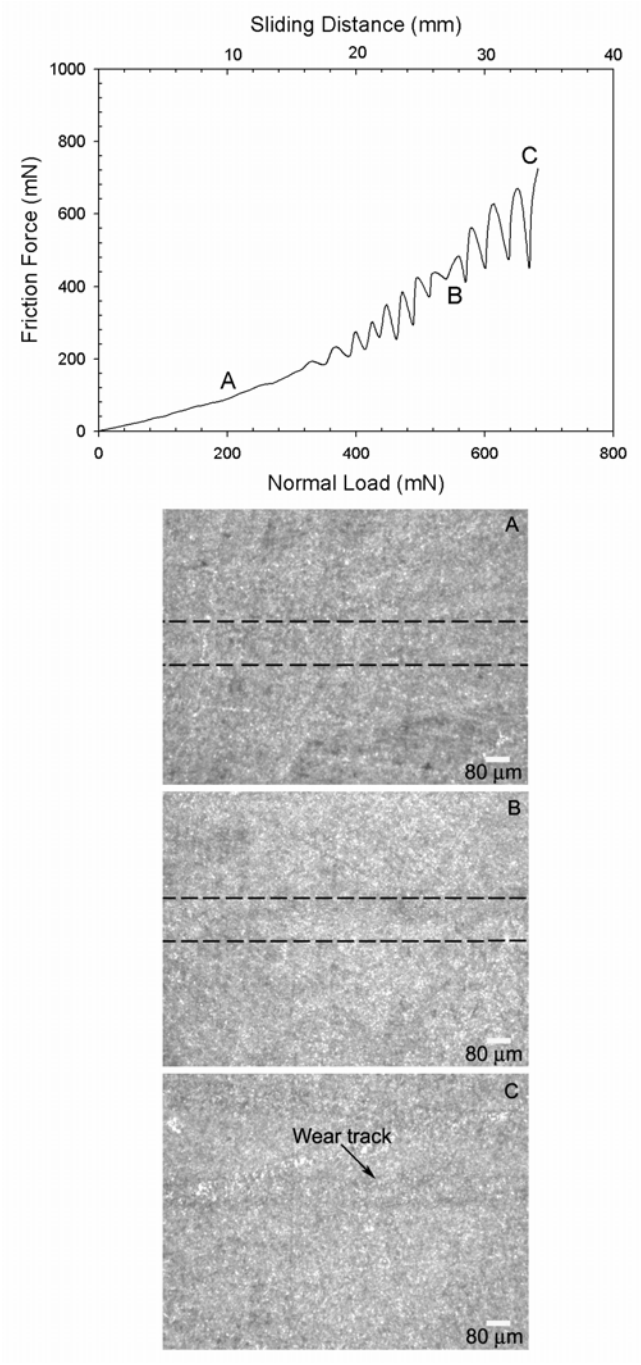

Figure 9. Representative friction force vs. normal load plots obtained from a scratch test using a conical diamond probe (for DVB 15). The optical micrographs represent three different regions from the friction trace indicated by A, B and C. The dashed lines in A and B are guides for the eye enclosing the region where the probe slid over the surface.

3.5.4 Wear against diamond probe

Figure 10 shows representative profiles of the resulting wear depth for each of the samples obtained after wear tests against the diamond probe. DVB 10 exhibited the maximum wear followed by DVB 20 and then DVB 15. The average wear depths are recorded in Table 2. SEM images of the wear tracks are shown in Figs. 11 and 12, with the latter being at higher magnification. It can be clearly seen that DVB 10 and DVB 20 exhibit grooves as well as presence of abraded material debris and some cracking along the groove edges. DVB 15 on the other hand displayed a high degree of cracking with negligible debris. Abrasive wear is manifested by the cutting or plowing of the surface by the harder material (diamond in our experiments). The abraded particles are either embedded in the counterface or get loose within the contact zone. All these samples can be considered to have experienced abrasive wear by the sharp conical probe.

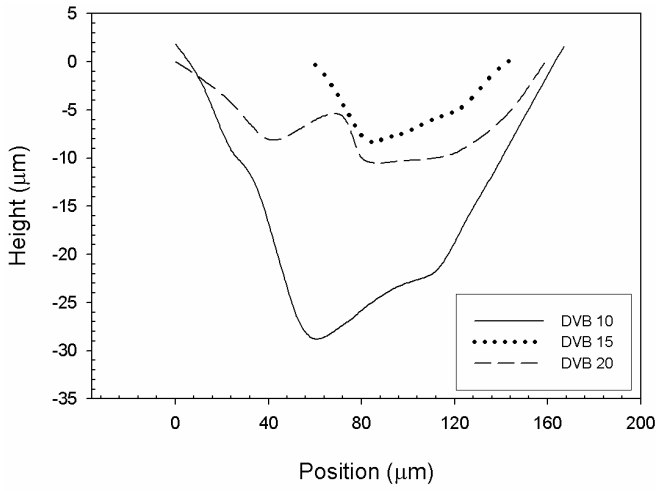

Figure 10. Representative profiles of the sliding wear depths for the tested materials against a sharp diamond probe obtained using a contact profilometer. The average wear depths were quantified using such profiles (listed in Table 2).

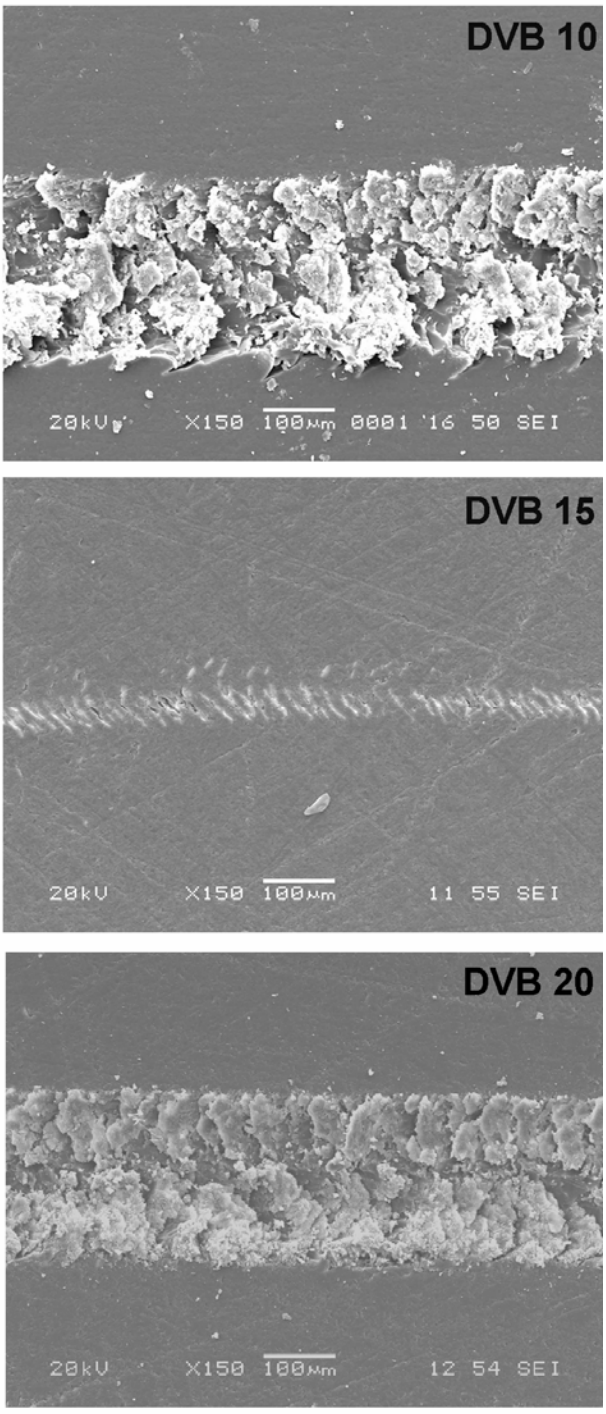

Figure 11. Scanning electron microscope images of the abrasive wear track on DVB 10, DVB 15 and DVB 20. Formation of cracks on all the three samples is clearly seen. In addition, DVB 10 and DVB 20 show ploughing and wear debris.

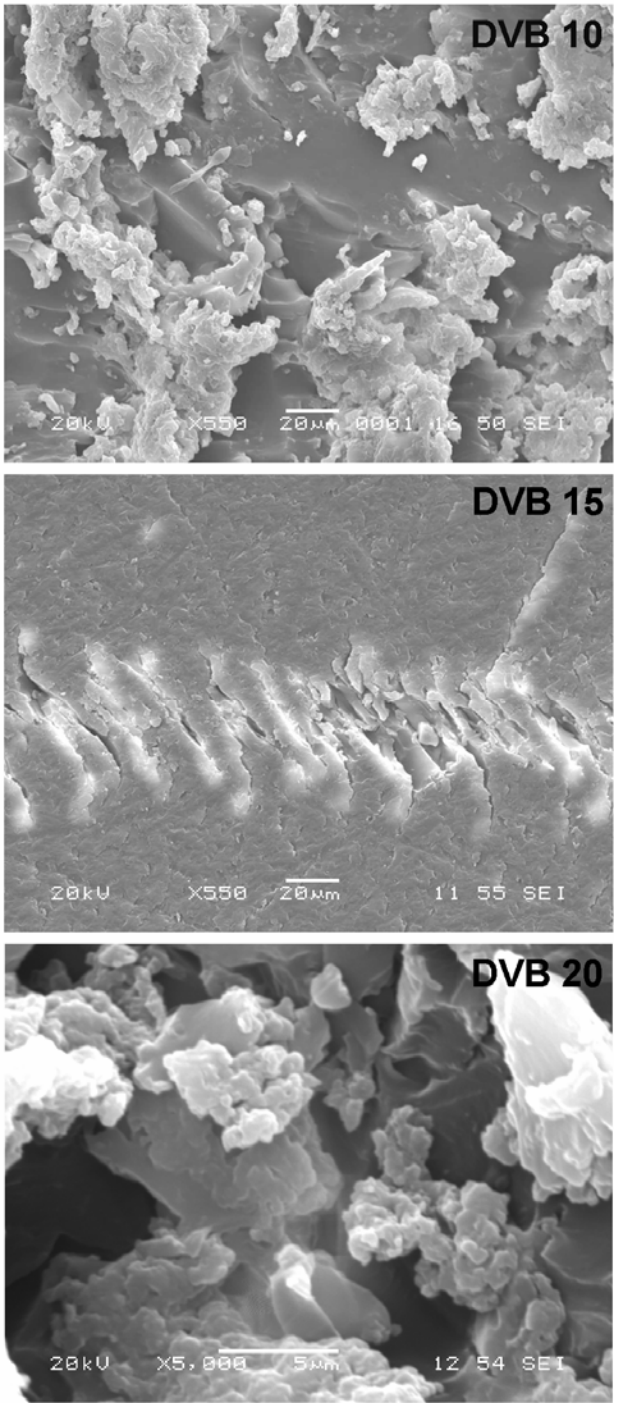

Figure 12. Higher magnification images of abrasive wear tracks. Wear debris in DVB 10 and DVB 20 appear to be loosely embedded while DVB 15 displays clear cracks.

Further, the degree of penetration, defined by the ratio of the depth of groove and the radius of contact [14], gave values less than 0.2 for all samples which indicates that dominant mechanism of abrasive wear is ploughing. The radii of curvature of the wear grooves were calculated be about 112-114 μm which is close to the radius of curvature, 100 μm, of the diamond probe. The fact that DVB 10 displayed cracking during the scratch test (i.e. 1 cycle) whereas DVB 15 and DVB 20 did not, suggests that DVB 10 underwent abrasive wear by plastic deformation whereas the other samples might have underwent wear by fatigue as well.

It is well known that rubbery materials like DVB 10 consist of long flexible chain-like molecules, which are interconnected at various points by crosslinks to form loose molecular networks [9]. When stress is applied on the surface the rubbery materials tend to break the networks. DVB 15 showed the least amount of abrasive wear. From Table 1, DVB 15 also has the highest toughness (area under stress-strain curve) amongst the three. Although DVB 20 has the highest crosslinking density, its low toughness value compared to DVB 15 can be attributed to the fact that there exist nonuniform crosslinking structures in the polymer network as well as occurrence of nonuniformity in polymer composition during the synthesis [9]. For example, flakes of divinyl benzene may precipitate to the bottom before the residual solution starts to gel. Therefore the density of a polymer may be dissimilar across the bulk, thereby resulting in varying mechanical properties. Another disadvantage is the inefficiency in divinyl benzene consumption [9]. This can lead to limited availability of the crosslinker and hence a softer and weaker region since it is the crosslinking which gives (or enhances) the material its strength. Table 2 shows that the wear depths of the soybean oil-

based polymers as a result of sliding against diamond probe are higher than UHMWPE. DVB 15 and DVB 20 showed comparable depths to that of epoxy (EP) resin, whereas DVB 10 compared poorly.

3.6 Conclusions

The tribological properties of novel soybean oil-based polymeric materials as a function of crosslinking density (10%, 15% and 20% of crosslinking agent DVB concentration by weight) were evaluated. The coefficients of friction of DVB 10 and DVB 20 were 37% and 4% lower respectively, when compared with DVB 15 which showed a value of 0.83. In sliding wear tests against a Si_3N_4 spherical probe, DVB 20 showed negligible wear whereas DVB 15 showed 19% less adhesive wear depth than DVB 10. In sliding wear tests with a conical diamond probe, all samples exhibited abrasive wear. DVB 10 showed the highest wear depth followed by DVB 20 (63% lower than DVB 10) and DVB 15 (72 % lower). The DVB 10 and DVB 15 samples exhibited delayed recovery of scratch grooves under intermediate loads, which warrants further investigation. Based on these studies, these novel bio-based materials show promise as replacements for conventional plastics as structural materials.

3.7 Acknowledgement

The authors would like to thank Professor Scott Chumbley of Material Science and Engineering Department at Iowa State University (ISU) for assistance with SEM operation. We are also grateful to Jerry Amenson of Materials Analysis and Research Laboratory at ISU for the use of their Allied Sample Polisher.

3.8 References

1. R.C. Brown, Biorenewable Resources: Engineering New Products from Agriculture, 1st ed, Iowa State Press, Ames,2003.
2. S. Kim and B.E. Dale, Global potential bioethanol production from wasted crops and crop residues, Biomass and Bioenergy 26(4) (2004) 361-375.
3. A. Adhvaryu, S.Z. Erhan and J.M. Perez, Tribological studies of thermally and chemically modified vegetable oils for use as environmentally friendly lubricants, Wear 257(3-4) (2004) 359-367.
4. S. Bhuyan, S. Sundararajan, L. Yao, E.G. Hammond and T. Wang, Boundary lubrication properties of lipid-based compounds evaluated using microtribological methods, Tribology Letters 22(2) (2006) 167-172.
5. G. Biresaw, Biobased dry-film metalworking lubricants, Journal of Synthetic Lubrication 21(1) (2004) 43-58.
6. F. Li, M.V. Hanson and R.C. Larock, Soybean oil–divinylbenzene thermosetting polymers: synthesis, structure, properties and their relationships, Polymer 42 (2001) 1567-1579.
7. S.-J. Park, F.-L. Jin, J.-R. Lee and J.-S. Shin, Cationic polymerization and physicochemical properties of a biobased epoxy resin initiated by thermally latent catalysts, European Polymer Journal 41(2) (2005) 231-237.
8. K. Matyjaszewski, Cationic polymerization: mechanisms, synthesis and applications, Marcel Dekker, New York,1996.

9. F. Li and R. Larock, New Soybean Oil-Styrene-Divinylbenzene Thermosetting Copolymers III Tensile Stress–Strain Behavior, Journal of Polymer Science: Part B: Polymer Physics 39 (2001) 60-77.

10. J. Check, K.S.K. Karuppiah and S. Sundararajan, Comparison of the effect of surface roughness on the micro/nanotribological behavior of ultra-high-molecularweight polyethylene (UHMWPE) in air and bovine serum solution, Journal of Biomedical Materials Research Part A 74A(4) (2005).

11. B.N.J. Persson, On the theory of rubber friction, Surface Science 401(3) (1998) 445-454.

12. B.N.J. Persson, Elastoplastic contact between randomly rough surfaces, Physical Review Letters 87(11) (2001) art. no.-116101.

13. C.M. Pooley and D. Tabor, Friction and Molecular Structure - Behavior of Some Thermoplastics, Proceedings of the Royal Society of London Series a-Mathematical and Physical Sciences 329(1578) (1972) 251.

14. K. Hokkirigawa and K. Kato, An experimental and theoretical investigation of ploughing, cutting and wedge formation during abrasive wear, Tribology International 21(1) (1988) 51-57.

CHAPTER 4. MICRO- AND NANO- TRIBOLOGICAL BEHAVIOUR OF SOYBEAN OIL-BASED POLYMERS OF DIFFERENT CROSSLINKING DENSITIES

Modified from a paper submitted to *Tribology Letters*

Satyam Bhuyan, Sriram Sundararajan, Dejan Andjelkovic and Richard Larock

4.1 Abstract

Biobased polymers produced from renewable and inexpensive natural resources, such as natural oils, have drawn considerable attention over the past decade, due to their low cost, ready availability, environmental compatibility, and their inherent biodegradability. In this study, the micro/nanotribological wear behavior of biopolymers of different crosslinking densities prepared from low saturated soybean oil (LSS) by Rh-catalyzed isomerization with divinyl benzene and polystyrene are evaluated and compared. Microtribological measurements were performed using a ball-on-flat reciprocating microtribometer using two different probes - 1.2 mm radius Si_3N_4 spherical probe and a 100 micron radius conical diamond probe with 90^0 cone angle. Nanoscale wear tests were performed using a DLC coated antimony (n) doped silicon probe of radius ~200 nm in an atomic force microscope (AFM). Wear volumes were estimated from AFM topography maps of groove geometry and wear coefficients were evaluated for the materials. Elastic modulus and hardness information were evaluated using tensile test and nanoindentation tests respectively. Correlations between crosslinking density and observed wear behavior across scales are discussed.

4.2 Introduction

In the past few decades the awareness and concern over the usage of petroleum-based products and their impact on the environment has created an opportunity and thrust to produce environmentally acceptable materials from bio-based feedstock. The benefits of using biobased feedstock as sources for engineering materials includes taking advantage of excess agricultural production, the potential for rural development and minimizing the nation's dependency on petroleum [1]. Research has been conducted on developing a variety of bio-based products including transportation fuels [2, 3], lubricants [4-6], polymers [7-10] and polymer composites [11-13].

Soybean oil is a biodegradable oil and readily available in bulk from a renewable natural resource. The polyunsaturation of soybean oil and low-saturation soybean oil with still higher polyunsaturated fatty acid content makes it possible to polymerize or copolymerize these natural oils into useful new materials [14]. Larock and coworkers have developed a variety of novel polymeric materials ranging from elastomers to tough, rigid plastics prepared by the cationic copolymerization of regular soybean oil, low-saturation soybean oil, and conjugated low-saturation soybean oil [7]. The advantages of these thermoset polymer materials are their low cost, availability from a renewable natural source, and their possible biodegradability. Extensive characterization of mechanical and interfacial properties of these materials are needed to evaluate their potential in replacing existing petroleum-based products for engineering applications. These polymers exhibit mechanical properties that are competitive with commercial unsaturated polyesters [15].

In this paper, we focus on the nanoscale wear behavior of these polymers together with microscale data. Mechanisms of observe wear behavior are discussed in conjunction with effect of crosslinking density.

4.3 Materials

The natural oil used to prepare the materials in this study was food-grade low-saturation (LSS) soybean oil commercially available in the supermarkets. The oil was used without further purification. The materials synthesis procedure is briefly described here and can be found in extensive detail elsewhere [7]. The LSS was subjected to cationic copolymerization with styrene (ST) and divinyl benzene (DVB) initiated by boron triflouride diethyl etherate ($BF_3.OEt_2$) and modified with Norway fish oil ethyl ester (NFO). This process yields viable polymers ranging from soft rubbers to hard, tough, or brittle plastics by varying oil content, cross-liking density and other parameters [7]. For this study, three materials were prepared with 45% (w/w) oil content and crosslinking agent (divinyl benzene) concentration of 10%, 15% and 20% by weight as listed in Table 1. The table also lists basic material properties and surface roughness data. Throughout the manuscript, these materials will be referred to as DVB 10, DVB 15 and DVB 20. DVB 10 is an elastomeric material whereas DVB 20 is quite brittle. This is reflected by the elongation at break data from Table 1.

Table 1: Mechanical properties of the test samples

Samples	Crosslinking Density[a] (moles/m^3)	Ultimate Tensile Strength[a] (MPa)	Elongatio at break[a] (%)	Toughness[a,b] (MPa)	RMS Roughness[c] (nm)
LSS 45-ST 37-DVB 10-(NFO 5-BFE 3)	2.0 x 10^2	2.7	96	1.64	99 ± 11
LSS 45-ST 32-DVB 15-(NFO 5-BFE 3)	5.3 x 10^2	6.0	64	2.86	102 ±9
LSS 45-ST 27-DVB 20-(NFO 5-BFE 3)	9.0 x 10^2	7.6	20	1.09	80 ± 1

[a] Values for LSS samples taken from Ref. [18].
[b] Toughness is defined as the fracture energy per unit volume (area under the tensile stress-strain curve).
[c] Measured using AFM, 15 μm X 15 μm scan size.

4.4 Methods

4.4.1 Nanoindentation tests

Nanoindentation test were performed on the polymers with a Berkovich indenter using a Hysitron Triboscope (Hysitron Inc., Minneapolis, Minnesota, USA) in conjunction with an Atomic Force Microscope (NanoScope Dimension™ 3100, Digital Instruments, Veeco Metrology Group). Two different loading profiles were used for the test. One is a trapezoidal loading profile with a peak indentation force of 25 μN (loading time 2.5 seconds, holding time 1 second, and unloading time 0.5 second, respectively). The other is a partial loading and unloading profile with an equal loading and unloading rate of 10 μN/s and 10 different peak indentation loads ranged from 5 to 50 μN. At each peak load, appropriate

holding time was assigned. During indentation test, the sample was hold firmly by the vacuum chuck of AFM. The mechanical properties namely hardness and elastic modulus were analyzed using Oliver and Pharr method [16].

4.4.2 Microscale Wear Tests

For the experiments described in this paper, a custom-built reciprocating ball-on-flat microtribometer that can produce a microscale (apparent area ~1000 square microns) multi-asperity contact [17] was used. To obtain wear a 500 cycle reciprocating sliding wear test was performed in which the normal load between a silicon nitride (Si_3N_4) ball (radius - 1.2 mm, RMS roughness - 4 nm, scan size 15 μm X 15 μm) and the sample was keep constant at 800 mN at a sliding speed of 5 mm/s. Preliminary tests showed that, for our load conditions, sliding speed had negligible effect on friction and wear relative to other factors. A 10 cycle reciprocating test with a conical diamond probe (100 micron radius, 90° cone angle) was then carried out at 700 mN at 5mm/s. For the loading condition used, the Hertzian contact pressures under the assumption of Hertzian contact theory predicted a plastic deformation response [18].

4.4.3 Nanoscale wear tests

Nanoscale reciprocating wear tests were performed using a Dimension ™ 3100 AFM (Nanoscope IV, Veeco Instruments, Santa Barbara, CA) in controlled low (14 ± 4 % RH) humidity conditions. V-shaped triangular silicon probes doped with antimony (n) and coated with DLC (from Veeco) with calibrated force constant of 41.1 N/m and measured tip radius of 200 nm were used for wear measurements. The spring constant of the cantilever used were

calibrated using the technique described by Sader [19]. The radius of the tip was characterized before and after the experiments using commercially available calibration samples (TGT01 from MikroMasch USA, Portland, OR). Tip contamination was monitored using a standard tipcheck sample (Tipcheck from Aurora Nanodevices). Tipcheck has a Ti thin film coated on a Si surface and TGT01 has sharp spiked silicon features. Both these samples exploit the reverse imaging to provide a fast and simple way of assessing tips. The sample's sharp features, when imaged using the AFM, result in height maps that contain information regarding the tip shape[17]. Deconvolution of these images using blind reconstruction methods results in a fairly accurate estimate of the tip shape and radius. The adhesive forces between the probe and the sample were measured from force-displacement curves after each test. For scratch tests the probe was moved back and forth at a constant normal load by disabling the slow scan axis which allowed it to scratch the sample along a line. Normal forces were varied from 0 to 10 μN as the wear depth was monitored after 10 cycles of scratching.

4.5 Results and discussion

4.5.1 Nanoindentation tests

Figure 1a shows the typical load penetration depth curves of nanoindentations on the polymer samples observed using a trapezoidal loading profile. As can be seen, the maximum load for indentation has not reached the peak load intended to apply due to the significant creep of the materials. For accurate determination of mechanical properties of polymeric and viscoelastic materials using nanoindentation test, the creep effect, which often results in bulging "nose" in the unloading curve must be accounted for before applying Oliver and Pharr method. This can be done by either introducing a sufficiently long holding segment [20]

or using a sufficiently fast unloading rate [21]. In this study, both appropriate holding segment and fast unloading rate have been employed to reduce creep effect on the measured mechanical properties. At the end of unloading, indentation force dropped below zero, which may indicate adhesion between indenter and the tested polymer materials. The average elastic modulus and hardness of 9 indentations for all polymers are shown in Table 2. It must be noted that these values may not represent the "true" properties of the materials since the Oliver-Pharr analysis assumes no creep. However, they are useful for relative comparisons in this study.

Figure 1b shows the typical load penetration depth curves of nanoindentations with partial loading and unloading profile. The elastic modulus and hardness are determined from the partial unloading curves at different peak loads. The variations of average elastic modulus and hardness with the average indentation contact depth of 5 indentations for all materials are plotted in Fig 2. Both elastic modulus and hardness for all the polymers decrease with the increase of contact depth. Partial loading and unloading tests shows a similar trend that polymer DVB 20 has the highest elastic modulus and hardness while DVB 10 has the lowest elastic modulus and hardness at different contact depths. From the data, one can see a correlation between hardness and crosslinking density. The hardness increases with crosslinking density. Nanoindentation test shows that polymer DVB 20 has the highest elastic modulus and hardness while DVB 10 has the lowest elastic modulus and hardness.

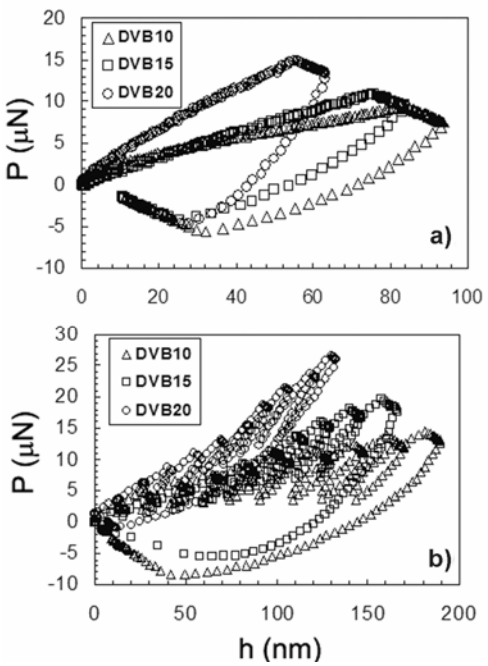

Figure 1. Load penetration depth curves of nanoindentations on the three samples with a) trapezoidal loading profile and b) partial loading and unloading profile.

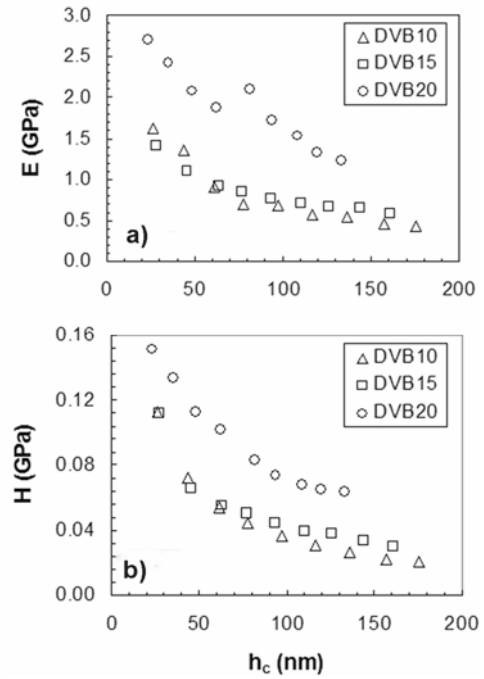

Figure 2. Variations of average (a) elastic modulus and (b) hardness with the average indentation contact depth of 5 indentations for all three samples.

Table 2: Average ± standard deviation of elastic modulus and hardness of polymers taken from 9 indentation tests.

Materials	Elastic modulus (GPa)	Hardness (GPa)
DVB 10	0.80 ± 0.06	0.035 ± 0.004
DVB 15	1.05 ± 0.07	0.060 ± 0.007
DVB 20	2.19 ± 0.31	0.130 ± 0.019

Crosslinking increases the tensile strength because the van der Waals force between neighboring polymer chains is replaced by covalent bonds [22]. To break the chemical bonds, an activation energy barrier needs to be overcome. By pulling a bond, the initial state increases its energy until thermal fluctuations are sufficient to overcome the activation barrier, revealing an increased mechanical response.

4.5.2 Sliding wear against Si_3N_4 ball

After dry sliding wear tests against a Si_3N_4 probe, SEM imaging (Fig 3) of the samples indicated the presence of clear wear tracks on DVB 10 and DVB 15 but not on DVB 20. It was therefore concluded that DVB 20 did not undergo any wear even after 500 cycles. It was also observed that DVB 10 displayed some material buildup and debris scattered along the track, whereas DVB 15 did not exhibit any significant features. Profiles obtained across the wear-track boundary using an AFM indicate that a very shallow groove has been formed (~100-150 nm) on both samples. These data were used to estimate average wear depths.

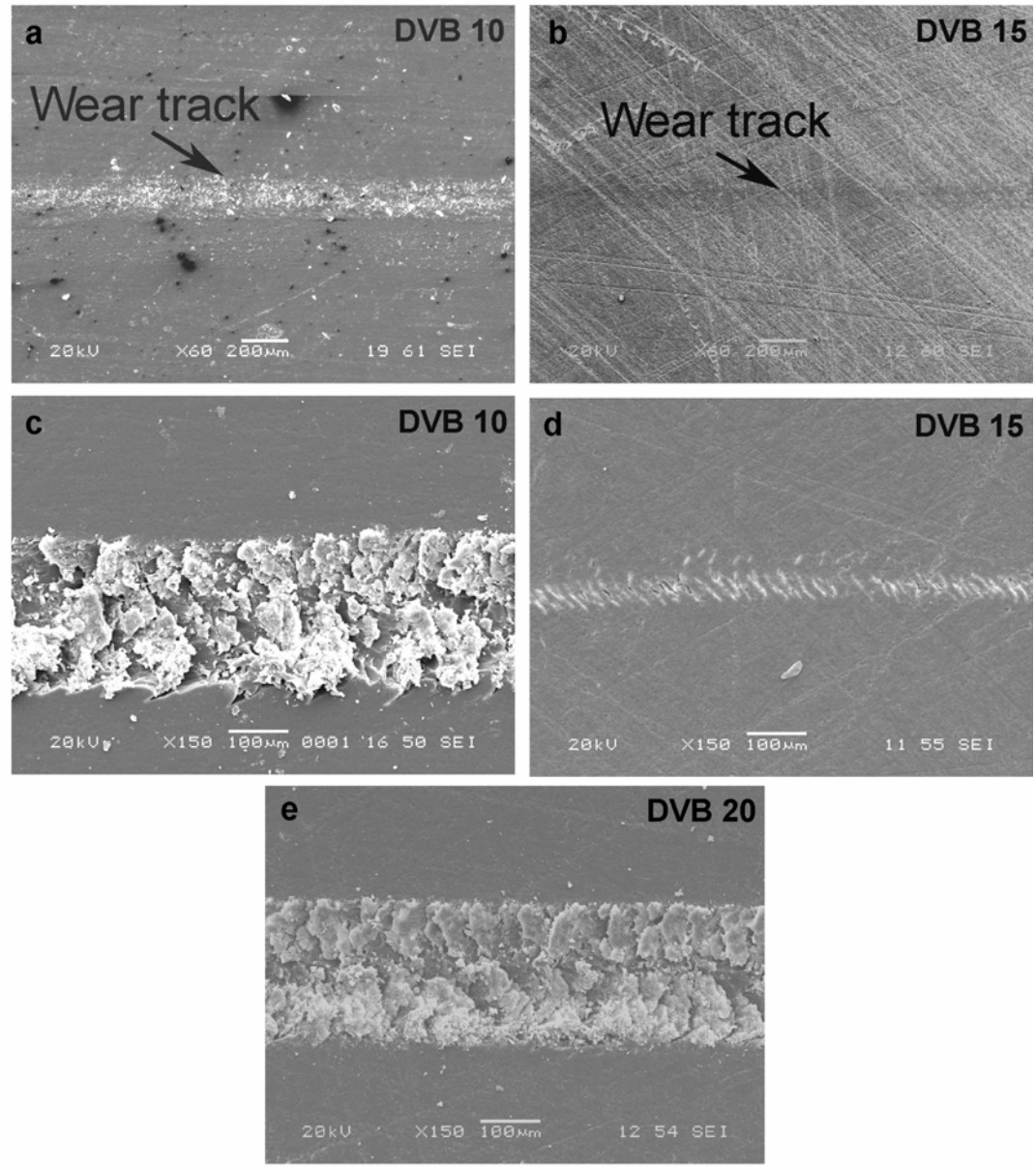

Figure 3. Scanning electron microscope images of the wear track on a) DVB 10 and b) DVB 15 with Si_3N_4 probe and on c) DVB 10, d) DVB 15 and e) DVB 20 with sharp diamond probe. Appearance of cracks due to abrasive wear with diamond probe on all the three samples is clearly seen.

Table 3: Summary of test results

	Microscale						Nanoscale	
Samples	**Average wear depth with Si_3N_4 probe[a] (nm)**	**Wear co-efficient with Si_3N_4 probe[a]**	**Wear rate with Si_3N_4 probe[a] (nm/s)**	**Average wear depth with diamond probe[b] (μm)**	**Wear co-efficient with diamond probe[b]**	**Wear rate with diamond probe[b] (μm/s)**	**Wear co-efficient with DLC coated Sb (n) doped Si probe[c]**	**Wear rate with DLC coated Sb (n) doped Si probe[c] (μm/s)**
DVB 10	157 ± 14.76	1.37×10^{-6}	2.63	27 ± 1.19	120×10^{-4}	807	0.91	93.7
DVB 15	127 ± 13.08	1.45×10^{-6}	7.57	7.68 ± 0.44	8.67×10^{-4}	91	0.17	12.5
DVB 20	-	-	-	9.92 ± 0.42	150×10^{-4}	873	0.15	8.03

[a] After 500 cycles at 800 mN normal load.
[b] After 10 cycles at 700 mN normal load.
[c] After 10 cycles at 5 μN normal load.

Average wear depth for DVB 10 was 157 nm which is slightly greater than DVB 15 with an average of 127 nm. When the Si_3N_4 probes were examined under the SEM transfer films on both the probes for DVB 10 and DVB 15 were seen. This suggests that adhesive wear was the dominant mechanism for these samples. The adhesive wear coefficients listed in table 3 give a value ~10^{-6} indicating a mild wear for these materials. No transfer film was observed on the probe that was run against DVB 20. The observed area of transfer film due to DVB 10 probe is larger than that due to DVB 15. This suggests that DVB 10 transfers more material compared to DVB 15. All these data indicate that the soybean oil-based polymers exhibit a decrease in adhesive wear propensity with an increase in crosslinking density. Table 3 summarizes the results in terms of wear rates and wear coefficients. These were calculated from the following equations (for plastic contacts) [18],

$$k = \frac{vH}{Wx} \tag{1}$$

$$\dot{d} = \frac{kpV}{H} \tag{2}$$

As one would expect from Archard's law, the material with the highest hardness showed the least wear against Si_3N_4 probe.

4.5.3 Sliding wear against diamond probe

Figure 3 shows representative SEM images of the resulting wear track for each of the samples obtained after dry sliding against the diamond probe. DVB 10 exhibited the maximum wear followed by DVB 20 and then DVB 15. It can be clearly seen that DVB 10 and DVB 20 exhibit grooves as well as presence of abraded material debris and some

cracking along the groove edges. DVB 15 on the other hand displayed a high degree of cracking with negligible debris. Abrasive wear is manifested by the cutting or ploughing of the surface by the harder material (diamond in our experiments). The abraded particles are either embedded in the counterface or get loose within the contact zone. All these samples can be considered to have experienced abrasive wear by the sharp conical probe. The average wear depths are recorded in Table 3. Although DVB 20 does not undergo any wear against the Si_3N_4 probe but does suffer a lot of abrasive wear with the sharp diamond probe possibly due to high contact pressures as shown in table 4. Further, the degree of penetration, defined by the ratio of the depth of groove and the radius of contact [23], gave values less than 0.2 for all samples which indicates that dominant mechanism of abrasive wear is ploughing. The radii of curvature of the wear grooves were calculated be about 112-114 μm which is close to the radius of curvature, 100 μm, of the diamond probe.

It is well known that rubbery materials like DVB 10 consist of long flexible chain-like molecules, which are interconnected at various points by crosslinks to form loose molecular networks [24]. When stress is applied on the surface the rubbery materials tend to break the networks. DVB 15 showed the least amount of abrasive wear. From Table 1, DVB 15 also has the highest toughness (area under stress-strain curve) amongst the three. Although DVB 20 has the highest crosslinking density, its low toughness value compared to DVB 15 can be attributed to the fact that there exist nonuniform crosslinking structures in the polymer network as well as occurrence of nonuniformity in polymer composition during the synthesis [24]. For example, flakes of divinyl benzene may precipitate to the bottom before the residual solution starts to gel. Therefore the density of a polymer may be dissimilar across

the bulk, thereby resulting in varying mechanical properties. Another disadvantage is the inefficiency in divinyl benzene consumption [24]. This can lead to limited availability of the crosslinker resulting a soft, weaker region since it is the crosslinking which gives (or enhances) the material its strength.

4.5.4 Nanoscale sliding wear against a DLC coated Si probe

In order to investigate the idea of non-uniformity of polymer crosslinking and hence wear response, nanoscale wear tests were conducted. The average wear depth as a function of the normal load obtained from the nanoscale wear tests for the three samples is shown in Fig 4. The soft, rubbery sample (DVB 10) shows the greatest wear depth; followed by the sample with intermediate hardness (DVB 15) while the hard and rigid sample (DVB 20) shows the least wear depth. The trend displayed by DVB 10 is linear. The average wear depths for DVB 15 and DVB 20 progressed non linearity with load with the latter showing a sharp rise at 10 μN.

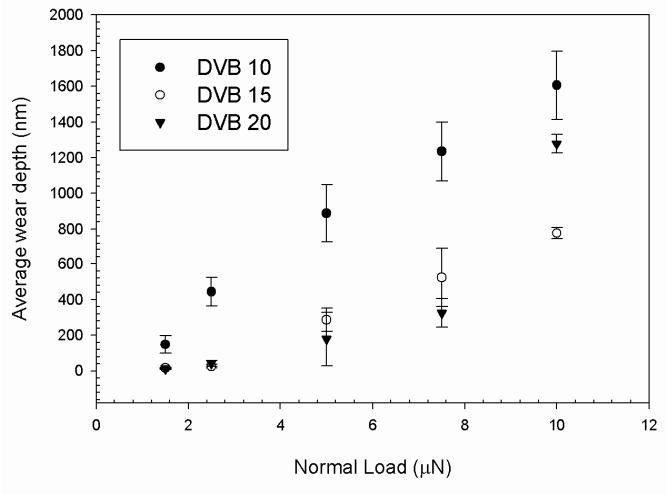

Figure 4. Wear depth plotted against five different normal loads. The average and standard deviations have been taken from five different measurements.

Three dimensional topographic images of the wear tracks are shown in Fig 5. In most cases of abrasive wear, scratching of the softer material can be observed as a groove parallel to the line of sliding. These features can be clearly seen in all samples from the images leading up to a profile depth of 1 micron. The formation of deep grooves on the surface after sufficient number of cycles indicates that the contact between tip and the surface could have become conformal [25]. Some material has been displaced on to the side of the grooves indicating that ploughing and wedge formation might have occurred. From Hertzian contact theory, the contact diameter is estimated to be at least 45–225 nm with mean pressures in the range of 113-235 MPa. Evidence of pile up on the top edge of the scratch indicate that the surface is being ploughed [26]. Repeated ploughing of the surface might have led to a low-cycle fatigue. The calculated degree of penetration falls with the range of 0.28 to 0.3 thereby indicating that cutting might have been a dominant mechanism in these nanoscale wear tests. For the two samples, DVB 15 and DVB 20, one can see that that the wear is not uniform at a load of 5 μN but this non-uniformity disappears at 10 μN load indicating that there exist a certain critical load between 5 and 10 μN beyond which the plastic deformation becomes even throughout the length of the scratch. Therefore, the observed non-uniformity in DVB 15 exists across the scales. The pressures from both the micro- and nano-scale tests have been studied and shown in table 4. The pressure required to make the wear uniform along the length of the track is much higher than the pressures from the microscale tests. The wear coefficients and wear rates listed in table 3 have been compared with those obtained from microtribometer tests.

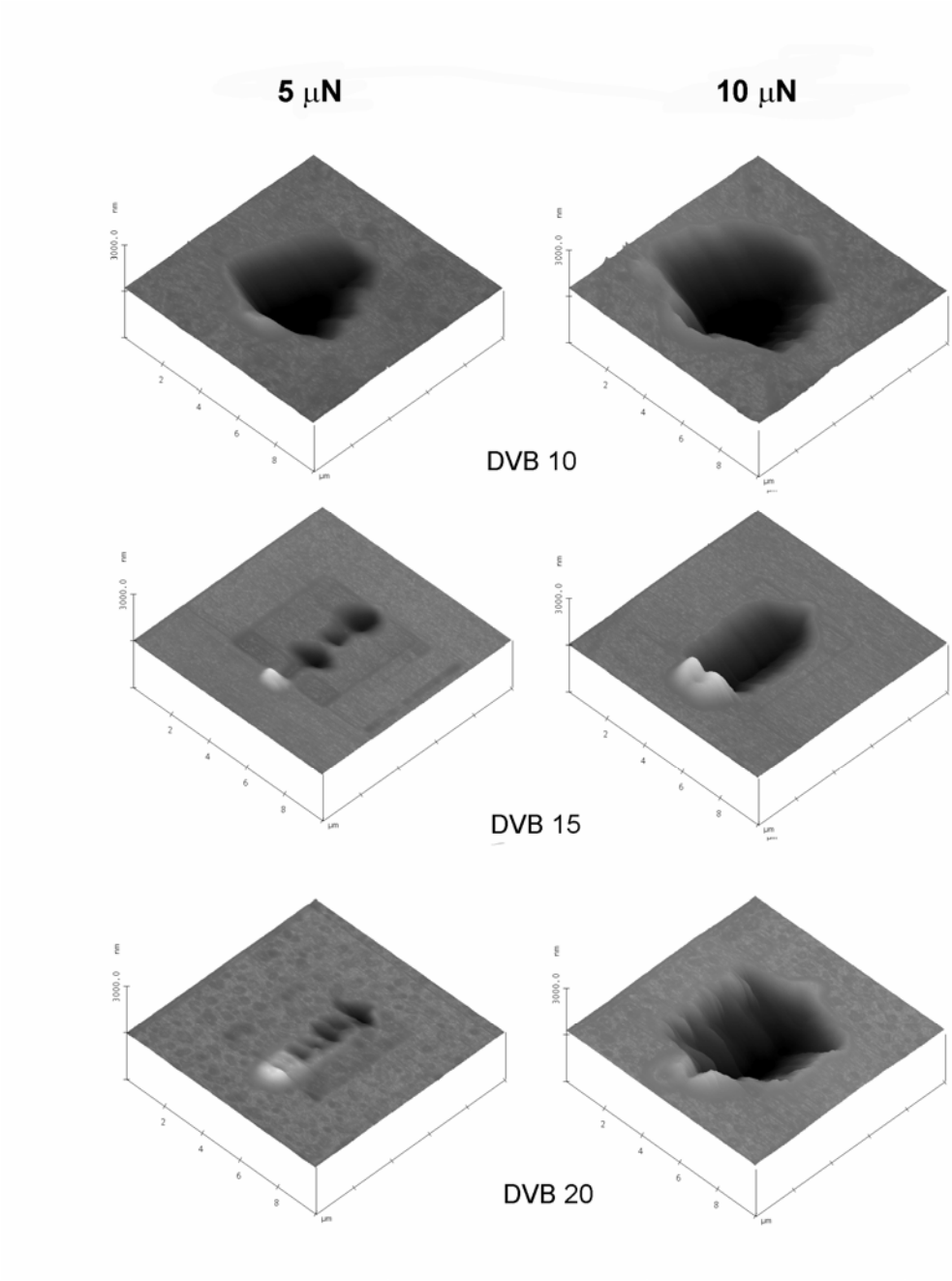

Figure 5 AFM images of the wear scratches for DVB 10, DVB 15 and DVB 20 at loads of 5 μN and 10 μN. DVB 15 and DVB 20 exhibit non-uniform wear behavior at 5 μN load but not at 10 μN load.

Table 4: Comparison of Hertzian contact pressures for microscale and nanoscale wear tests.

Sample	Mean pressure in microscale regime at 700 mN of normal force[a] (MPa)	Mean pressure in nanoscale regime at 5 μN of normal force[b] (MPa)	Mean pressure in nanoscale regime at 10 μN of normal force[b] (MPa)
DVB 10	8.53	25	31.5
DVB 15	23.2	30	37.9
DVB 20	27.6	48.8	61.5

[a] Test conducted using diamond probe of radius 100 μm
[b] Tests conducted using DLC coated AFM probe of radius 200 nm

4.6 Conclusions

Experimental data corresponding to the case of the plastic interaction with wear of a hard rigid tip of different radii with the polymer surface have been presented and elucidated. In conclusion, it was observed that the trends displayed by the polymeric materials were similar both in microscale and nanoscale studies. The material with higher crosslinking displayed more resistance to wear. Crosslinking results in strong bonding amongst polymer network and reduces the mobility of molecular chain thereby making the molecule hard and wear resisting. Non-uniformity in wear behavior for the samples with higher crosslinker concentrations was observed both in microscale and nanoscale regime. This non-uniformity is attributed to non-uniform crosslinking in the polymer network during synthesis. This irregularity in composition appears to be present at small scales on the surface. This non-uniformity in observed wear depths was found to be contact pressure dependent and invariant of the Hertzian contact scale. This non-uniformity disappears at contact pressures higher than a threshold for each of the samples.

4.7 Acknowledgement

The authors would like to thank Professor Scott Chumbley of Material Science and Engineering Department at Iowa State University (ISU) for assistance with SEM operation. We are also grateful to Jerry Amenson of Materials Analysis and Research Laboratory at ISU for the use of their Allied Sample Polisher.

4.8 References

1. R.C. Brown, *Biorenewable Resources: Engineering New Products from Agriculture*. 1st ed. 2003, Ames: Iowa State Press.
2. S. Kim and B.E. Dale, *Global potential bioethanol production from wasted crops and crop residues.* Biomass and Bioenergy, 2004. **26**(4): p. 361-375.
3. S. Kim and B. Dale, *Allocation procedure in ethanol production system from corn grain: I. system expansion.* International Journal of Life Cycle Assessment, 2002. **7**(4): p. 237–243.
4. A. Adhvaryu, S.Z. Erhan, and J.M. Perez, *Tribological studies of thermally and chemically modified vegetable oils for use as environmentally friendly lubricants.* Wear, 2004. **257**(3-4): p. 359-367.
5. S. Bhuyan, et al., *Boundary lubrication properties of lipid-based compounds evaluated using microtribological methods.* Tribology Letters, 2006. **22**(2): p. 167-172.
6. G. Biresaw, *Biobased dry-film metalworking lubricants.* Journal of Synthetic Lubrication, 2004. **21**(1): p. 43-58.

7. F. Li, M.V. Hanson, and R.C. Larock, *Soybean oil–divinylbenzene thermosetting polymers: synthesis, structure, properties and their relationships.* Polymer, 2001. **42**: p. 1567-1579.

8. S.-J. Park, et al., *Cationic polymerization and physicochemical properties of a biobased epoxy resin initiated by thermally latent catalysts.* European Polymer Journal, 2005. **41**(2): p. 231-237.

9. F. Li and R. Larock, *Synthesis, Structure and Properties of New Tung Oil-Styrene-Divinlybenzene Copolymers Prepared by Thermal Polymerization.* Biomacromolecules, 2003. **4**: p. 1018-1025.

10. S. Bhuyan, et al., *Effect of crosslinking on the friction and wear behavior of soy-bean oil-based polymeric materials.* Wear, 2007. : p. in press.

11. Y. Lu and R.C. Larock, *Novel Biobased Nanocomposites from Soybean Oil and Functionalized Organoclay.* Biomacromolecules, 2006. **7**(9): p. 2692-2700.

12. Y. Lu and R.C. Larock, *Corn oil-based composites reinforced with continuous glass fibers: Fabrication and properties.* Journal of Applied Polymer Science, 2006. **102**(4): p. 3345-3353.

13. D. Pfister, et al., *Preparation and Properties of Tung Oil-Based Composites Using Spent Germ as a Natural Filler.* Journal of Applied Polymer Science, 2008. **108**: p. 3618-3625.

14. K. Matyjaszewski, *Cationic polymerization: mechanisms, synthesis and applications*. 1996, New York: Marcel Dekker.

15. R.P.W. Jue Lu, *Novel thermosetting resins for SMC applications from linseed oil: Synthesis, characterization, and properties.* Journal of Applied Polymer Science, 2006. **99**(5): p. 2481-2488.

16. W.C. Oliver and G.M. Pharr, *An improved technique for determining hardness and elastic modulus using load and displacement sensing indentation experiments* Journal of Materials Research 1992. **7**(6): p. 1564-83.

17. J. Check, K.S.K. Karuppiah, and S. Sundararajan, *Comparison of the effect of surface roughness on the micro/nanotribological behavior of ultra-high-molecularweight polyethylene (UHMWPE) in air and bovine serum solution.* Journal of Biomedical Materials Research Part A, 2005. **74A**(4): p. 687-695.

18. B. Bhushan, *Principles and Application of Tribology*. 1999, New York: John Wiley & Sons, Inc.

19. J.E. Sader, J.W.M. Chon, and P. Mulvaney, *Calibration of rectangular atomic force microscope cantilevers.* Review of Scientific Instruments, 1999. **70**: p. 3967-3969.

20. B.J. Briscoe, L. Fiori, and E. Pelillo, *Nano-indentation of polymeric surfaces.* Journal of Physics D-Applied Physics, 1998. **31**: p. 2395-2405.

21. Y. Cheng, C. Cheng, and W. Ni, *Methods of obtaining instantaneous modulus of viscoelastic solids using displacement-controlled instrumented indentation with axisymmetric indenters of arbitrary smooth profiles.* Material Science and Engineering A-Structural Material Properties Microstructure and Processing, 2006. **423**: p. 2-7.

22. R. Berger, et al., *Nanowear on polymer films of different architecture.* Langmuir, 2007. **23**(6): p. 3150-3156.

23. K. Hokkirigawa and K. Kato, *An experimental and theoretical investigation of ploughing, cutting and wedge formation during abrasive wear.* Tribology International, 1988. **21**(1): p. 51-57.

24. F. Li and R. Larock, *New Soybean Oil-Styrene-Divinylbenzene Thermosetting Copolymers III Tensile Stress–Strain Behavior.* Journal of Polymer Science: Part B: Polymer Physics, 2001. **39**: p. 60-77.

25. A. Khurshudov and K. Kato, *Volume increase phenomena in reciprocal scratching of polycarbonate studied by atomic force microscopy.* J. Vac. Sci. Technol. B, 1995. **13**(5): p. 1938-1944.

26. C. Gibbs and J.W. Bender, *A study of the nanotribological fatigue of ultra-high molecular weight polyethylene.* Tribology Letters, 2006. **22**(1): p. 85-93.

CHAPTER 5. EFFECT OF CROSSLINKING ON TRIBOLOGICAL BEHAVIOR OF TUNG OIL-BASED POLYMERS

Modified from a paper submitted to *Tribology International*

Satyam Bhuyan, Sriram Sundararajan , Dejan Andjelkovic and Richard Larock

5.1 Abstract

In this study, the tribological properties of tung oil-based polymers synthesized by the cationic copolymerization of tung oil with divinyl benzene and styrene are evaluated as a function of crosslink density. Tribological measurements were performed using a ball-on-flat reciprocating microtribometer on samples with three crosslinking densities of 20%, 30% and 40% by weight of the crosslinking agent. Friction and wear characteristics during dry sliding was evaluated using a spherical (1.2 mm radius) silicon nitride probe as well as a conical (100 micron radius, 90° cone angle) diamond probe. Friction behavior was evaluated from single strokes at ramped normal loads, whereas wear experiments were evaluated from 100 to 500 reciprocating cycles at fixed normal loads. Elastic modulus and hardness information were evaluated using nanoindentation tests. Scanning electron microscopy of wear tracks were used to elucidate deformation mechanisms in the various samples. All samples showed friction coefficients ranging from 0.06 to 0.49. It was found that a higher crosslinking density resulted in lower abrasive wear due to increased hardness. These results provide some insight into the friction and wear behavior of tung oil-based polymers.

5.2 Introduction

In the past few decades there has been an awareness and concern over the usage of petroleum-based products and their influence on the environment. This has created an opportunity for scientists and researchers to produce environmentally acceptable materials from agricultural feedstock. The benefits of using environmental friendly products include reducing pollution, minimal health and safety risks and easier disposal due to their superficial biodegradability. The benefits of using agricultural feedstock as sources for engineering materials include taking advantage of excess agricultural production, the potential for rural development and minimizing the nation's dependency on foreign sources of oil [1]. Research is being conducted on developing a variety of biobased products including transportation fuels [2, 3], lubricants [4-6], polymers [7-11] and polymeric composites[12-14].

A variety of novel polymeric materials ranging from elastomers to tough, rigid plastics can be prepared by the cationic copolymerization of natural oils and its conjugates [15, 16]. These polymers exhibit mechanical properties that are competitive with commercial unsaturated polyesters [17]. The advantages of these polymer materials are their low cost, availability from a renewable natural source, and their presumed ability to biodegrade in an environmentally compassionate manner after service. Extensive characterization of mechanical and interfacial properties of these materials are needed to evaluate their potential in replacing existing petroleum-based products for engineering and structural applications.

Tung oil is biodegradable oil which is readily available as a major product from the seeds of a tung tree [18]. Its principal constituent is a glyceride of elaeostearic acid, a conjugated triene. This highly unsaturated, conjugated system makes it largely responsible for the rapid polymerization in to useful new materials [19]. Due to the conjugated C=C double

bonds in tung oil, it is expected to undergo facile cationic polymerization [20, 21]. Past studies by Li and Larock have shown that the cationic polymerization of tung oil with aromatic comonomers like styrene and divinyl benzene initiated by borontriflouride diethyl etherate have resulted in a variety of yellow, transparent polymeric materials ranging from rubbery elastomers to tough and rigid plastics by varying the stoichoiometry and other parameters [9, 10].

In this paper, the tribological (friction and wear) properties of these tung oil-based polymeric materials are evaluated as a function of the crosslinking density of the polymers. Crosslinking increases the tightness of the polymer network and reduces the molecular mobility of chains between the junctions. As a result, the number of conformations that a polymer can adopt decreases as the crosslink density increases [22]. Thus, crosslinking increases the stiffness of the polymers, which should in turn affect the tribological properties. Mechanisms of wear and correlations between material composition and wear behavior are identified and discussed.

5.3 Materials

The tung oil was commercially available in the markets. The oil was used without further purification. The materials synthesis procedure is briefly described here and can be found in extensive detail elsewhere [10]. The tung oil (TUN) was subjected to cationic polymerization with styrene (ST) and divinyl benzene (DVB). This process yields viable polymers ranging from soft rubbers to hard, tough, or brittle plastics by varying oil content, crossliking density and other parameters. For this study, three materials were prepared with 50% (w/w) oil content and crosslinking agent (divinyl benzene) concentrations of 20%, 30%

and 40% by weight. The concentration of (ST+DVB) was kept constant at 50%. Throughout the manuscript, these materials will be referred to as DVB 20, DVB 30 and DVB 40. Prior to tribological measurements, the RMS roughness of all samples was characterized using an atomic force microscope (AFM, Dimension 3100, Nanoscope IV, Veeco Instruments, Santa Barbara, California). Table 1 lists the basic material properties and the surface roughness data of the samples under study. All materials were brittle in nature. This is reflected by the compressive strength data in Table 1.

5.4 Methods

5.4.1 Nanoindentation tests

Nanoindentation test were performed on the polymer samples with a Berkovich indenter using a Hysitron Triboscope (Hysitron Inc., Minneapolis, Minnesota, USA) in conjunction with an Atomic Force Microcope (NanoScope Dimension^{TM} 3100, Digital Instruments, Veeco Metrology Group). Two different loading profiles were used for the test. One was a trapezoidal loading profile with a peak indentation force of 25 μN (loading time 2.5 seconds, holding time 1 second, and unloading time 0.5 second, respectively). The other was a partial loading and unloading profile with an equal loading and unloading rate of 10 μN/s and 10 different peak indentation loads ranged from 5 to 50 μN. At each peak load, appropriate holding time was assigned. During indentation test, the sample was hold firmly by the vacuum chuck of AFM. The mechanical properties namely hardness and elastic modulus were analyzed using Oliver and Pharr method [23].

Table 1: Material properties of the samples used in the study.

Sample	Glass transition temperature[a] (T_g)	Crosslinking density[a] (moles/m^3)	Compressive strength[a] (MPa)	RMS Roughness[b] (nm)
DVB 20	77	3.5×10^3	44	10.6 ± 0.6
DVB 30	82	6.1×10^3	89	10.4 ± 0.2
DVB 40	71	17×10^3	110	11.6 ± 0.7

[a] Values taken from Ref. [10]
[b] Measured using AFM at 15 μm X 15 μm scan size.

5.4.2 Microscale friction and wear tests

For the experiments described in this paper, a custom-built reciprocating ball-on-flat microtribometer that can produce a microscale (apparent area ~1000 square microns) multi-asperity contact was used [24]. A schematic of its major components is shown in Fig. 1. A desired probe of specific radius is placed at the end of a crossed I-beam structure which is lowered using a linear stage to apply a desired normal load to the sample. The normal and friction (lateral) forces are measured using semiconductor strain gages on the cantilevers. Friction forces can be resolved to approximately ±5 μN and normal forces to approximately ±15 μN. The signal from the normal load is monitored and used in a simple proportional-integral (PI) feedback loop to maintain the desired normal force regardless of any slope or waviness in the surface of the sample. The desired sample is affixed to another stage set perpendicular to the beam, which provides linear motion.

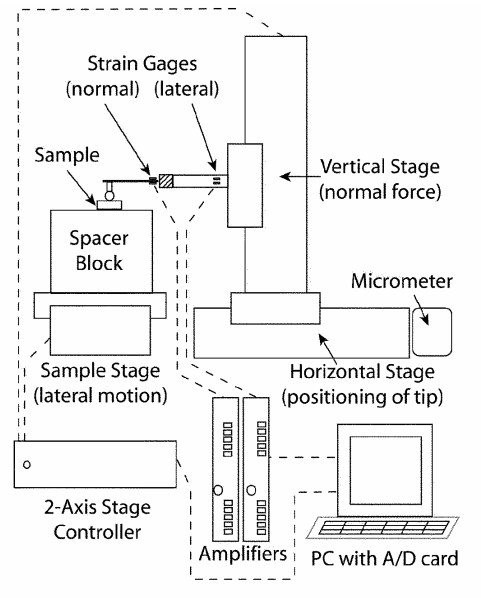

Figure 1. Schematic of the microtribometer set up used for friction and wear tests.

To obtain the coefficient of friction, ramped load tests were performed in which the normal load between a silicon nitride (Si_3N_4) ball (radius - 1.2 mm, RMS roughness - 4 nm, scan size 15 μm X 15 μm) and the sample was increased linearly with the sliding distance while the friction force was monitored. The load was increased from 0.2 to 200 mN as the probe was moved across a stroke distance of 50 mm at 1 mm/s. Preliminary tests showed that, for our load conditions, sliding speed had negligible effect on friction and wear relative to other factors. A set of four ramped load tests were performed on each batch to obtain an average value of the friction coefficient.

A 500 cycle reciprocating sliding wear test was performed against the Si_3N_4 probe at a constant load of 800 mN and a stroke speed of 5 mm/s for a total sliding distance of 30 m. A preliminary scratch response study of the materials was performed in order to evaluate normal loads to be used for sliding wear tests using a conical (100 micron radius, 90° cone

angle) diamond probe. Consequently, a 100 cycle reciprocating test with the diamond probe was then carried out at 800 mN at 5mm/s. All tests were performed at 23 $^{\circ}$C and 30±2 % relative humidity. Wear track profiling was carried out using a contact profilometer (Dektak II). A JOEL JSM-6060LV Scanning Electron Microscope (SEM) was used to obtain high resolution images of the wear tracks. These polymeric samples were coated with gold before performing electron microscopy.

5.5 Results and Discussion

5.5.1 Nanoindentation tests

Figure 2a shows the typical load-penetration depth curves of nanoindentations on the three polymer samples with trapezoidal loading profile. The maximum load for indentation did not reached the peak load intended to apply due to the significant creep of the materials. For accurate determination of mechanical properties of polymeric and viscoelastic materials using nanoindentation test, the creep effect, which often results in bulging "nose" in the unloading curve, must be accounted for before applying Oliver and Pharr method. This can be done by either introducing a sufficiently long holding segment [25] or using a sufficiently fast unloading rate [26]. In this study, both appropriate holding segment and fast unloading rate have been employed to reduce creep effect on the measured mechanical properties. At the end of unloading, indentation force dropped below zero, which may indicate adhesion between indenter and the tested polymer materials. The average elastic modulus and hardness of five indentations for all polymers are reported in Table 2. It must be noted that these values may not represent the "true" properties of the materials since the Oliver-Pharr analysis assumes no creep. However, they are used for relative comparisons in this study.

Nanoindentation test shows that polymer DVB 40 has the highest elastic modulus and hardness while DVB 20 has the lowest elastic modulus and hardness.

Figure 2b shows the typical load-penetration depth curves of nanoindentations with partial loading and unloading profile. The elastic modulus and hardness are determined from the partial unloading curves at different peak loads. The variations of average elastic modulus and hardness with the average indentation contact depth of five indentations for all materials are plotted in Fig. 3. Both elastic modulus and hardness for all the polymers decrease with the increase of contact depth. Partial loading and unloading tests shows a similar trend that elastic modulus and hardness of DVB 40 are much higher than those of DVB 20 and DVB 30. From the data, one can see a correlation of the observed elastic modulus and hardness with crosslinking density. Both, elastic modulus and hardness increases with crosslinking density.

Table 2: Average elastic modulus and hardness of tung oil-based polymers taken from five indentations.

Materials	Young's Modulus (GPa)	Hardness (GPa)
DVB 20	0.658 ± 0.009	0.071 ± 0.001
DVB 30	0.947 ± 0.013	0.091 ± 0.002
DVB 40	1.373 ± 0.020	0.158 ± 0.003

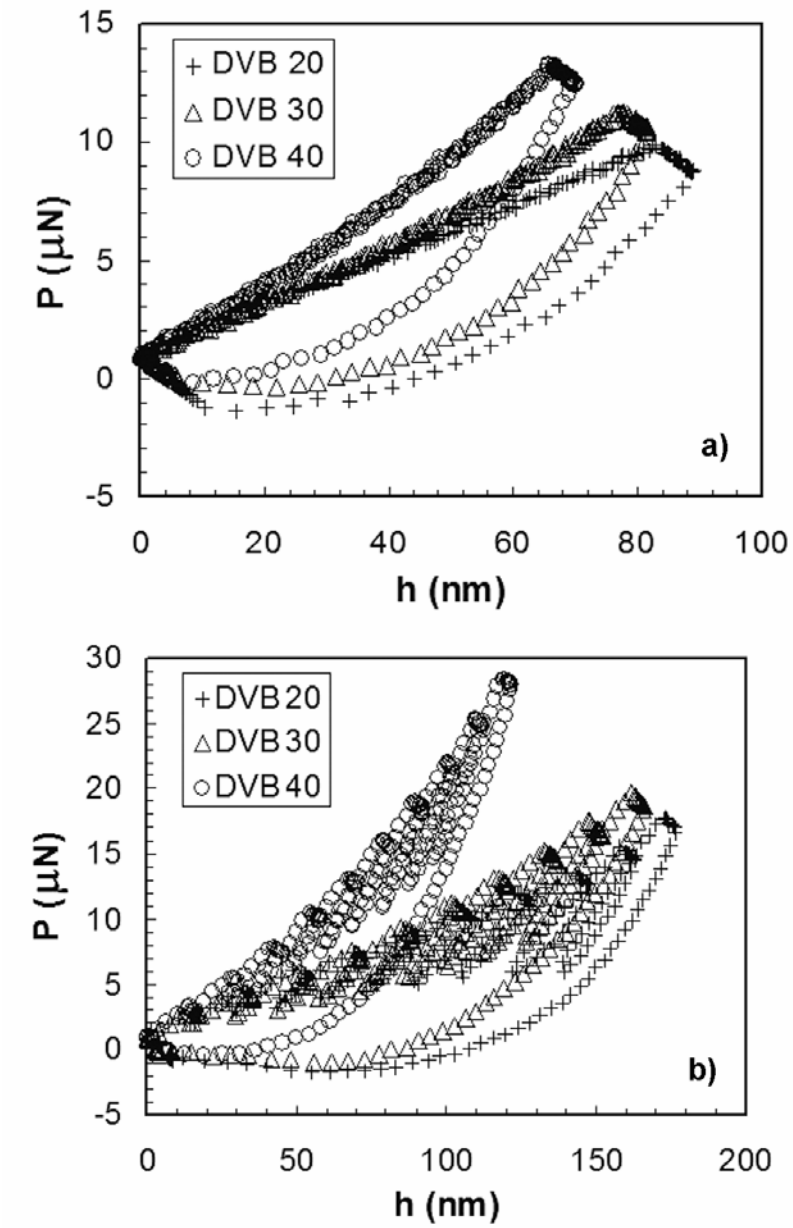

Figure 2. Load penetration depth curves of nanoindentations on the three samples with a) trapezoidal loading profile and b) partial loading and unloading profile.

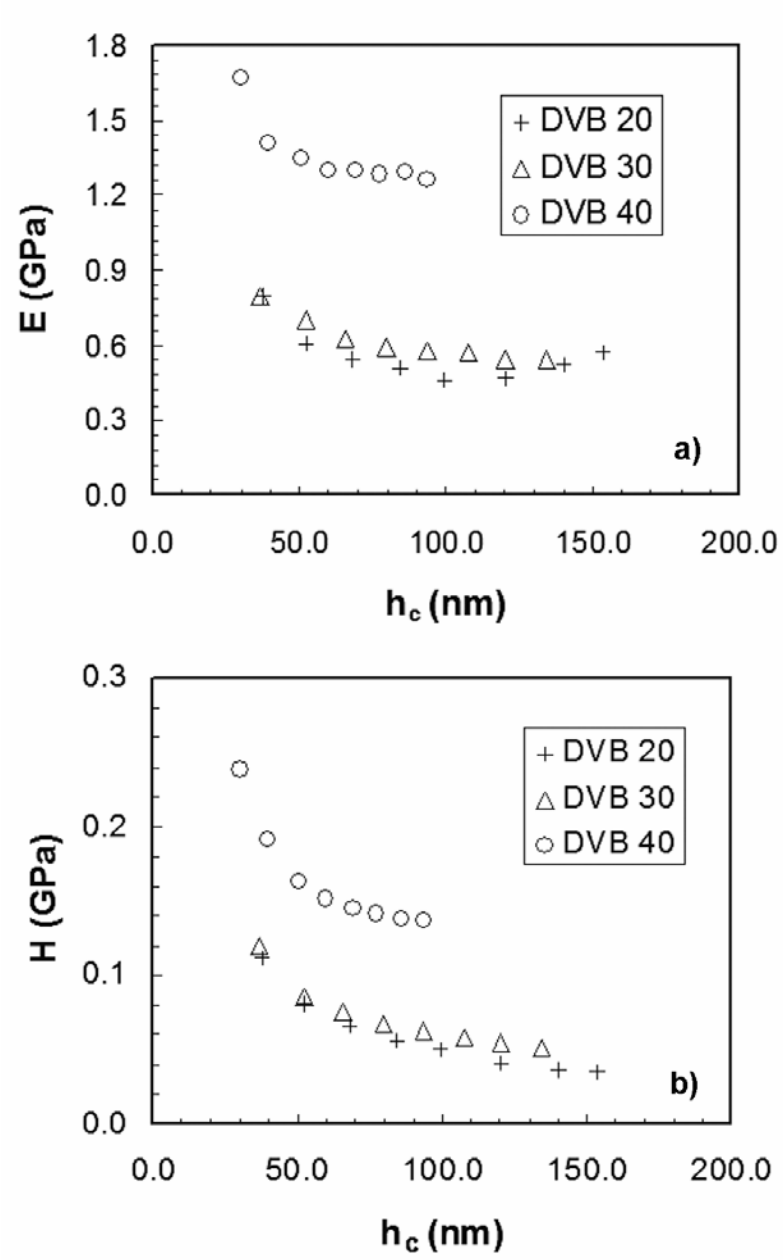

Figure 3. Variations of average (a) elastic modulus and (b) hardness with the average indentation contact depth of five indentations for all three samples.

5.5.2 Microscale friction and wear tests with Si_3N_4 probe

The results from the microscale friction experiments are shown in Fig. 4. Selected friction traces of dry sliding during microscale friction tests against Si_3N_4 ball are shown in Fig. 4a. The materials generated a fairly smooth friction trace probably due to its self-lubricating nature. It has been found out through Soxhlet extraction and proton-NMR studies that the structure of the bulk polymer is that of crosslinked polymer network plasticized by a certain amount of unreacted free oil [9]. The sudden drop in friction force (indicated by X in Fig. 4a) may be due to oil seeping out of the surface. Figure 4b is a bar chart representation of the coefficient of friction. The polymeric material and the ceramic probe produced friction coefficients in the range of 0.06-0.49. It can be seen that the coefficient of friction increases with DVB concentration, and hence, the crosslinking density.

A sample friction test on the softer DVB 20 sample up to 1 N load did not exhibit any observable evidence of damage on the surface. Consequently, a normal load of 800 mN was chosen for constant load reciprocating wear tests. Even after 500 cycles of loading with Si_3N_4 probe there was still no evidence of damage on the surface. Calculated mean Hertzian contact pressures [27] ranged from 26.3 to 42.8 MPa for the various samples.

5.5.3 Microscale friction and wear tests with diamond probe

The results from the microscale friction test using the conical diamond probe are shown in Fig. 5. The figure plots the friction force as a function of increasing normal load as well as the sliding distance. The friction data appears to exhibit an increase in slope at higher normal loads. Such an increase is typically associated with onset of additional energy

dissipative mechanisms including increased damage. However, no damage was observed on the samples.

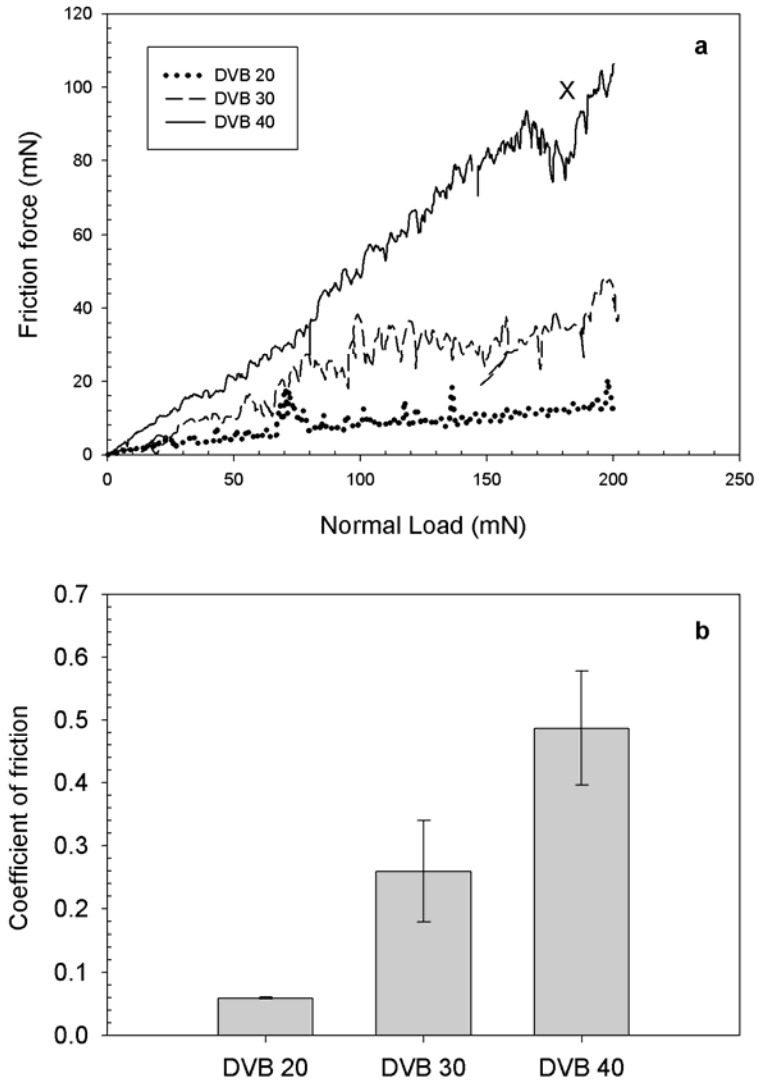

Figure 4. (a) Friction force vs. normal load plots obtained from friction tests for DVB 20, DVB 30 and DVB 40 using a spherical Si_3N_4 probe. A sudden drop in friction force was observed (indicated by X). (b) Coefficient of friction ± standard deviation using bar diagram.

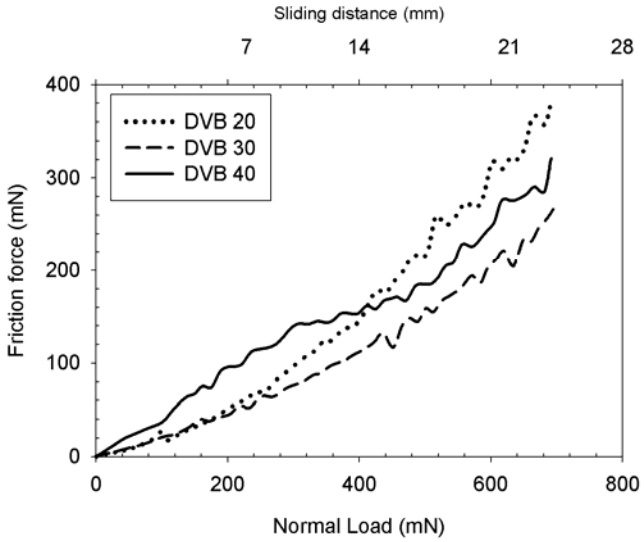

Figure 5. Friction force vs. normal load plots obtained from friction tests for DVB 20, DVB 30 and DVB 40 using a spherical conical diamond probe.

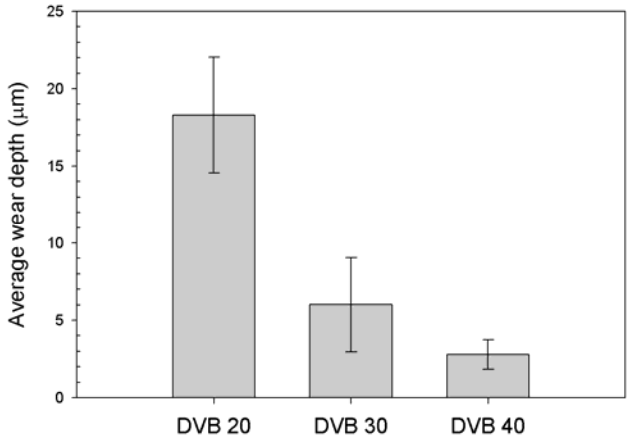

Figure 6. Plots of the average wear depth of with increasing concentrations of DVB. The average and standard deviation have been taken from a set of three tests.

When reciprocating tests were done with the sharp diamond probe at 800 mN normal load, damage was seen. Under these conditions the contact pressures ranged from 138 to 225 MPa for the various samples. The wear depth was quantified and average wear depths with

increasing DVB concentrations are shown and compared in Fig. 6. From the data one can see that DVB 40 shows the least wear depth of 2.79 μm followed by DVB 30 whose wear depth is 6μm, and finally, DVB 20 with an average wear depth of 18.3 μm. Thus the wear behavior against a diamond probe improves with increasing crosslinking density.

SEM images of the wear tracks generated by tests with diamond probe are shown in Figs. 7 and 8; the latter being at higher magnification. It can be clearly seen that all samples exhibit grooves as well as presence of abraded material debris and some cracking along the groove edges. Abrasive wear is manifested by the cutting or ploughing of the surface by the harder material [28]. In these experiments, a sharp diamond probe was used. The abraded particles are either embedded in the counterface or get loose within the contact zone. All these samples can be considered to have experienced abrasive wear by the conical diamond probe. Further, the degree of penetration, defined by the ratio of the depth of groove and the radius of contact [29], gave values less than 0.2 for all samples which indicates that dominant mechanism of abrasive wear is ploughing.

The observed wear behavior of polymeric materials against the diamond probe is consistant with Archard's wear equation for abrasive wear [30]. According to this theory, the wear volume is inversely proportional to hardness of the material. The hardness increased with crosslinking density for the samples studied. As a result, DVB 40 with the highest hardness is more resistant to wear than DVB 20 and DVB 30. A similar trend can be observed for elastic modulus as well. DVB 20 with the lowest elastic modulus showed the highest abrasive wear depth.

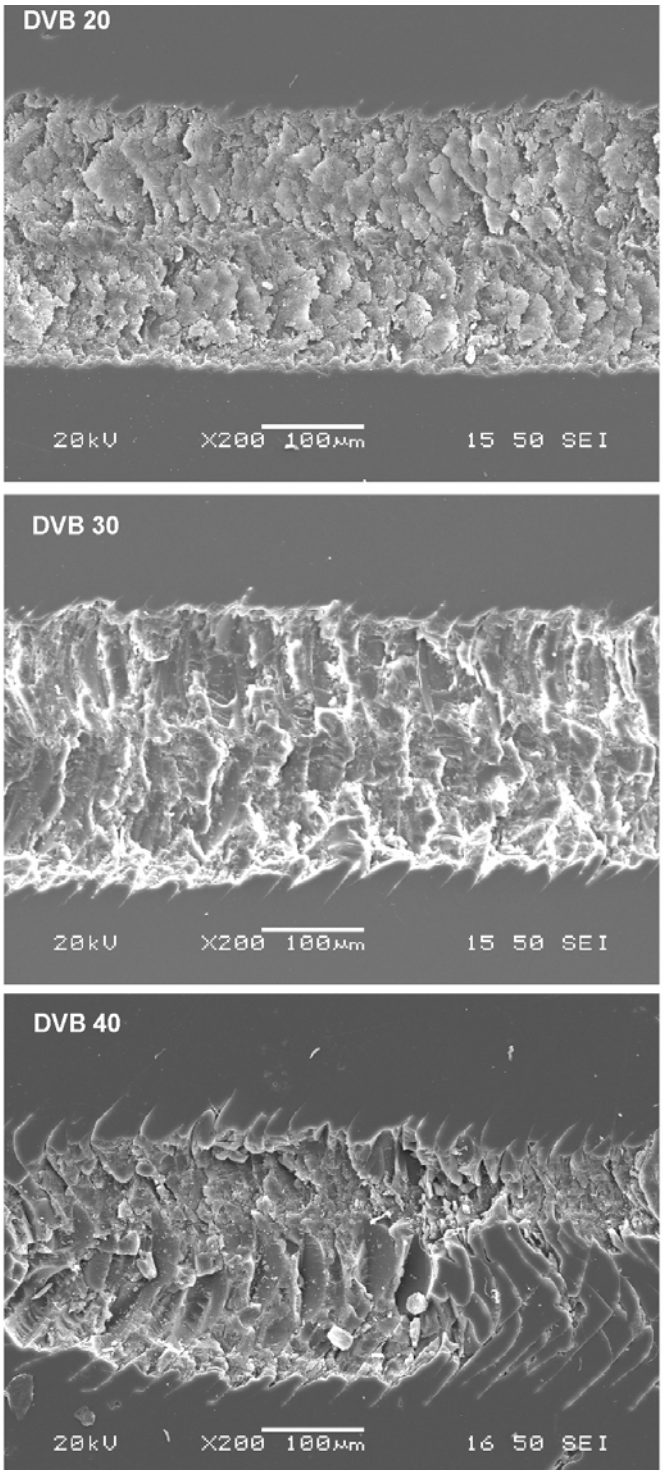

Figure 7. Scanning electron microscope (SEM) images of the abrasive wear track on DVB 20, DVB 30 and DVB 40. Formation of cracks on all the three samples can be clearly seen.

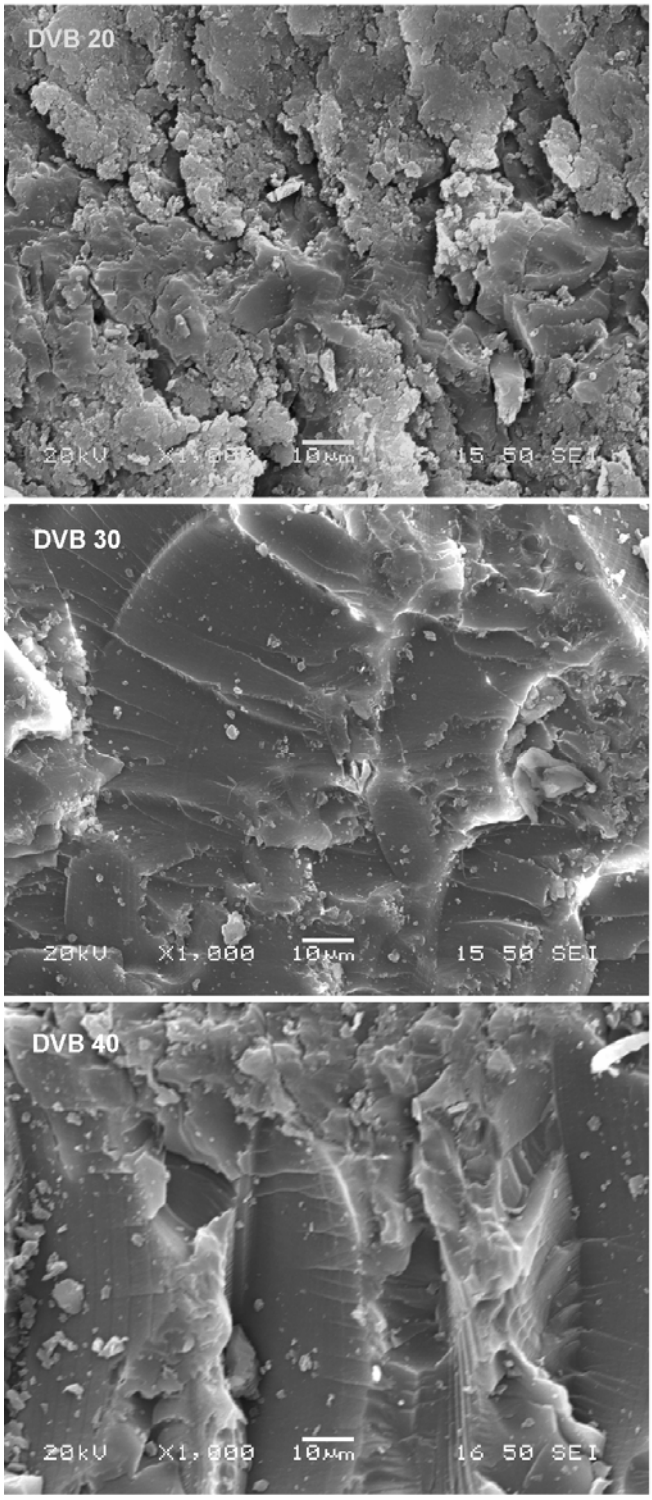

Figure 8. Higher magnification SEM images of abrasive wear tracks indicating that the dominant mechanism of wear in these polymeric materials is abrasive in nature.

5.6 Conclusions

The tribological properties of novel tung oil-based polymeric materials as a function of crosslinking density (20%, 30% and 40% of crosslinking agent DVB concentration by weight) were evaluated. Nanoindentation tests have shown that the material with highest crosslinking density resulted in higher elastic modulus and hardness. When compared with DVB 40 the coefficients of friction of DVB 20 and DVB 30 against a spherical Si_3N_4 probe were 87.8% and 46.8% lower respectively. In sliding wear tests against the Si_3N_4, all samples showed negligible wear even after 500 cycles of sliding. An increase in crosslinking density resulted in better wear performance against the conical diamond probe. DVB 20 showed the highest wear depth of 18.3 μm followed by DVB 30 (67.2% lower than DVB 20) and DVB 40 (84.8% lower than DVB 20). All samples exhibited abrasive wear as indicated by high magnification SEM images. Based on these studies, these novel biobased materials show promising tribological properties.

5.7 Acknowledgement

The authors would like to thank Professor Scott Chumbley of Material Science and Engineering department at Iowa State University for assistance with SEM operation. We are also grateful to Zhi-Hui Xu and Xiaodong Li from University of Southern Carolina for their help with the nanoindentation tests. This work was partially supported by seed funding from Plant Science Institute at Iowa State University.

5.8 References

1. Brown RC. Biorenewable Resources: Engineering New Products from Agriculture. 1st ed. Ames: Iowa State Press, 2003.
2. Kim S and Dale BE. Global potential bioethanol production from wasted crops and crop residues. Biomass and Bioenergy 2004;26(4):361-375.
3. Kim S and Dale B. Allocation procedure in ethanol production system from corn grain: I. system expansion. International Journal of Life Cycle Assessment 2002;7(4):237–243.
4. Adhvaryu A, Erhan SZ and Perez JM. Tribological studies of thermally and chemically modified vegetable oils for use as environmentally friendly lubricants. Wear 2004;257(3-4):359-367.
5. Bhuyan S, Sundararajan S, Yao L, Hammond EG and Wang T. Boundary lubrication properties of lipid-based compounds evaluated using microtribological methods. Tribology Letters 2006;22(2):167-172.
6. Biresaw G. Biobased dry-film metalworking lubricants. Journal of Synthetic Lubrication 2004;21(1):43-58.
7. Li F, Hanson MV and Larock RC. Soybean oil–divinylbenzene thermosetting polymers: synthesis, structure, properties and their relationships. Polymer 2001;42:1567-1579.
8. Li FK, Hasjim J and Larock RC. Synthesis, structure, and thermophysical and mechanical properties of new polymers prepared by the cationic copolymerization of

corn oil, styrene, and divinylbenzene. Journal of Applied Polymer Science 2003;90(7):1830-1838.

9. Li F and Larock RC. Thermosetting polymers from cationic copolymerization of tung oil: Synthesis and characterization. Journal of Applied Polymer Science 2000;78(5):1044-1056.

10. Li F and Larock R. Synthesis, Structure and Properties of New Tung Oil-Styrene-Divinlybenzene Copolymers Prepared by Thermal Polymerization. Biomacromolecules 2003;4:1018-1025.

11. Park S-J, Jin F-L, Lee J-R and Shin J-S. Cationic polymerization and physicochemical properties of a biobased epoxy resin initiated by thermally latent catalysts. European Polymer Journal 2005;41(2):231-237.

12. Lu Y and Larock RC. Corn oil-based composites reinforced with continuous glass fibers: Fabrication and properties. Journal of Applied Polymer Science 2006;102(4):3345-3353.

13. Lu Y and Larock RC. Novel Biobased Nanocomposites from Soybean Oil and Functionalized Organoclay. Biomacromolecules 2006;7(9):2692-2700.

14. Pfister D, Baker JR, Henna PH, Lu Y and Larock RC. Preparation and Properties of Tung Oil-Based Composites Using Spent Germ as a Natural Filler. Journal of Applied Polymer Science 2008;108:3618-3625.

15. Andjelkovic DD, Li FK and Larock RC. Novel polymeric materials from soybean oils - synthesis, properties, and potential applications. Bozell JJ and Patel MK, editors. Feedstocks for the Future: Renewables for the Production of Chemicals and Materials, 2006.

16. Li F and Larock RC. Synthesis, Properties, and Potential Applications of Novel Thermosetting Biopolymers from Soybean and Other Natural Oils. Mohanty AK, Misra M and Druzal LT, editors. Natural Fibers, Biopolymers and Biocomposites, 2005.

17. Lu J and Wool RP. Novel thermosetting resins for SMC applications from linseed oil: Synthesis, characterization, and properties. Journal of Applied Polymer Science 2006;99(5):2481-2488.

18. Wood EC. Tung Oil: A new American Industry, 1949.

19. Kinabrew RG. Tung Oil in Mississippi, The Competitive Position of the Industry. MS: University of Mississippi, 1952.

20. Matyjaszewski K. Carbocationic Polymerizations: Mechanisms, Synthesis and Applications. New York: Marcel Dekker, 1996.

21. Kennedy JP and Marechal E. Carbocationic Polymerizations. New York: Wiley, 1982.

22. Li F and Larock R. New Soybean Oil-Styrene-Divinylbenzene Thermosetting Copolymers III Tensile Stress–Strain Behavior. Journal of Polymer Science: Part B: Polymer Physics 2001;39:60-77.

23. Oliver WC and Pharr GM. An improved technique for determining hardness and elastic modulus using load and displacement sensing indentation experiments Journal of Materials Research 1992;7(6):1564-83.

24. Check J, Karuppiah KSK and Sundararajan S. Comparison of the effect of surface roughness on the micro/nanotribological behavior of ultra-high-molecularweight polyethylene (UHMWPE) in air and bovine serum solution. Journal of Biomedical Materials Research Part A 2005;74A(4).

25. Briscoe BJ, Fiori L and Pelillo E. Nano-indentation of polymeric surfaces. Journal of Physics D-Applied Physics 1998;31:2395-2405.

26. Cheng Y, Cheng C and Ni W. Methods of obtaining instantaneous modulus of viscoelastic solids using displacement-controlled instrumented indentation with axisymmetric indenters of arbitrary smooth profiles. Material Science and Engineering A-Structural Material Properties Microstructure and Processing 2006;423:2-7.

27. Bhushan B. Principles and Application of Tribology. New York: John Wiley & Sons, Inc., 1999.

28. Friedrich K. Friction and Wear of Polymer Composites. Pipes RB, editor. Composite materials Series Vol 1. Amsterdam: Elsevier, 1986.

29. Hokkirigawa K and Kato K. An experimental and theoretical investigation of ploughing, cutting and wedge formation during abrasive wear. Tribology International 1988;21(1):51-57.

30. Archard JF. Contact and Rubbing of Flat Surfaces. J. Appl. Phys. 1953;24:981-988.

CHAPTER 6. A STUDY OF THE PHYSICAL AND TRIBOLOGICAL PROPERTIES OF BIOBASED POLYMER-CLAY NANOCOMPOSITES AT DIFFERENT CLAY CONCENTRATIONS

Modified from a paper submitted to *Wear*

Satyam Bhuyan, Sriram Sundararajan, Yongshang Lu and Richard Larock

6.1 Abstract

Novel biobased nanocomposites have been prepared by the cationic copolymerization of conjugated low saturated soybean oil with styrene and divinlybenzene, and a reactive organomodified montmorillonite (VMMT) clay as reinforcing phase. Microscale tribological measurements were performed on samples with different concentration of VMMT (0%, 1% and 5 % by weight) using a ball-on-flat reciprocating microtribometer. Friction and wear behavior during dry sliding was evaluated using spherical (1.2 mm radius) steel probe as well as a conical (100 μm radius, 90 degree cone angle) diamond probe. Friction behavior was evaluated from single strokes at ramped normal loads, whereas wear experiments were evaluated from 10 to 1000 reciprocating cycles at fixed normal loads. Contact profilometry and scanning electron microscopy of wear tracks were used to elucidate deformation mechanisms in the various samples.

6.2 Introduction

In the past few decades the awareness and concern over the usage of petroleum-based products and their impact on the environment has created an opportunity and thrust to

produce environmentally acceptable materials from biobased feedstock. The benefits of using biobased feedstock as sources for engineering materials includes taking advantage of excess agricultural production, the potential for rural development and minimizing the nation's dependency on petroleum [1]. Research has been conducted on developing a variety of biobased products including transportation fuels [2, 3], lubricants [4-6], polymers [7-10] and polymer composites [11-13]. Soybean oil is a biodegradable oil and readily available in bulk from a renewable natural resource. The carbon-carbon double bonds are conjugated in the low saturated soybean oil to give rise to conjugated low saturated soybean oil (CLS) , which imparts a higher reactivity than the regular soybean oil and which in turn results in polymers with much improved properties [7].

Polymer-clay nanocomposites have attracted increasing attention from science and industry [14]. Compared with conventional composites with higher filler concentrations, nanocomposites often exhibit a great improvement in modulus [15-18] creep resistance [19] and strength [20, 21] at very low clay contents of generally less than 5% by weight. The enhancement of material properties can be attributed to the fact that there exist strong interfacial interactions between the polymer matrix and the layered silicate [22]. Montmorillonite (MMT), by far, is the most commonly used clay for the preparation of polymer-clay nanocomposites. The crystal structure consists of a layered clay mineral with a central alumina octahedral sheet sandwiched between two silica tetrahedral sheets [23]. Apart from enhancing the material strength of polymers, nanoparticle fillers have dramatically improved in the reduction in the wear rate of the polymer matrix at very low loadings [24]. Because nanoparticles are of the same size scale as counterface asperities, they may polish

the highest asperities and develop tribologically favorable transfer films. Once formed, the transfer films shield the composite from direct asperity contact and damage [25].

Within the past decade there have been a number of studies conducted to investigate the role of nanoparticles in tribological performance of polymer nanocomposites. For example, Xue *etal* [26] looked directly at the effects of particle size and morphology on the tribological behavior of the composite. They found that the nanoparticles effectively reduced the wear rate of high performance engineering polymeric materials like PEEK (polyetheretherketone) by 44% and a reduction in friction coefficient of 50%. Sawyer *etal* [27] reported favorable tribological properties of alumina-PTFE nanocomposites. They varied the loading of 38 nm alumina from 0.02–10%. With as little as 0.02% loading, a two times increase in wear resistance was detected.

This paper explores the friction and wear characteristics of the novel biobased nanocomposites prepared by the cationic polymerization of conjugated low saturated soybean oil (CLS) with styrene (ST) and divinlybenzene (DVB) in the presence of an organoclay and modified boron triflouride diethyl etherate (BFE) as the catalyst. The organoclay used in this work, Montmorillonite (MMT), was modified with (4-vinylbenzyl)triethylammonium chloride (VTAC), so that the resultant organoclay (VMMT) can be polymerized into the polymer matrix through chemical bonding, leading to a significant performance improvement in thermal stability and compressive strength for the resulting nanocomposites when compared with the corresponding pure polymers [12].

6.3 Materials

The natural oil used to prepare the materials in this study was food-grade low-saturation soybean oil commercially available in the supermarkets. The oil was used without further purification. The materials synthesis procedure is briefly described here and can be found in extensive detail elsewhere [12]. A desired amount of VMMT was dispersed into the mixture consisting of 50 g CLS, 25 g of ST and 10 g of DVB. The resulting mixture was vigorously stirred for 24 h, followed by sonication for 4 h at room temperature. Then, 15 g of the modified BFE initiator, prepared by mixing the Norway fish oil ethyl ester (NFO) with BFE in a 2:1 weight ratio, was added. By changing the VMMT concentration of 0, 1 and 5 wt %, a series of nanocomposites were prepared in which the VMMT is expressed as a percent of the total weight. For the purpose of nomenclature we label them as clay 0, clay 1 and clay 5 respectively. All samples were prepared in three batches. The compressive mechanical properties have been shown in table 1.

Table 1: Compressive mechanical properties of biobased nanocomposites[a].

Sample	Compressive modulus (MPa)	Compressive strength (MPa)	Compressive strain at failure (%)
Clay 0%	260	25	57
Clay 1%	592	48	64
Clay 5%	340	35	60

[a] Values taken from Ref. [12]

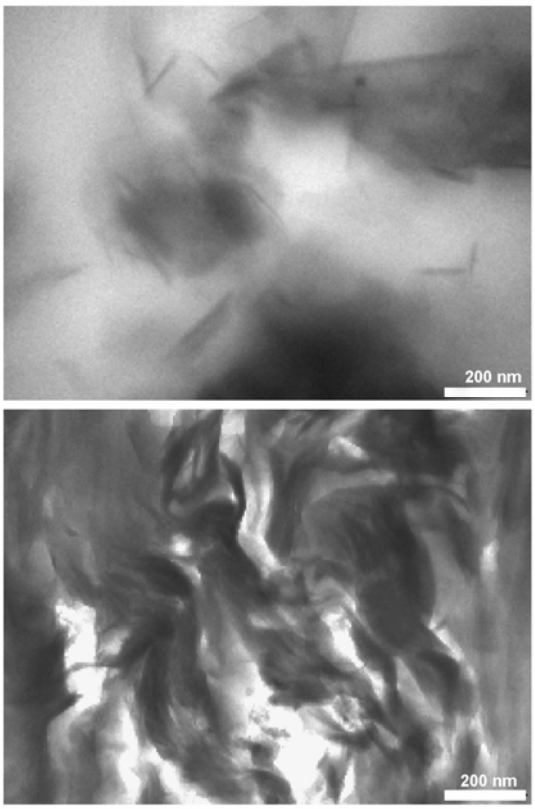

Figure 1. TEM images of nanocomposites with 1% and 5% wt of VMMT

The samples were molded in vials from which a rectangular-shaped cross section was cut out using a band saw. The shear marks on the surface were sanded later to maintain a similar roughness across the samples. Roughness measurements over a scan area of 50 μm x 50 μm obtained using atomic force microscopy yielded values of 600-900 nm (RMS) for the samples. All samples have been prepared in three batches at each clay concentration. TEM images (Fig.1) of clay 1 and clay 5 show that these materials have intercalated structures, in which the dispersed phase between the layers of the silicates is on a nanometer-length scale and hence, they can be classified as nanocomposites.

6.4 Methods

6.4.1 Microscale Friction and Wear Tests

For the experiments described in this paper, a custom-built reciprocating ball-on-flat microtribometer that can produce a microscale (apparent area ~1000 square microns) multi-asperity contact was used [28]. A schematic of its major components is shown in Fig. 2. A probe with a specific radius is placed at the end of a crossed I-beam structure which is lowered using a linear stage to apply a desired normal load to the sample. The normal and friction (lateral) forces are measured using semiconductor strain gages on the cantilevers. Friction forces can be resolved to approximately ±5 μN and normal forces to approximately ±15 μN. The signal from the normal load is monitored and used in a simple proportional-integral (PI) feedback loop to maintain the desired normal force regardless of any slope or waviness in the surface of the sample. The desired sample is affixed to another stage set perpendicular to the beam, which provides linear motion.

To obtain the coefficient of friction, ramped load tests were performed in which the normal load between a steel ball (radius - 1.2 mm, RMS roughness - 8 nm, scan size 15 μm X 15 μm) and the sample was increased linearly with the sliding distance while the friction force was monitored. The load was increased from 0.2 to 800 mN as the probe was moved across a stroke distance of 40 mm at 5 mm/s. Preliminary tests showed that, for our load conditions, sliding speed had negligible effect on friction and wear relative to other factors. A set of four tests were performed on each batch to obtain an average value of the friction coefficient.

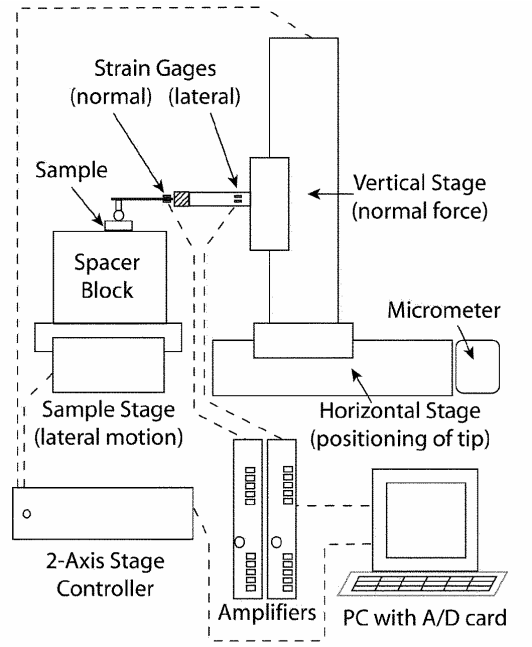

Figure 2. Schematic of the reciprocating microtribometer used for friction and wear tests

A 1000 cycle reciprocating sliding wear test was performed against the steel probe at a constant load of 500 mN and a stroke speed of 5 mm/s for a total sliding distance of 60 m. A preliminary scratch response study of the materials was performed in order to evaluate normal loads to be used for sliding wear tests using a conical (100 micron radius, 90° cone angle) diamond probe. A 10 cycle reciprocating test with the diamond probe was then carried out at 300 mN at 5mm/s. All tests were performed at 28 $^{\circ}$C and 30 ± 3 % relative humidity. All reciprocating wear tests were repeated twice on each batch of the samples. Wear track profiling was carried out using a contact profilometer (Dektak II). The average wear depth reported in this paper has been taken from an average of 15 data points. A JOEL JSM-6060LV Scanning Electron Microscope (SEM) was used to obtain high resolution images of the wear tracks as well as to check for and image transfer films on the probes.

Table 2: Summary of microtribometer tests.

Sample	Friction[a] (0-800 mN)	Average wear depth with steel probe[b] (μm)	Average wear depth with diamond probe[c] (μm)
Clay 0%	0.741 ± 0.189	14.9 ± 8.83	22.2 ± 17.6
Clay 1%	0.598 ± 0.083	2.33 ± 0.809	5.41 ± 5.42
Clay 5%	0.771 ± 0.104	3.18 ± 1.443	25 ± 10.1

[a] Tests conducted using a steel probe of radius 1.2 mm
[b] After 1000 cycles at 500 mN normal load
[c] After 10 cycles at 300 mN normal load

6.5 Results and Discussion

6.5.1 Microscale friction and wear tests

Figure 3 plots the co-efficient of friction (COF) for all three batches of clay 0, clay 1 and clay 5 samples. The friction coefficients of all the batches of all samples ranged from 0.3-0.9 which is typically higher than what one would expect from steel on polymer contact [29]. This may be partly due to the high roughness of the samples. Table 2 summarizes the average friction coefficient of all three samples from which it has been found that the coefficient of friction of clay 0 and clay 5 are similar but clay 1 shows a 19.2% decreases in friction coefficient from clay 0.

Figure 4 shows the wear depth resulting from dry sliding tests against the steel probe and the diamond probe. The average values of the wear depth have been reported in table 2 which indicates that the wear in clay 0 is the highest with an average wear depth of 14.9 μm followed by clay 5 whose average depth is 3.18 μm, which is comparable to clay 1, which had a wear depth of 2.33 μm. This particular trend is same in all the three batches of samples. Wear tests with diamond probe showed that the average wear depth for clay 1 was the least

with a value of 5.41 μm compared to clay 0 and clay 5 samples which had average wear depth values of 22.2 μm and 25 μm respectively.

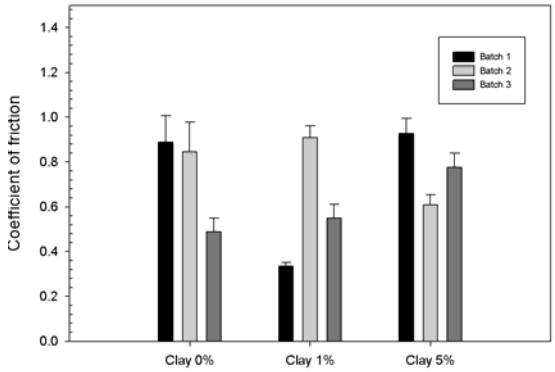

Figure 3. Histogram plot of the co-efficient of friction for three batches of all samples measured using the microtribometer.

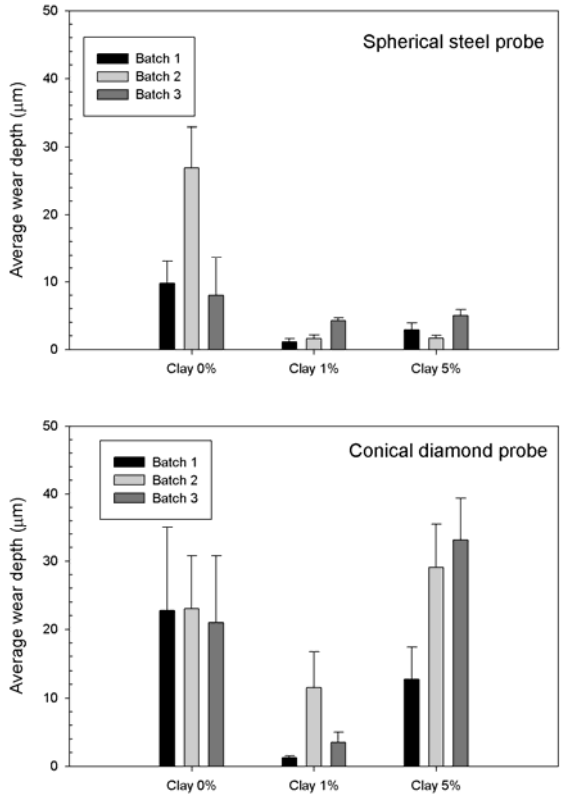

Figure 4. Histogram plot of the average wear depth for three batches of all samples subjected to tests against a spherical steel probe (top) and a sharp conical diamond probe (bottom).

SEM images of the worn surfaces (Fig. 5) displayed clear wear tracks on all samples after tests using the steel probe. The wear morphology of nanocomposites typically exhibits local flaking and diffused microcracking on the worn surfaces. This indicates that all samples undergo wear after 1000 cycles with the steel probe. There was clear evidence of material being removed as well as generation of cracks on the surfaces. Wear behavior of nanocomposites is generally governed by microchipping and microcracks due to transgranular fracture types which lead to wear debris [30]. Wear debris is generated by microchipping due to microcracks. When the steel probe was examined under the SEM transfer films were seen as shown in Fig. 6. High magnification SEM image (inset, Fig. 6) of the transfer film revealed distinct striation mark along the direction of stroke after tests in all samples. This suggests that adhesive wear was dominant mechanism for these samples.

SEM images of the wear tracks with diamond probe are shown in Fig. 7. It can be clearly seen that all samples exhibited grooves as well as presence of abraded material debris and some cracking along the groove edges. All samples exhibited similar degree of cracking with negligible debris. Abrasive wear is manifested by the cutting or plowing of the surface by the harder material (diamond in our experiments). The abraded particles are either embedded in the counterface or get loose within the contact zone. All these samples can be considered to have experienced abrasive wear by the sharp conical probe. Further, the degree of penetration, defined by the ratio of the depth of groove and the radius of contact [31], gave values less than 0.2 for all samples which indicates that dominant mechanism of abrasive wear is plowing.

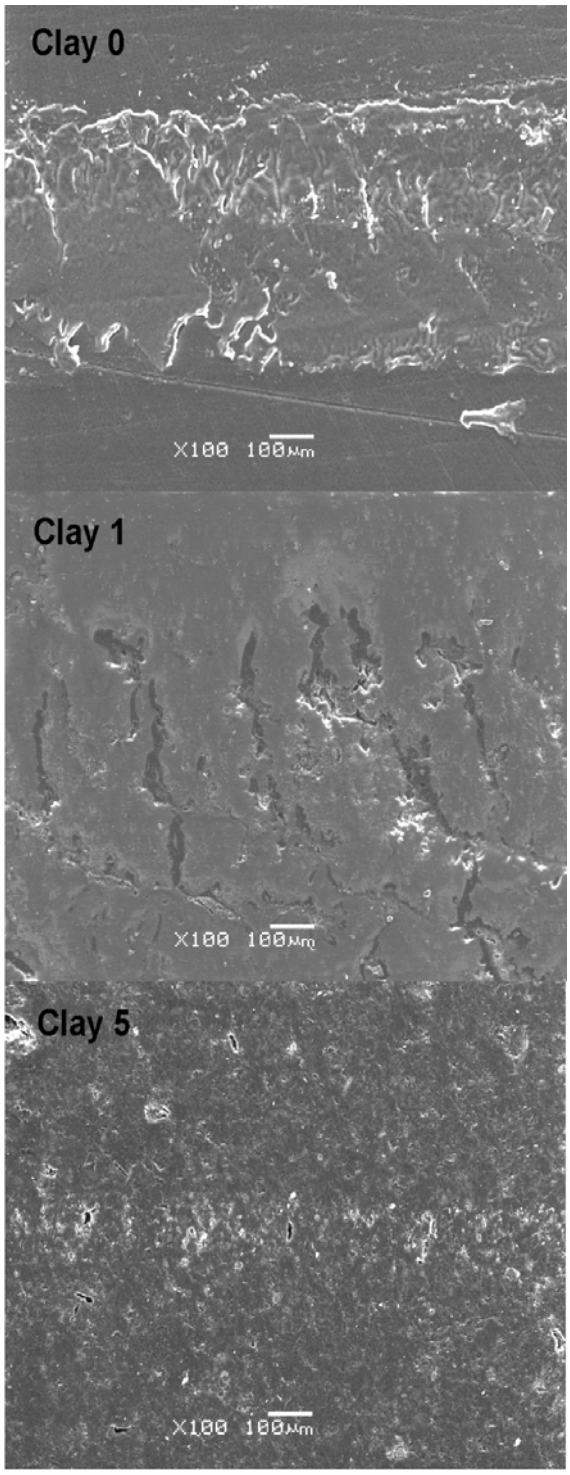

Figure 5. Scanning electron microscope images of the wear track with steel probe on clay 0, clay 1 and clay 5 samples. Formation of cracks on all the three samples is clearly seen.

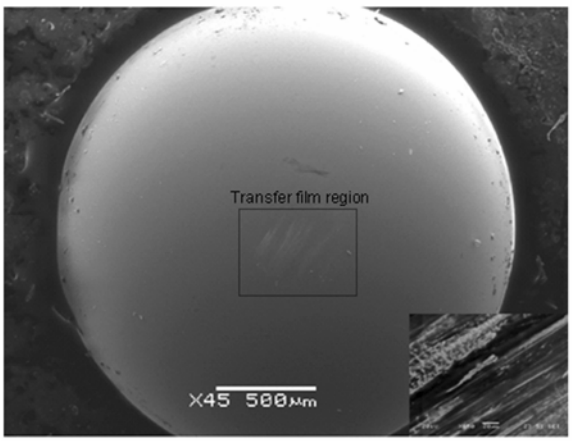

Figure 6. Scanning electron microscopy images of the transfer film formed on the steel probe during sliding wear tests. The high magnification images (inset) of the films reveal distinct striations parallel to the direction of stroke.

The results clearly show that a VMMT concentration of 1% resulted in improved wear performance in both adhesive and abrasive wear conditions. A further increase in VMMT concentration to 5% results in increased abrasive wear. This trend appears to correlate with compressive strength data reported in table 1. It is expected that addition of VMMT at 1% results in improvement in elasticity of the nanocomposites, which can be due to the strong interfacial interaction between the soybean oil-based polymer and the silicate platelets and to the presence of immobilized or partially immobilized polymer phases [18]. The degradation of properties upon increased loading of VMMT is attributed to defects in polymer networks and by the agglomeration and subsequent intercalation of VMMT that decreases the polymer-layered silicate interfacial bonding and prevents the monomers from penetrating into the galleries of the VMMT [12]. Another way to look in to this is that the clay particles are rigid fillers and make the resulting nanocomposite more brittle at high VMMT content [18].

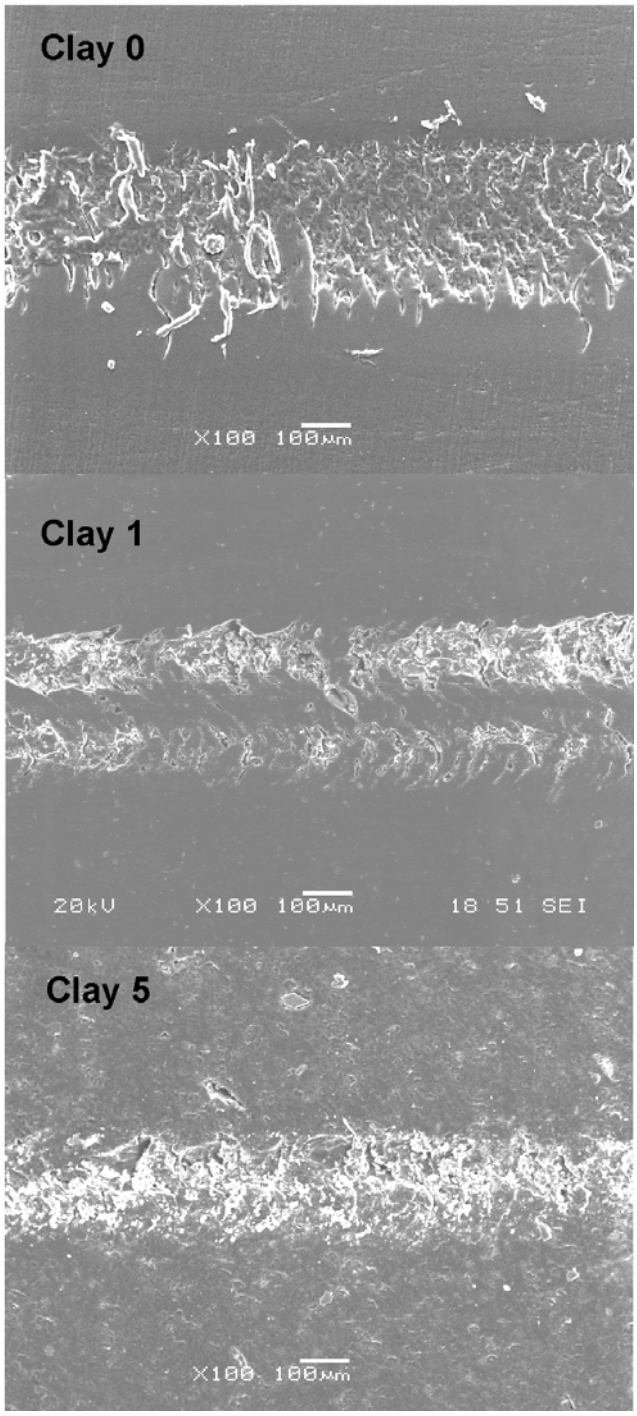

Figure 7. Scanning electron microscope images of the wear track with diamond probe on clay 0, clay 1 and clay 5 samples. All samples exhibit grooves as well as presence of abraded material debris and some cracking along the groove edges.

6.6 Conclusions

The tribological properties of novel biobased nanocomposites from soybean oil and functionalized organoclay as a function of clay concentration (0%, 1% and 5% concentration by weight) were evaluated. The coefficient of friction of the sample with 1% (clay 1) clay concentration is 19.2 % and 22.4% lower than the ones with 0% (clay 0) and the 5% (clay 5) respectively. However, the friction coefficients are typically higher than one would expect from steel on polymer contact. In sliding wear tests against a Si_3N_4 spherical probe, clay 0 showed the highest wear depth whereas the wear depth in clay 1 and clay 5 were lowered by 78.7% and 84.3% respectively. In sliding wear tests with a conical diamond probe, all samples exhibited abrasive wear. Clay 1 showed the lowest wear depth with a value 75.7% less than clay 0 and 78.3% less than clay 5. Thus, the addition of clay by 1% by weight resulted in a nanocomposite material with superior wear behavior than the ones with higher and lower clay concentrations. Based on these studies, it can be said that the VMMT in the polymer matrix play an important role in enhancing the wear behavior of the resulting nanocomposites.

6.7 Acknowledgement

The authors would like to thank Professor Scott Chumbley of Material Science and Engineering Department at Iowa State University for assistance with SEM operation.

6.8 References

1. R.C. Brown, Biorenewable Resources: Engineering New Products from Agriculture, 1st ed, Iowa State Press, Ames,2003.
2. S. Kim and B.E. Dale, Global potential bioethanol production from wasted crops and crop residues, Biomass and Bioenergy 26(4) (2004) 361-375.
3. S. Kim and B. Dale, Allocation procedure in ethanol production system from corn grain: I. System Expansion, International Journal of Life Cycle Assessment 7(4) (2002) 237–243.
4. A. Adhvaryu, S.Z. Erhan and J.M. Perez, Tribological studies of thermally and chemically modified vegetable oils for use as environmentally friendly lubricants, Wear 257(3-4) (2004) 359-367.
5. S. Bhuyan, S. Sundararajan, L. Yao, E.G. Hammond and T. Wang, Boundary lubrication properties of lipid-based compounds evaluated using microtribological methods, Tribology Letters 22(2) (2006) 167-172.
6. G. Biresaw, Biobased dry-film metalworking lubricants, Journal of Synthetic Lubrication 21(1) (2004) 43-58.
7. F. Li, M.V. Hanson and R.C. Larock, Soybean oil–divinylbenzene thermosetting polymers: synthesis, structure, properties and their relationships, Polymer 42 (2001) 1567-1579.
8. S.-J. Park, F.-L. Jin, J.-R. Lee and J.-S. Shin, Cationic polymerization and physicochemical properties of a biobased epoxy resin initiated by thermally latent catalysts, European Polymer Journal 41(2) (2005) 231-237.

9. F. Li and R. Larock, Synthesis, Structure and Properties of New Tung Oil-Styrene-Divinlybenzene Copolymers Prepared by Thermal Polymerization, Biomacromolecules 4 (2003) 1018-1025.

10. S. Bhuyan, S. Sundararajan, L.S. Holden, D. Andjelkovic and R. Larock, Effect of crosslinking on the friction and wear behavior of soy-bean oil-based polymeric materials, Wear 263 (2007) 965-973.

11. Y. Lu and R.C. Larock, Corn oil-based composites reinforced with continuous glass fibers: Fabrication and properties, Journal of Applied Polymer Science 102(4) (2006) 3345-3353.

12. Y. Lu and R.C. Larock, Novel Biobased Nanocomposites from Soybean Oil and Functionalized Organoclay, Biomacromolecules 7(9) (2006) 2692-2700.

13. D. Pfister, J.R. Baker, P.H. Henna, Y. Lu and R.C. Larock, Preparation and Properties of Tung Oil-Based Composites Using Spent Germ as a Natural Filler, Journal of Applied Polymer Science 108 (2008) 3618-3625.

14. S. Sinha-Ray and M. Okamoto, Polymer/layered silicate nanocomposites: a review from preparation to processing, Progress in Polymer Science 28(11) (2003) 1539-1641.

15. E.P. Giannelis, Polymer Layered Silicate Nanocomposites Advanced Materials 8(1) (1996) 29-35.

16. J.-I. Weon and H.-J. Sue, Effects of clay orientation and aspect ratio on mechanical behavior of nylon-6 nanocomposite, Polymer 46 (2005) 6325-6334.

17. Tianxi Liu, W.C. Tjiu, Y. Tong, C. He, S.S. Goh and T.-S. Chung, Morphology and fracture behavior of intercalated epoxy/clay nanocomposites, Journal of Applied Polymer Science 94(3) (2004) 1236-1244.

18. C. Basara, U. Yilmazer and G. Bayram, Synthesis and characterization of epoxy based nanocomposites, Journal of Applied Polymer Science 98(3) (2005) 1081-1086.

19. A. Lee and J.D. Lichtenhan, Thermal and viscoelastic property of epoxy-clay and hybrid inorganic-organic epoxy nanocomposites, Journal of Applied Polymer Science 73(10) (1999) 1993-2001.

20. H.M. Park, X. Liang, A.K. Mohanty, M. Misra and L.T. Drzal, Effect of Compatibilizer on Nanostructure of the Biodegradable Cellulose Acetate/Organoclay Nanocomposites, Macromolecules 37(24) (2004) 9076-9082.

21. X. Dai, J. Xu, X. Guo, Y. Lu, D. Shen, N. Zhao, X. Luo and X. Zhang, Study on Structure and Orientation Action of Polyurethane Nanocomposites, Macromolecules 37(15) (2004) 5615-5623.

22. Jir-Shyr Chen, Mark D. Poliks, Christopher K. Ober, Yuanming Zhang, Ulrich Wiesner and E. Giannelis, Study of the interlayer expansion mechanism and thermal-mechanical properties of surface-initiated epoxy nanocomposites, Polymer 43 (2002) 4895-4904.

23. P. Dubois and M. Alexandre, Performant Clay/Carbon Nanotube Polymer Nanocomposites, Advanced Engineering Materials 8(3) (2006) 147-154.

24. D.L. Burris, B. Boesl, G.R. Bourne and W.G. Sawyer, Polymeric Nanocomposites for Tribological Applications, Macromol. Mater. Eng. 292 (2007) 387-402.

25. S. Bahadur, The development of transfer layers and their role in polymer tribology, Wear 245(1-2) (2000) 92-99.

26. Q.-J. Xue and Q.-H. Wang, Wear mechanisms of polyetheretherketone composites filled with various kinds of SiC, Wear 213(1-2) (1997) 54-58.

27. W.G. Sawyer, K.D. Freudenberga, P. Bhimaraj and L.S. Schadler, A study on the friction and wear behavior of PTFE filled with alumina nanoparticles Wear 254(1-2) (2003) 573-580.

28. J. Check, K.S.K. Karuppiah and S. Sundararajan, Comparison of the effect of surface roughness on the micro/nanotribological behavior of ultra-high-molecularweight polyethylene (UHMWPE) in air and bovine serum solution, Journal of Biomedical Materials Research Part A 74A(4) (2005) 687-695.

29. M.E. Kinsella, B. Lilly, B.E. Gardner and N.J. Jacobs, Experimental determination of friction coefficients between thermoplastics and rapid tooled injection mold materials, Rapid Prototyping Journal 11(3) (2005) 167-173.

30. S.-H. Kim, Y.H. Kim, S.W. Lee, T. Sekino and K. Niihara, Fracture and Tribological Behaviors of Al2O3 / 5 vol.% SiC Nanocomposites, Materials Science Forum 439 (2003) 90-94.

31. K. Hokkirigawa and K. Kato, An experimental and theoretical investigation of ploughing, cutting and wedge formation during abrasive wear, Tribology International 21(1) (1988) 51-57.

CHAPTER 7. EFFECT OF FILLER COMPOSITION AND CROSSLINKER CONCENTRATION ON THE TRIBOLOGICAL BEHAVIOR OF SPENT GERM PARTICLES AND TUNG OIL-BASED POLYMERIC COMPOSITES

Modified from a paper submitted to *Tribology International*

Satyam Bhuyan, Sriram Sundararajan, Daniel Pfister and Richard Larock

7.1 Abstract

Thermosetting composites have been prepared by the use of a biobased resin and spent germ filler, which is a byproduct from a wet ethanol production plant. Tribological measurements were performed on samples with different concentrations of the filler as well as the crosslinker using a ball-on-flat reciprocating microtribometer. Friction and wear behavior during dry sliding was evaluated using a spherical silicon nitride probe (radius 1.2 mm) as well as a conical diamond (radius 100 μm, cone angle 90^0) probe. Finally, a pin-on-disc tribometer was used to study the wear properties at high loads. Scanning electron microscopy (SEM) images of wear tracks were obtained to elucidate deformation mechanisms. All samples showed abrasive wear. It was found that an increase in the concentration of the crosslinker lowered the abrasive wear depth. These results provide some insight into the effectiveness of using biobased spent germ-tung oil polymer composites as potential tribomaterials.

7.2 Introduction

In the past few decades the awareness and concern over the usage of petroleum-based products and their impact on the environment has created an opportunity and thrust to produce environmentally acceptable materials from biobased feedstock. The benefits of using biobased feedstock as sources for engineering materials includes taking advantage of excess agricultural production, the potential for rural development and minimizing the nation's dependency on petroleum [1]. Research has been conducted on developing a variety of biobased products including transportation fuels [2, 3], lubricants [4-6], polymers [7-10] and polymeric composites[11-13]. Natural oils are among the most promising renewable resources to be used for the production of biopolymers. Considerable recent research on the development of polymeric materials from these oils has been conducted [14-16]

Polymer-matrix composites are progressively finding applications in the industry because of their unique combination of mechanical, electrical and thermal properties [17-19]. In recent years, there has been much interest in particle-reinforced polymers not only because it is cheaper to produce them, but also they can be used as high quality engineering materials [20, 21]. A number of studies on polymer-matrix composites subjected to sliding and abrasive wear indicate that wear resistance depends on the detailed properties of the material as well as the external wear conditions such as applied pressure and contact velocity [22-25] . Furthermore, fiber addition to polymers does not necessarily improve their wear resistance [26].

Larock and coworkers has focused their attention on the preparation of crosslinked networks by polymerization of the unfunctionalized double bonds in natural oils [27]. Fillers are often added to polymers to increase dimensional strength, toughness, and environmental resistance [28]. Over the years composite materials have successfully found its way in

numerous applications in the automobile, aircraft, military, sporting goods and marine industries. The term biocomposites in its broader definition can be used to describe composites resulting from biobased resins and synthetic fibers, petroleum-based resins and natural fibers, or biobased resins and natural fibers. Natural fibers, as a replacement for synthetic fibers, have drawn much attention in the past several years, because of their low cost, low density, suitable specific strength, ability to renew and biodegradability [18]. The mechanical properties of the resulting materials are improved to a significant extent, making them suitable for applications in automobile and other industries. In this paper, the tribological properties of thermoset composites prepared using a biobased resin (tung-oil) and spent germ filler are investigated. The effect of filler composition and crosslinker concentration on the tribological response of the materials is reported.

7.3 Materials

Tung oil is triglyceride oil which is extracted from the seeds of a tung tree. The main chemical composition (~84%) is alpha-elaeostearic acid (cis-9, trans-11, trans-13-octadecatrienoic acid) [10]. The high number of fatty acid side chains containing a conjugated triene makes it reactive toward free radical polymerization. The tung oil based resin (TUN) was prepared by bulk free radical polymerization with divinylbenzene (DVB), t-butyl peroxide (TBPO) and n-Butyl methacrylate (BMA). The DVB, here, is used as the crosslinker. The synthesis procedure has been described here briefly and has been discussed extensively elsewhere [13]. The designated amounts of TUN, BMA, DVB, and TBPO were mixed and cured in a proper curing sequence. Then the spent germ (SG) particles (size ~180 μm) were added and this mixture was stirred until all the SG was wetted and was then

placed in the cavity of the preheated (130 ^{0}C) steel mold coated with the PTFE release agent. The mold was closed and cured at 130 ^{0}C under the designated pressure for 4 h. The mold was then moved to an oven and cured under atmospheric pressure.

The standard composition by weight and conditions used for preparing the composites were 50% TUN, 35% BMA, 15% DVB, 50% SG and 3000 psi molding pressure. When one variable was changed, the rest were held constant. In all cases, the matrix composition was TUN 50-(BMA + DVB) 50. For example, a composite designated SG 50 refers to TUN 50-BMA 30-DVB 20 (resin), 50% SG (filler) and 3000 psi molding pressure. We studied the effect of SG filler composition and the effect of DVB crosslinker concentration. For the first study, SG concentration of 40%, 50% and 60% were tested at a DVB concentration of 15%. The samples are termed SG 40, SG 50 and SG 60. For the second study, DVB concentration of 10%, 15% and 20% were tested at 50% SG concentration. These samples are termed as DVB 10, DVB 15 and DVB 20. The material properties of all samples are listed in Table 1.

7.4 Methods

7.4.1 Microscale friction and wear tests

For the experiments described in this paper, a custom-built reciprocating ball-on-flat microtribometer that can produce a microscale (apparent area ~1000 μm^2) multi-asperity contact was used [29]. A schematic of its major components is shown in Fig. 1. A probe with a specific radius is placed at the end of a crossed I-beam structure which is lowered using a linear stage to apply a desired normal load to the sample. The normal and friction (lateral) forces are measured using semiconductor strain gages on the cantilevers. Friction forces can

be resolved to approximately ±5 μN and normal forces to approximately ±15 μN. The signal from the normal load is monitored and used in a simple proportional-integral (PI) feedback loop to maintain the desired normal force regardless of any slope or waviness in the surface of the sample. The desired sample is affixed to another stage set perpendicular to the beam, which provides linear motion.

To obtain the coefficient of friction, ramped load tests were performed in which the normal load between a silicon nitride (Si_3N_4) ball (radius - 1.2 mm, RMS roughness - 4 nm, scan size 15 μm X 15 μm) and the sample was increased linearly with the sliding distance while the friction force was monitored. The load was increased from 0.2 to 800 mN as the probe was moved across a stroke distance of 40 mm at 5 mm/s. Preliminary tests showed that, for our load conditions, sliding speed had negligible effect on friction and wear relative to other factors.

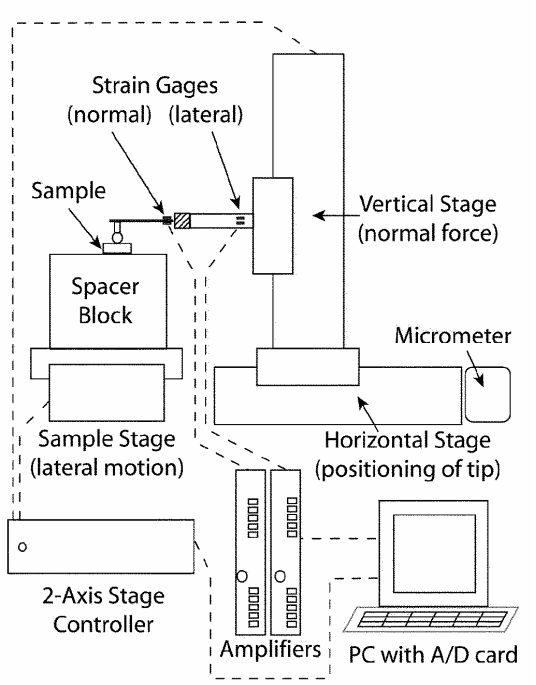

Figure 1. Schematic of a reciprocating microtribometer used for friction and wear tests.

Table 1. Mechanical properties of spent germ-based composites. Samples with varying spent germ (SG) concentrations as well as samples with varying divinyl benzene (DVB) concentrations by weight were studied.

Samples	Break Strength (MPa)	Modulus (MPa)	Toughness (MPa)	Ultimate Break Strain (%)	Ultimate Strength (MPa)
SG 40[a]	13.1	516	0.296	4.28	13.0
SG 50[a]	12.3	470	0.279	4.21	12.2
SG 60[a]	6.70	335	0.097	2.73	6.68
DVB 10[b]	6.96	196	0.200	5.27	6.95
DVB 15[b]	12.3	470	0.279	4.21	12.2
DVB 20[b]	13.5	678	0.208	3.07	13.4

[a] at a DVB concentration of 15% by weight
[b] at a SG concentration of 50% by weight

A 500 cycle reciprocating sliding wear test was performed against the Si_3N_4 probe at a constant load of 800 mN and a stroke speed of 5 mm/s for a total sliding distance of 30 m. A preliminary scratch response study of the materials was performed in order to evaluate normal loads to be used for sliding wear tests using a conical (100 micron radius, 90° cone angle) diamond probe. A 20 cycle reciprocating test with the diamond probe was then carried out at 800 mN at 5mm/s. All tests were performed at 30 $^{\circ}$C and 25±5 % relative humidity. Wear track profiling was carried out using a contact profilometer (Dektak II). High resolution images of the wear tracks were obtained using a JOEL JSM-6060LV Scanning Electron Microscope (SEM). These polymeric samples were coated with gold before performing electron microscopy.

7.4.2 Macroscale wear tests

Macroscale tests were done to verify trends seen in microscale tests. A pin-on-disc wear tester was used for wear experiments in which the stationary alumina pin was in contact with a rotating polymeric disk. Rectangular pins of size 6 mm X 6 mm in cross-section and 16 mm long were machined for use as the specimens for the tests. The disc used was 8 mm in diameter and 5 mm in thickness with a RMS surface roughness of 102 ± 21 nm at 15 X 15 μm scale. Dry sliding at ambient condition with a normal load of 15 N and a sliding speed of 0.123 m/s was performed in a track of 7 mm in diameter giving rise to a total sliding distance of 200 m. Before testing, the pins were abraded against a 600 grade SiC paper to ensure good contact between the sliding pin surface and the counterface during a sliding experiment. The surface of both the pin and disc were cleaned with a soft paper soaked in ethyl alcohol and thoroughly dried. The specimens were weighed both before and after the tests to an accuracy of 0.0001 g in a precision balance. Each specimen was tested once.

7.5 Results and discussions

The results of the microscale friction experiments are shown in Fig. 2 as bar charts. Figures 2a and 2b compares the friction data for samples with different SG filler composition against the Si_3N_4 and the diamond probe respectively. It can be seen that the coefficient of friction against Si_3N_4 increases with filler composition whereas for friction against diamond there is no apparent trend with all samples showing comparable friction levels. Upon examination of the friction tracks under an optical microscope, no clear evidence of damage or plastic deformation was observed.

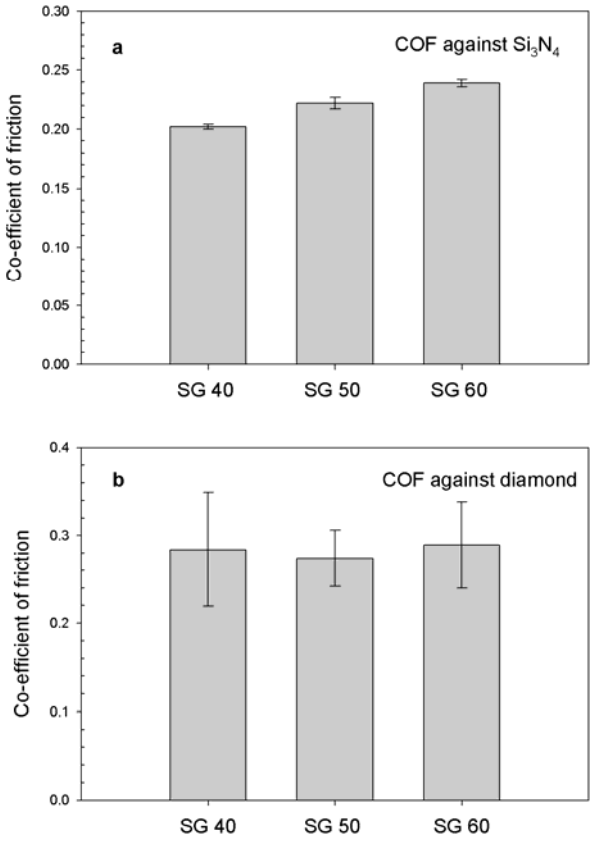

Figure 2. Plots of the average coefficient of friction (COF) of spent germ-based polymer composites with increasing SG filler composition under dry sliding against a) Si_3N_4 and b) diamond. The average and standard deviation have been taken from a set of four tests.

Consequently, a normal load of 800 mN was chosen for constant load reciprocating wear tests. Even after 500 cycles of loading with Si_3N_4 probe there was still no evidence of damage on the surface. Calculated Hertzian contact pressures ranged from 11.7 to 26.8 MPa. However, when reciprocating tests were done with a sharp diamond probe at 800 mN of normal load damages were seen on the surfaces of all materials. Under these conditions the contact pressures ranged from 61.4 to 779 MPa for the various samples. The wear depth was quantified and average wear depths have been reported. Figure 3(a) shows the effect of SG

composition on the wear behavior. From the data one can see that the SG 40 shows the least wear depth of 2.4 μm followed by SG 50 with a depth of 10 μm and finally, SG 60 whose average wear depth is 29.7 μm. Thus, an increase in the concentration of spent germ resulted in increased wear depth. This trend was seen in the macroscale wear tests as well. Mass loss data from pin-on-disc tests are shown in Fig. 3(b). The mass loss for SG 60 is the highest followed by SG 50 and then SG 40.

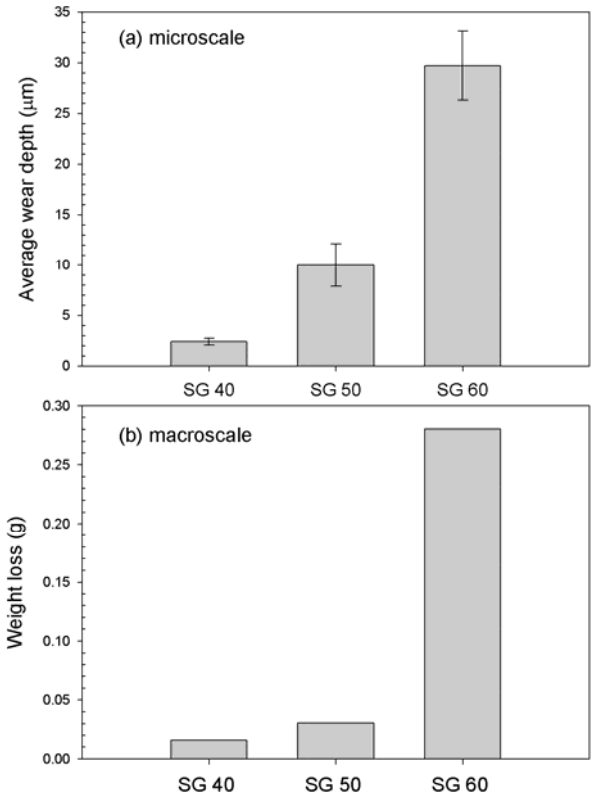

Figure 3. Wear data of the composites as a function of SG filler composition under dry sliding conditions - (a) Microscale wear data against a diamond probe and (b) macroscale wear data against an alumina pin. The average and standard deviation of the average wear depth have been taken from a set of three tests.

In order to determine the wear mechanisms responsible for the observed variations in wear depth, the morphology of the worn surfaces were examined using scanning electron microscopy (SEM). Polymers, by nature, can be abraded by rubbing against a hard surface resulting in abrasive wear [30]. Abrasive wear of particle reinforced polymers occurs mainly by three mechanisms: (a) microploughing, (b) microcutting, and (c) microcracking [22]. Using SEM images, it is possible to identify qualitatively the dominant mechanisms that operate, and thus, gain an insight into the influence that the reinforcement and crosslinking are having upon the abrasive wear process.

Figure 4 shows the damage due to wear over a 20 cycle reciprocating tests using the diamond probe. It is quite noticeable that the extent of wear damage on the samples increases with the concentration of spent germ. The SEM images of the wear tracks reveal the presence of cracks with debris scattered along the track. The non-uniform edges are a result of plastic deformation and cutting. The deep longitudinal cracks observed on the surface are consistent with a repeated ploughing mechanism causing surface fatigue.

Figure 5 shows the wear damage on SG 60 from the macroscale pin-on-dics tests. Evidence for particle pull-out and voids left by debonding of polymer-matrix are observed in the micrograph. At higher magnifications (insert), distinct evidence of particle-matrix debonding and fatigue damage of the tung-oil based resin matrix can be seen on the surface. Voids caused by the removal of particles are also seen on the surface and appear to be due to the abrasion of alumina on the debonded particles. Layers of resin appear to be removed by micro-cracking resulting again from surface fatigue. Exposed particles are then debonded and fractured from the surface as a consequence of inadequate matrix support owing to poor adhesion between filler and matrix. At this stage, the particles show minimum resistance to

removal through wear. Fracture by crack propagation is the predominant mechanism of material removal from the polymer matrix.

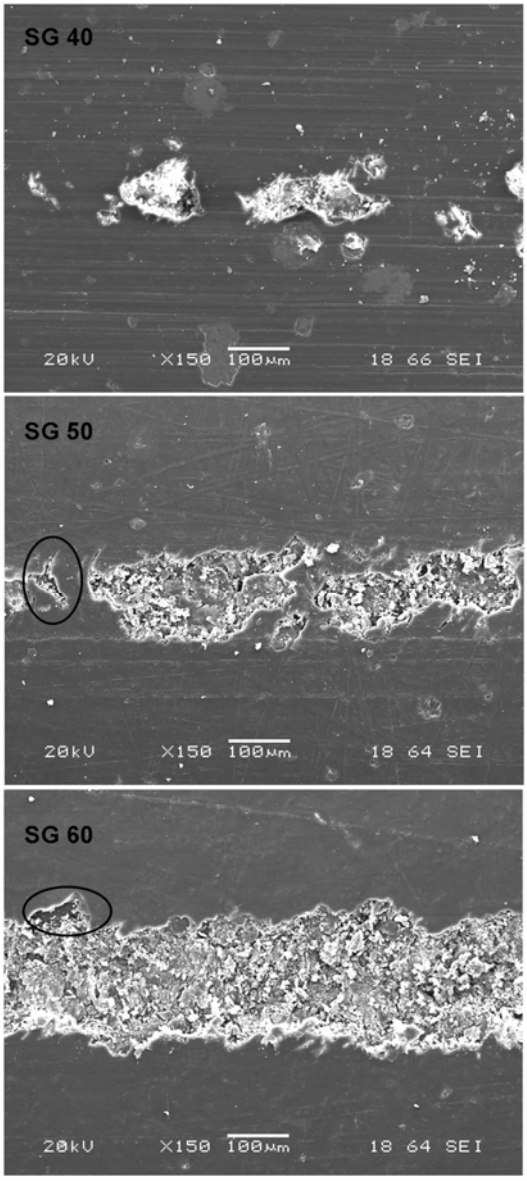

Figure 4. Scanning electron microscope images of the abrasive wear track on SG 40, SG 50 and SG 60 against the sharp diamond probe. Cracks on all the three samples are indicated by black ovals.

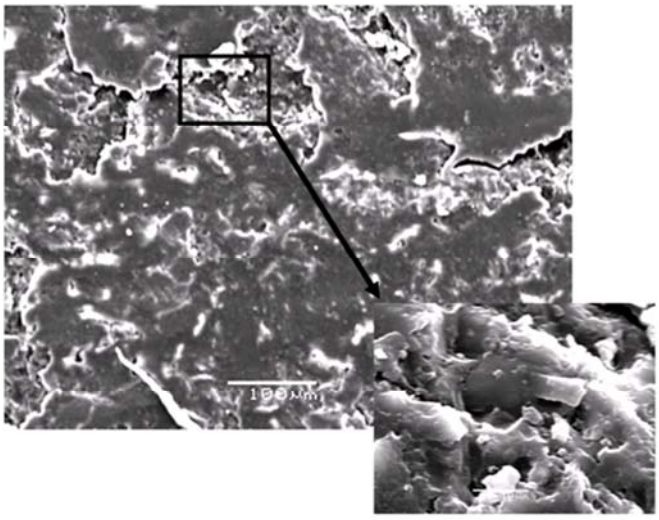

Figure 5. Scanning electron microscope images of the abrasive wear track on SG 60 DVB 15 against an alumina pin at a load of 15 N. Evidence of particle pull-out from the resin matrix can be observed (insert).

It has been suggested that the addition of spent germ as filler particles in composites disrupts the chain propagation by suppressing the initiator and as a result, the amount of crosslinking decreases [11]. Incomplete wetting of the filler by the resin are also believed to result in an increase in voids and filler–filler agglomerations [31]. Further, it has been found that the spent germ has 10% unreactive crude corn oil which can sometimes act as a plasticizer in the matrix [13] and increases the number of voids in the matrix which in turn weakens the material strength [11]. This is also evident from the material strength in Table 1.

Data from friction tests of samples with different crosslinker (DVB) concentration for a fixed SG concentration are shown in Fig. 6. No definite trend is seen for tests against a Si_3N_4 probe as the concentration is increased (Fig. 6a). On the other hand, in Fig. 6b, which

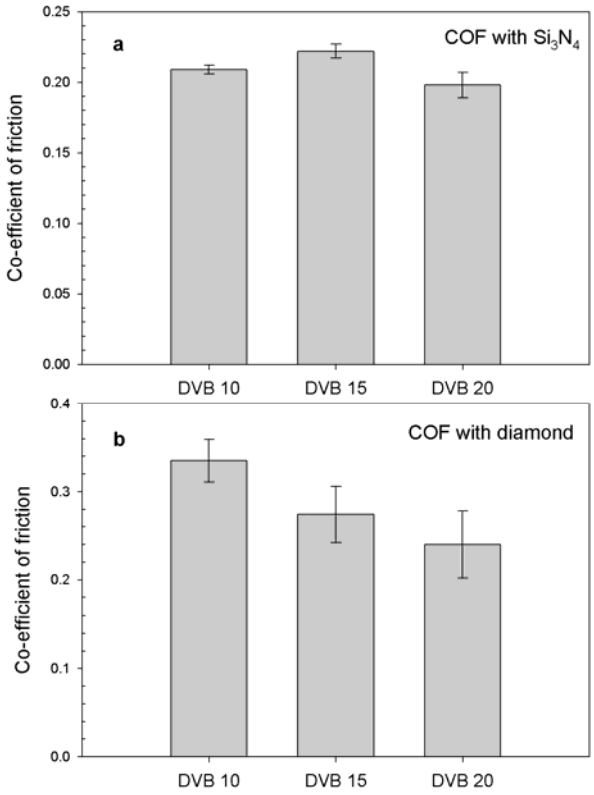

Figure 6. Plots of the average coefficient of friction of spent germ-based polymer composites with increasing concentration of the DVB crosslinker under dry sliding against a) Si_3N_4 and b) diamond. The average and standard deviation have been taken from a set of four measurements.

plots the friction data against diamond probe, it was found that the coefficient of friction decreases as the concentration of DVB is increased.

Figure 7(a) shows the observed wear as a function of the DVB concentration. It can be seen that DVB 10 shows a wear depth of 17.8 μm which is more than DVB 15, with a wear depth of 10 μm, followed by DVB 20 which has the least average wear depth of 3.2 μm. This trend is also evident from mass loss data in Fig. 7(b) during the macroscale wear

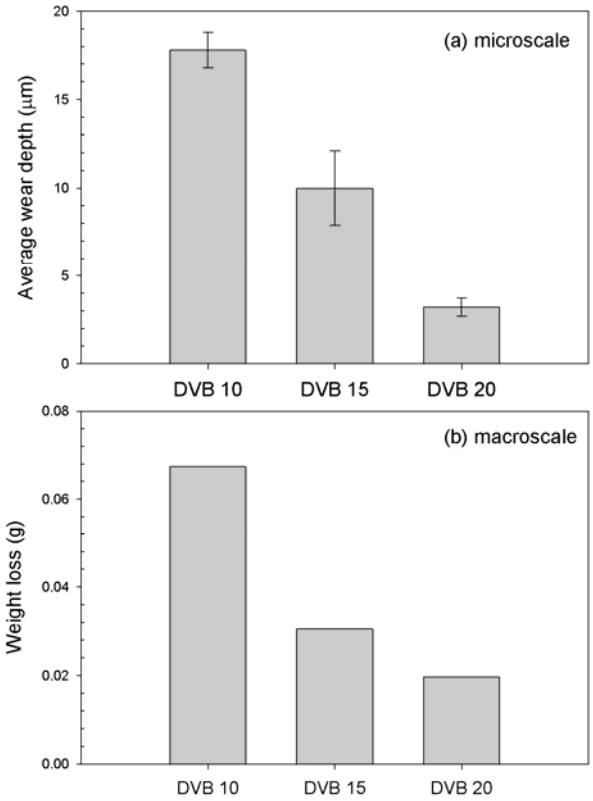

Figure 7. Wear data of the composites as a function of DVB crosslinker concentration under dry sliding conditions - (a) Microscale wear data against a diamond probe and (b) macroscale wear data against an alumina pin. The average and standard deviation of the average wear depth have been taken from a set of three tests

test. Mass loss for DVB 10 is more than DVB 15 which in turn is more than DVB 20. The SEM images of the wear tracks from tests against the diamond probe are shown in Fig. 8. It can be seen that the material gets plastically deformed under load through ploughing and with subsequent applications of load; microcracks are created along the deformed material, which are eventually removed by brittle fracture. Thin scratch like grooves along the wear direction present on the surface is formed by micro-cutting by the abrasive particles. Thus,

the coefficient of friction and the average wear depth against the sharp diamond probe were observed to decrease with an increase in the crosslinker concentration.

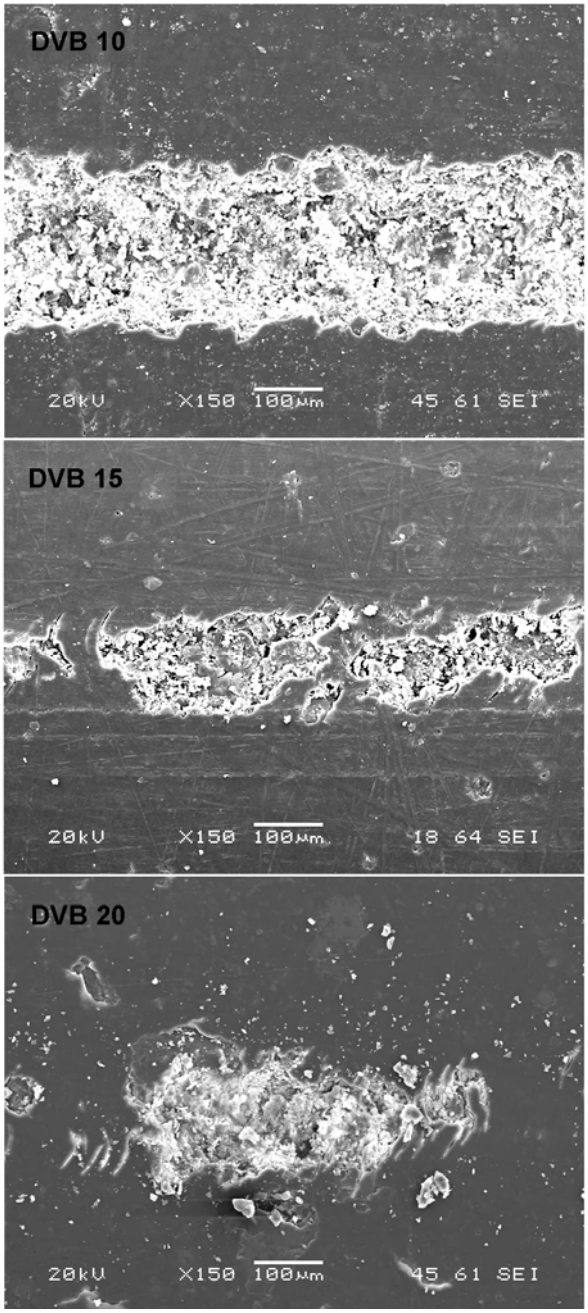

Figure 8. Scanning electron microscope images of the abrasive wear track on DVB 10, DVB 15 and DVB 20 against the sharp diamond probe. Formation of cracks on all the three samples is clearly seen.

These studies support past work which suggests that divinyl benzene (DVB) can be used as an effective crosslinker in increasing the material strength as well as reduction the wear of the material [7]. Crosslinking increases the tightness of the polymer network and reduces the molecular mobility of chains between the junctions. It could be possible the higher crosslinking reduces the number of conformations that the matrix can take on while being under an applied force [13]. Thus, crosslinking increases the stiffness of the polymers, which in turn affects the tribological properties.

7.6 Conclusions

The tribological properties of novel biobased polymer-composites from a tung oil-based resin and spent germ particles as a function of filler composition (40%, 50% and 60% by weight of spent germ) and as a function of crosslinker concentration (10%, 15% and 20% concentration by weight of divinyl benzene) were evaluated. The data from friction tests indicated that the coefficient of friction (COF) against a Si_3N_4 ball increases with filler composition. During the reciprocating wear tests, there was no evidence of damage on all samples against the Si_3N_4 ball indicating that these materials are resistance to wear under given loading conditions. On the other hand, wear against the sharp diamond probe was predominantly abrasive in nature and data showed that an increase in filler composition had an adverse impact on abrasive wear. A similar trend was observed with macroscale wear tests implying that the spent germ as filler does not improve wear resistance. This is attributed to the fact that the spent germ has 10% unreactive crude corn oil which can sometimes act as a plasticizer in the matrix resulting in the formation of voids which in turn weakens the material strength. On the other hand, addition of divinyl benzene (DVB) as the crosslinker

not only enhances the material strength but improves the tribological properties as well for a given filler composition. The COF and the average wear depth against diamond were observed to decrease with an increase in the crosslinker concentration. Micro-cracking of the matrix caused by surface fatigue was found to be the dominant mechanism of abrasive wear of polymer matrix composites caused by bulk solids.

7.7 Acknowledgements

The authors would like to thank Professor Scott Chumbley of Material Science and Engineering Department at Iowa State University for assistance with SEM operation. This work was partially supported by seed funding from Plant Science Institute at Iowa State University.

7.8 References

1. Brown RC. Biorenewable Resources: Engineering New Products from Agriculture. 1st ed. Ames: Iowa State Press, 2003.
2. Kim S and Dale BE. Global potential bioethanol production from wasted crops and crop residues. Biomass Bioenergy 2004;26(4):361-375.
3. Kim S and Dale B. Allocation procedure in ethanol production system from corn grain: I. system expansion. Int J Life Cycle Assess 2002;7(4):237–243.
4. Adhvaryu A, Erhan SZ and Perez JM. Tribological studies of thermally and chemically modified vegetable oils for use as environmentally friendly lubricants. Wear 2004;257(3-4):359-367.

5. Bhuyan S, Sundararajan S, Yao L, Hammond EG and Wang T. Boundary lubrication properties of lipid-based compounds evaluated using microtribological methods. Tribol Lett 2006;22(2):167-172.

6. Biresaw G. Biobased dry-film metalworking lubricants. J Synth Lubr 2004;21(1):43-58.

7. Bhuyan S, Sundararajan S, Holden LS, Andjelkovic D and Larock R. Effect of crosslinking on the friction and wear behavior of soy-bean oil-based polymeric materials. Wear 2007;263:965-973.

8. Li F, Hanson MV and Larock RC. Soybean oil–divinylbenzene thermosetting polymers: synthesis, structure, properties and their relationships. Polymer 2001;42:1567-1579.

9. Park S-J, Jin F-L, Lee J-R and Shin J-S. Cationic polymerization and physicochemical properties of a biobased epoxy resin initiated by thermally latent catalysts. Eur Polym J 2005;41(2):231-237.

10. Li F and Larock R. Synthesis, Structure and Properties of New Tung Oil-Styrene-Divinlybenzene Copolymers Prepared by Thermal Polymerization. Biomacromolecules 2003;4:1018-1025.

11. Lu Y and Larock RC. Corn oil-based composites reinforced with continuous glass fibers: Fabrication and properties. J Appl Polym Sci 2006;102(4):3345-3353.

12. Lu Y and Larock RC. Novel Biobased Nanocomposites from Soybean Oil and Functionalized Organoclay. Biomacromolecules 2006;7(9):2692-2700.

13. Pfister D, Baker JR, Henna PH, Lu Y and Larock RC. Preparation and Properties of Tung Oil-Based Composites Using Spent Germ as a Natural Filler. J Appl Polym Sci 2008;108:3618–3625.

14. Mosiewicki M, Aranguren MI and Borrajo J. Mechanical properties of linseed oil monoglyceride maleate/styrene copolymers. J Appl Polym Sci 2005;97(3):825-836.

15. Can E, Küsefoglu S and Wool RP. Rigid thermosetting liquid molding resins from renewable resources. II. Copolymers of soybean oil monoglyceride maleates with neopentyl glycol and bisphenol A maleates. J Appl Polym Sci 2002;83(5):972-980.

16. Can E, Küsefoglu S and Wool RP. Rigid, thermosetting liquid molding resins from renewable resources. I. Synthesis and polymerization of soy oil monoglyceride maleates. J Appl Polym Sci 2001;81(1):69-77.

17. Cenna AA, Allen S, Page NW and Dastoor P. A polyethylene-reinforced polymer composite abraded by bulk solids. Wear 2001;249:663.

18. Mohanty AK, Misra M, Drzal LT, Selke SE, Harte BR and Hinrichsen G. Mohanty AK, Misra M and Drzal LT, editors. Natural Fibers, Biopolymers and Biocomposites, 2005.

19. Mohanty AK, Misra M and Hinrichsen G. Biofibres, biodegradable polymers and biocomposites: An overview. Macromol Mater Eng 2000;276/277:1-24.

20. Robertson CG, Lin CJ, Rackaitis M and Roland CM. Influence of particle size and polymer-filler coupling on viscoelastic glass transition of particle-reinforced polymers. Macromolecules 2008;41(7):2727-2731.

21. Kim BC, Park SW and Lee DG. Fracture toughness of the nano-particle reinforced epoxy composite. Compos Struct 2008;86(1-3):69-77.

22. Friedrich K. Friction and Wear of Polymer Composites. Pipes RB, editor. Composite materials Series Vol 1. Amsterdam: Elsevier, 1986.

23. Cirino M, Friedrich K and Pipes RB. The effect of fiber orientation on the abrasive wear behavior of polymer composite materials. Wear 1988;121(1):127-141.

24. Friedrich K and Cyffka M. On the wear of reinforced thermoplastics by different abrasive papers. Wear 1985;105(4):333-344.

25. Cirino M, Friedrich K and Pipes RB. Evaluation of polymer composites for sliding and abrasive wear applications. Composites 1988;19(5):383-392.

26. Cirino M, Pipes RB and Friedrich K. The abrasive wear behaviour of continuous fibre polymer composites J Mater Sci 1987;22 2481.

27. Li F and Larock RC. Synthesis, Properties, and Potential Applications of Novel Thermosetting Biopolymers from Soybean and Other Natural Oils. Mohanty AK, Misra M and Druzal LT, editors. Natural Fibers, Biopolymers and Biocomposites, 2005.

28. Jones RF. editor. Guide to Short Fiber Reinforced Plastics. Cincinnati, OH: Hanser Gardner Publications 1998.

29. Check J, Karuppiah KSK and Sundararajan S. Comparison of the effect of surface roughness on the micro/nanotribological behavior of ultra-high-molecularweight polyethylene (UHMWPE) in air and bovine serum solution. Journal of Biomedical Materials Research Part A 2005;74A(4):687-695.

30. Bhushan B. Principles and Application of Tribology. New York: John Wiley & Sons, Inc., 1999.

31. Mosiewicki M, Borrajo J and Aranguren MI. Mechanical properties of woodflour/linseed oil resin composites. Polym Int 2005;54(5):829-836.

CHAPTER 8. INFLUENCE OF CROSSLINKING DENSITY ON THE TRIBOMECHANICAL BEHAVIOR OF RING-OPENING METATHESIS POLYMERIZED (ROMP) THERMOSETTING POLYMERS AND OTHER POLYMERIC MATERIALS

Modified from a paper submitted to *Journal of Tribology*

Satyam Bhuyan, Sriram Sundararajan, Xia Sheng and Michael Kessler

8.1 Abstract

In this study, the friction and wear behavior of norbonene-based polymers prepared by ring-opening metathesis polymerization (ROMP) reaction are evaluated as a function of crosslinking density. Tribological measurements were performed using a ball-on-flat reciprocating microtribometer. Friction and wear experiments under dry sliding were evaluated using a 1.2 mm radius Si_3N_4 spherical probe as well as a 100 micron radius conical diamond probe with a 90° cone angle. Wear experiments were evaluated at constant normal loads for 100-500 reciprocating cycles. Wear depths were estimated from wear grooves using a contact profilometer and scanning electron microscopy was used to elucidate deformation mechanisms in the various samples. Correlations between crosslinking density and wear behavior were observed. Data from wear tests of ROMP polymers as well as biobased polymers from past work by the authors were used understand the relationship between wear behavior and crosslinking density.

8.2 Introduction

A new type of study has set foot in material design and that is through the development of self healing composites[1]. A unique feature of the healing concept is the use of the un-terminated chain-end polymerization catalysts, thus enabling multiple healing events. Engineering this self-healing composite involves the challenge of combining polymer science, experimental and analytical mechanics, and composites processing principles[2]. During damage, microcracks rupture the embedded capsules and release the healing agent in to the crack plane. The released healing agent comes in contact with an embedded catalyst and polymerizes, thereby, bonding the crack faces back together [3].

Past studies have shown that the norbornene-based monomer *Endo*-dicyclopentadiene (*endo*-DCPD) has been used effectively as the healing agent in self-healing composites [4-11]. Their works has shown that Grubbs' first generation catalyst was used as the embedded trigger to set off the ring-opening metathesis polymerized (ROMP) reaction. The end product is crosslinked structure with high toughness and strength. In the work done by Kessler and coworkers, *endo*-DCPD was polymerized in presence of ruthenium-based Grubbs catalyst to form crosslinked polymers of high toughness [12]. They have found out that the addition of a norbornene-based crosslinker to the monomer significantly affects the thermal properties of the resulting polymer.

In this paper, the friction and wear behavior of norbornene-based polymers under dry sliding have been reported as a function of the crosslinking density. Consequently, results from the authors' previous work on the wear of biobased polymers have been listed [13-15]. Finally, an empirical relationship between the wear volume and the crosslinking density has been developed for the various materials.

8.3 Materials

The reagents used to prepare the polymers were obtained from chemical suppliers. The endo-DCPD was used as received without further purification. The preparation of the norbornene-based crosslinker have been discussed elsewhere [12]. The mixture of crosslinker and monomers were prepared at five different loadings of the crosslinker – 0, 5, 10, 15 and 20%. The crosslinking densities, the storage moduli and the hardness of the samples have been shown in Table 1. The table also lists the RMS roughness of the samples taken at a scan area of 100 μm x 100 μm with an atomic force microscope. By adding the crosslinker at varying concentrations to the monomers, the properties of the resulting polymers can be tailored. As it can be seen from the table, that, with increase loadings of the crosslinker, the crosslinking density increases indicating the formation of a highly crosslinked network. This has been further substantiated by swelling tests [12]. Throughout the paper, the samples have been labeled as CL-0, CL-5, CL-10, CL-15 and CL-20.

Table 1. Material properties of the samples used in this study

Sample	Crosslinking density (moles/m^3)	Storage Modulus (MPa)	Hardness[a] (MPa)	RMS roughness[b] (nm)
CL-0	1.91 x 10^3	22.5	-	6.97 ± 1.59
CL-5	2.65 x 10^3	31.7	-	15.8 ± 0.94
CL-10	3.05 x 10^3	37	254 ± 5.10	9.66 ± 2.30
CL-15	3.10 x 10^3	37.9	325 ± 19.5	306 ± 15.7
CL-20	3.75 x 10^3	46	394 ± 39.8	240 ± 12.5

[a] Rockwell Hardness tests could not be performed on CL-0 and CL-5.
[b] Taken from a 100 μm x 100 μm scan

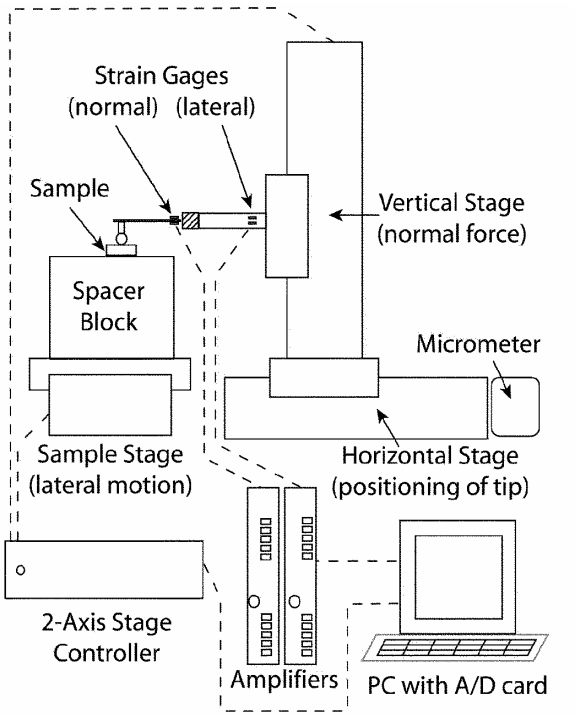

Figure 1. Schematic of the reciprocating microtribometer used for friction and wear tests.

8.4 Methods

8.4.1 Microscale Friction and Wear Tests

For the experiments described in this paper, a custom-built reciprocating ball-on-flat microtribometer producing a microscale (apparent area ~1000 square microns) multi-asperity contact was used [16]. A schematic of its major components is shown in Figure 1. A probe is placed at the end of a crossed I-beam structure which is lowered using a linear stage to apply a desired normal load to the sample. The normal and friction (lateral) forces are measured using semiconductor strain gages on the cantilevers. Friction forces can be resolved to approximately ±5 μN and normal forces to approximately ±15 μN. The signal from the normal load is monitored and used in a simple proportional-integral (PI) feedback loop to

maintain the desired normal force regardless of any slope or waviness in the surface of the sample. The desired sample is affixed to another stage set perpendicular to the beam, which provides linear motion.

To obtain the coefficient of friction, ramped load tests were performed in which the normal load between a silicon nitride (Si_3N_4) ball (radius - 1.2 mm, RMS roughness - 4 nm, scan size 15 μm X 15 μm) and the sample was increased linearly with the sliding distance while the friction force was monitored. The load was increased from 0 to 1 N as the probe was moved across a stroke distance of 30 mm at 2.5 mm/s. Average values of coefficient of friction have been calculated from four ramped load tests. A 500 cycle reciprocating sliding wear test was performed against the Si_3N_4 probe at a constant load of 800 mN and a stroke speed of 5 mm/s for a total sliding distance of 30 m. Preliminary scratch response study of the materials were performed in order to evaluate normal loads to be used for sliding wear tests using a conical (100 micron radius, 90° cone angle) diamond probe. A 100 cycle reciprocating test with the diamond probe was then carried out at 800 mN at 5mm/s. All tests were performed at 21 $^{\circ}$C and 30 ± 3% relative humidity. Wear track profiling was carried out using a contact profilometer (Dektak II) and average wear depths have been calculated from a set of three tests. A JOEL JSM-6060LV Scanning Electron Microscope (SEM) was used to obtain high resolution images of the wear tracks as well as to check for and image transfer films on the probes. Each sample was gold coated before the SEM studies. The hardness of the materials was measured with a Rockwell Hardness tester.

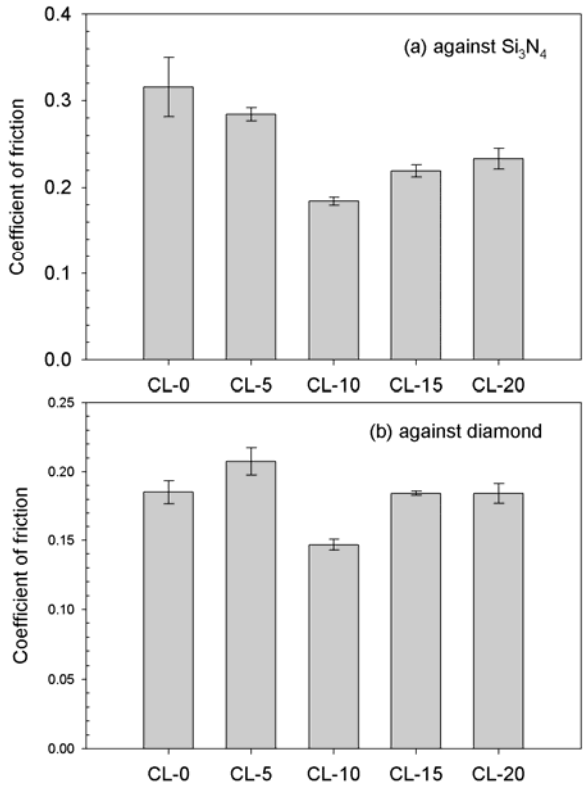

Figure 2. Histogram plot of the coefficient of friction of all samples subjected to tests with the microtribometer against (a) Si_3N_4 probe and (b) diamond probe.

8.5 Results and discussion

8.5.1 Microscale friction and wear tests

Figure 2a plots the average co-efficient of friction (COF) and its standard deviation for all five samples at under dry sliding against Si_3N_4 probe. The friction coefficients of all samples that were tested ranged from 0.184-0.316 as shown in the figure. The material without any crosslinker, CL-0, showed the highest friction coefficient. Addition of 5% (w/w) of the crosslinking agent reduces the COF by 10% indicating that crosslinking improves the friction response of these polymeric materials against Si_3N_4. Compared to CL-10 the COF of

CL-15 and CL-20 appears to be higher. Upon examining the surfaces and the probes under an optical microscope there was no evidence of any grooving or transfer film. Figure 2b plots the average friction coefficient and its standard deviation for all five samples under dry sliding against diamond probe. From this plot no definite trend in COF can be seen amongst the samples. However, CL-10 shows the least value of COF against diamond as well.

When the samples were subjected to a 500 cycle reciprocating wear tests with the Si_3N_4 probe, distinctive wear tracks were seen only on the CL-0 samples. Although no measurable depth was obtained using the profilometer, AFM measurements over a 100 μm x 100 μm area showed an average RMS roughness of 81.2 nm inside the track and 6.79 nm outside. The morphology of the wear surface was studied with a SEM and shown in Fig. 3. Few traces of microcracks can be seen on the wear grooves that are most likely caused by fatigue mechanisms associated with predominantly elastic deformation.

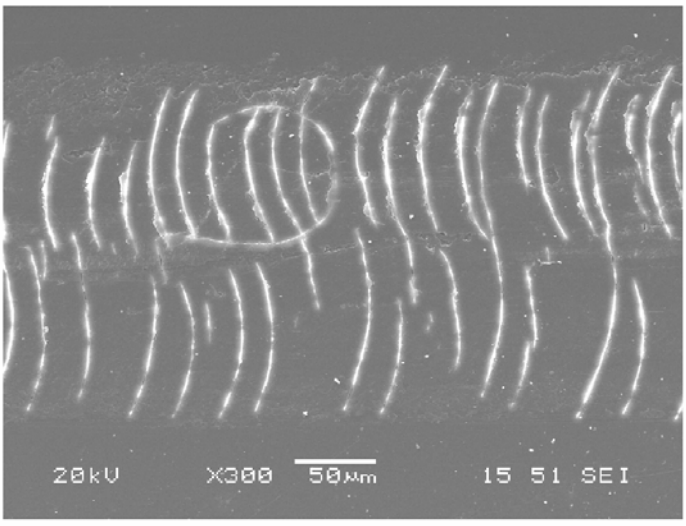

Figure 3. Scanning electron microscope (SEM) images of the wear track with Si3N4 probe on CL-0 sample. Formation of cracks is clearly evident.

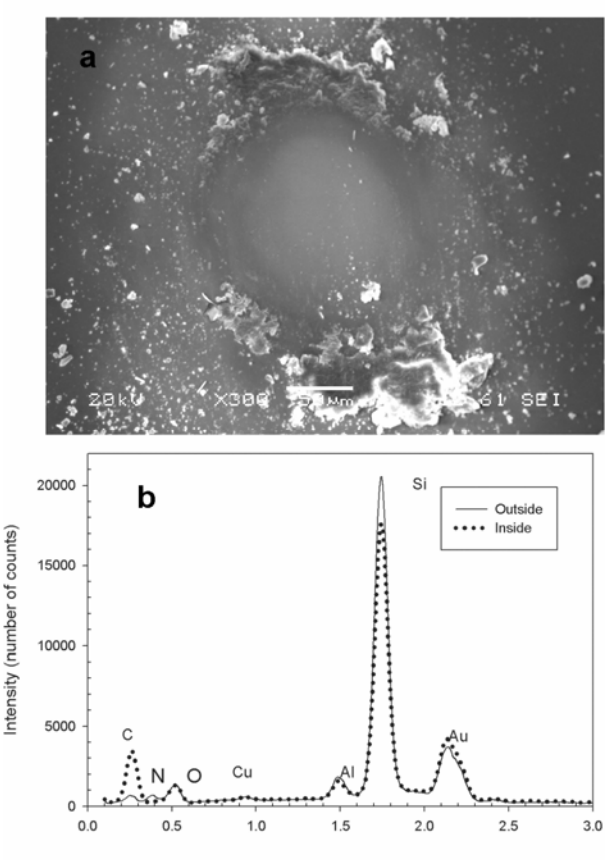

Figure 4. (a) Scanning electron microscopy (SEM) images of the transfer film during sliding wear tests on the Si3N4 probe. (b) Comparison of Energy Dispersive Spectroscopy (EDS) spectra of the probe both inside and outside the film indicates the presence of carbon in the film.

Polymers commonly transfers to the counterface when rubbing against other metals or ceramics [17]. In this study, surface morphology examination and surface analysis confirmed this tendency. A transfer layer was easily identified on the Si_3N_4 ball (see Fig. 4a.). The energy dispersive spectroscopy (EDS) analysis of the transfer film detected carbon as shown in Fig. 4b. These observations suggest that the material underwent adhesive wear.

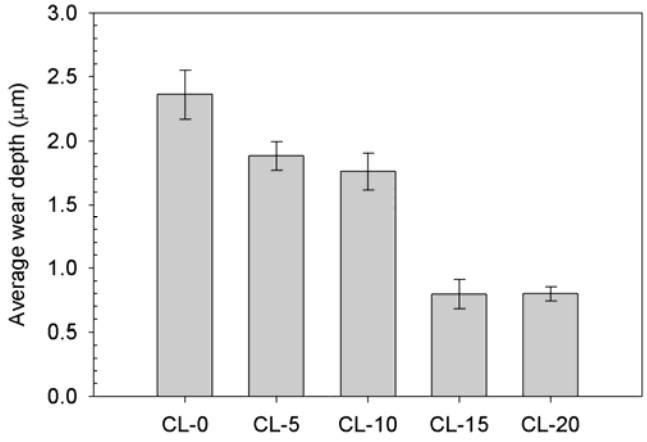

Figure 5. Histogram plot of the average wear depth (in μm) against diamond probe for all samples subjected to tests with the microtribometer.

Figure 5 shows the average wear depth resulting from dry sliding tests against the diamond probe. Clearly, the material without the crosslinker showed the highest wear depth of 2.36 μm. Upon loading with 5% (w/w) of the crosslinker (CL-5), the wear depth reduces by 20%. The CL-10 showed a much better improvement with a reduction by 25%. CL-15 and CL-20 showed wear depths that were comparable to one another and which were lower than CL-0 by 66%. These results clearly indicate that an increase in crosslinking reduces the propensity for wear for the given test conditions.

SEM images of the worn surfaces (Fig. 6.) from tests against the diamond probe displayed clear wear tracks on all samples. The wear morphology exhibits a groove along with crack formation along the edge or within the groove of the wear track, which is consistent with fatigue mechanisms associated with brittle polymers. Abrasive wear by repeated action of the reciprocating probe promotes crack extension and intersection, which leads to formation of wear debris. Evidence of material pull-out and voids left by the cracks

are observed in the micrograph (see Fig. 6f.). This cracking region represents the extent of damages that should be directly related to loss of material through abrasive wear.

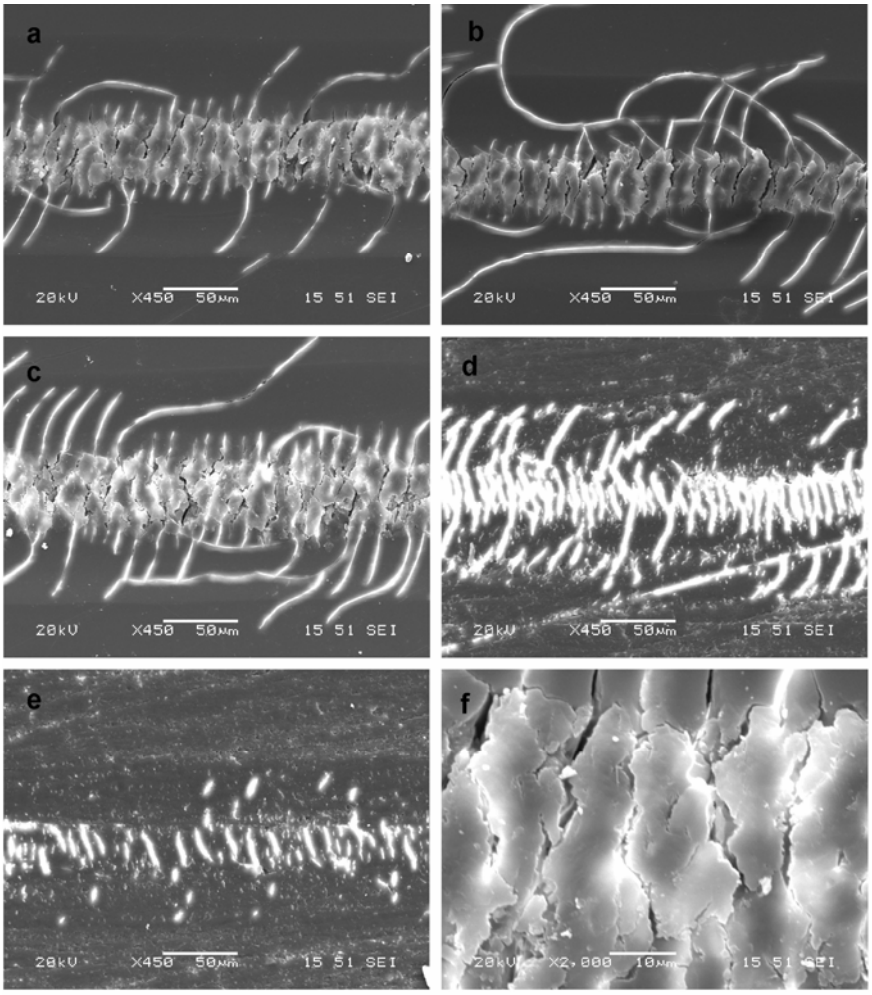

Figure 6. Scanning electron microscopy (SEM) images of the wear track with diamond probe on (a) CL-0, (b) CL-5, (c) CL-10, (d) CL -15 and (e) CL-20 samples. Clear evidence of cracks is noticeable on these brittle materials. (f) High magnification image on CL-0 shows evidence of material pull out and formation of voids.

8.5.2 Discussions

Abrasive wear of materials have been described by Archard [17] who showed that for abrasive wear involving plastic deformation, the wear volume (v) can be described as follows

$$v = \frac{k_{abs} W x}{H} \tag{1}$$

where k_{abs} is the nondimentional abrasive wear coefficient, W is the applied load, x is the total sliding distance and H is the hardness.

The wear volumes have been calculated from the groove geometry and measured hardness values were used to obtain wear coefficients, which are listed in Table 2. Since the only variable affecting material properties is crosslinking density, it stands to reason that the resulting hardness can be related to crosslinking density. Figure 7 plots the hardness and the wear coefficient as a function of crosslinking density. In general, hardness increases with crosslinking density while the wear coefficient decreases. This trend is supported from past work done by the authors on biobased polymers - low saturated soybean oil (LSS) and tung oil (TUN)[13, 14] in which divnyl benzene (DVB) was used as the cross linking agent. Figure 8 shows the hardness and wear data on these polymers as well. Although the exact relationship between crosslinking density and hardness would depend on the material system, based on the data on three systems, it can be assumed that a first order linear relationship exists between the two. Regression analyses have confirmed this type of behavior with regression values of 0.7909 for ROMP polymers, 0.9462 for LSS polymers and 0.9985 for TUN polymers. Therefore, Eq. (1). can be rewritten as,

$$v = \frac{k_{abs} W x}{a \nu_e} \tag{2}$$

where a is an empirical constant whose value depends upon the system under study. Thus crosslinking density affects the resulting abrasive wear volume by affecting the hardness of the materials.

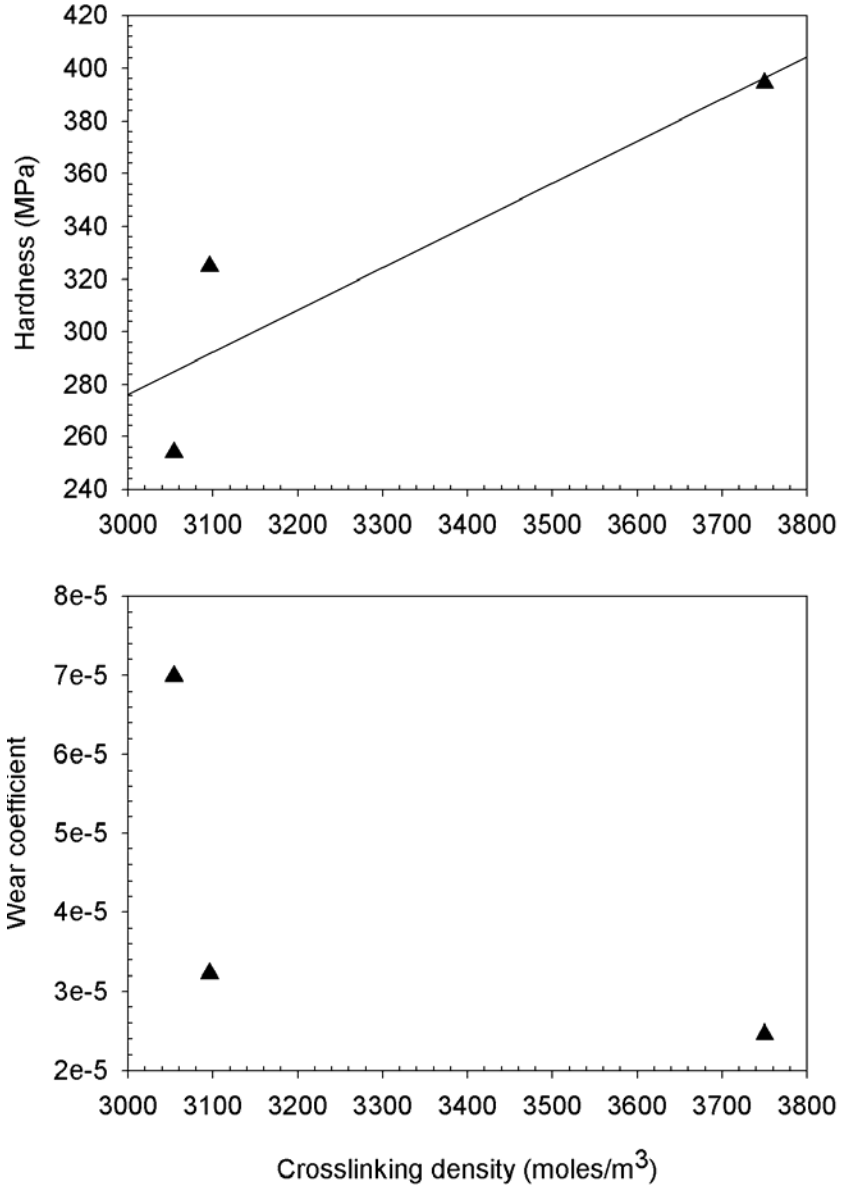

Figure 7. (a) Linear regression plot of hardness vs crosslinking density for ROMP thermosetting polymers. (b) Wear coefficients vs the crosslinking density.

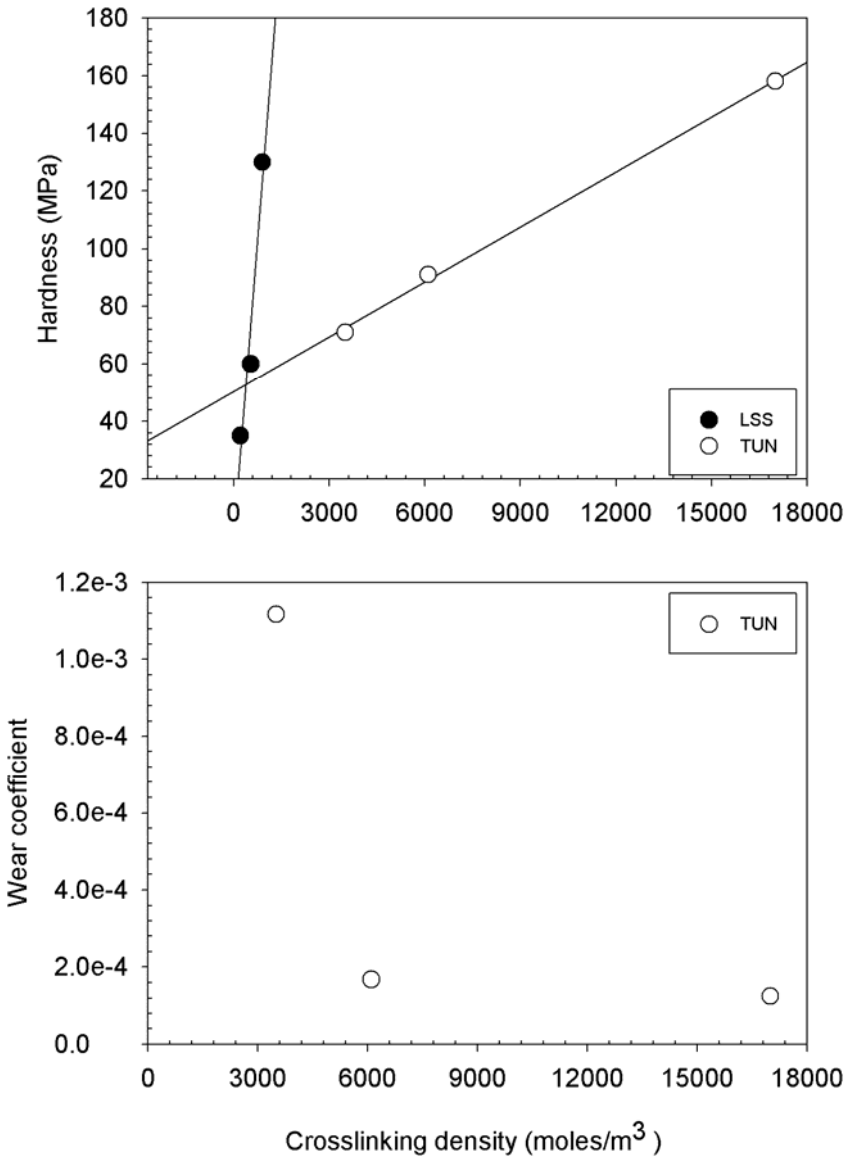

Figure 8. (a) Linear regression plot of hardness vs crosslinking density for low saturated soybean (LSS) oil and tung (TUN) oil-based polymers. (b) Wear coefficients vs crosslinking density for TUN samples.

Table 2: Determination of wear coefficients of the ROMP thermosetting polymeric samples as well as the biobased polymeric samples from past studies.

Sample	Crosslinking density (moles/m^3)	Estimated wear volume (m^3)	Wear coefficient
LSS DVB 10[a]	200	7.15×10^{-11}	5.63×10^{-4}
LSS DVB 15[a]	530	3.03×10^{-12}	1.42×10^{-4}
LSS DVB 20[a]	900	2.38×10^{-11}	7.32×10^{-4}
TUN DVB 20[b]	3500	7.55×10^{-11}	1.12×10^{-3}
TUN DVB 30[b]	6100	8.86×10^{-12}	1.68×10^{-4}
TUN DVB 40[b]	17000	3.79×10^{-12}	1.25×10^{-4}
CL-10	3054	1.32×10^{-12}	6.99×10^{-5}
CL-15	3096	4.77×10^{-13}	3.22×10^{-5}
CL-20	3750	2.99×10^{-13}	2.46×10^{-5}

[a] Discussed in Ref [14, 15]
[b] Discussed in Ref [13]

8.6 Conclusions

The tribological properties of ring opening metathesis polymerization thermosetting polymeric materials as a function of crosslinking density (0%, 5%, 10%, 15% and 20% of crosslinking agent CL concentration by weight) were evaluated. The sample without crosslinking, CL-0, showed a coefficient of friction of 0.316 against Si_3N_4. The COF of CL-5 and CL-10 were 10% and 42% lower respectively than CL-0. It was also found that the hardness of these materials increases with crosslinking density which significantly affected the wear behavior. In sliding wear tests against the Si_3N_4 spherical probe, CL-5, CL-10, CL-

15 and CL-20 showed negligible wear whereas CL-0 showed adhesive wear which was observed by a change in roughness as well as by the formation of transfer film on the probe. In sliding wear tests with a sharp conical diamond probe, all samples exhibited abrasive wear. CL-0 showed the highest wear depth followed by CL-5 (20% lower than CL-0), CL-15 (25 % lower than CL-0) with CL-15 and CL-20 showing comparable wear depths (66% lower than CL-0). Based on this study and past studies on biobased polymers, an empirical relationship between the wear volume and the crosslinking density was established.

8.7 References

[1] Kessler, M., 2007Proc of the Inst of Mech Eng. J Aerosp Engrg Part G, 221, pp. 479-495.

[2] White, S. R., Sottos, N. R., Geubelle, P. H., Moore, J. S., Kessler, M. R., Sriram, S. R., Brown, E. N. and Viswanathan, S., 2001, "Autonomic healing of polymer composites," Nature, 409, pp. 794-797.

[3] Sheng, X., Lee, J. and Kessler, M., 2008, "Influence of cross-link density on the properties of ROMP thermosets," submitted.

[4] Kessler, M. R. and White, S. R., 2001, "Self-activated healing of delamination damage in woven composites," Composites Part a-Applied Science and Manufacturing, 32(5), pp. 683-699.

[5] Brown, E. N., Sottos, N. R. and White, S. R., 2002, "Fracture testing of a self-healing polymer composite," Experimental Mechanics, 42(4), pp. 372-379.

[6] Kessler, M. R. and White, S. R., 2002, "Cure kinetics of the ring-opening metathesis polymerization of dicyclopentadiene," Journal of Polymer Science Part a-Polymer Chemistry, 40(14), pp. 2373-2383.

[7] Kessler, M. R., Sottos, N. R. and White, S. R., 2003, "Self-healing structural composite materials," Composites Part a-Applied Science and Manufacturing, 34(8), pp. 743-753.

[8] Brown, E. N., White, S. R. and Sottos, N. R., 2004, "Microcapsule induced toughening in a self-healing polymer composite," Journal of Materials Science, 39(5), pp. 1703-1710.

[9] Rule, J. D., Brown, E. N., Sottos, N. R., White, S. R. and Moore, J. S., 2005, "Wax-protected catalyst microspheres for efficient self-healing materials," Advanced Materials, 17(2), pp. 205-208.

[10] Brown, E. N., White, S. R. and Sottos, N. R., 2005, "Retardation and repair of fatigue cracks in a microcapsule toughened epoxy composite - Part 1: Manual infiltration," Composites Science and Technology, 65(15-16), pp. 2466-2473.

[11] Brown, E. N., White, S. R. and Sottos, N. R., 2005, "Retardation and repair of fatigue cracks in a microcapsule toughened epoxy composite - Part II: In situ self-healing," Composites Science and Technology, 65(15-16), pp. 2474-2480.

[12] Sheng, X., Kessler, M. and Lee, J., 2007, "The influence of cross-linking agents on ring-opening metathesis polymerized thermosets," Journal of Thermal Analysis and Calorimetry, 89(2), pp. 459-464.

[13] Bhuyan, S., Sundararajan, S., Andjelkovic, D. and Larock, R., 2008, "Effect of crosslinking on tribological properties of tung oil oil-based polymeric materials," Wear, submitted.

[14] Bhuyan, S., Sundararajan, S., Andjelkovic, D. and Larock, R., 2008, "Micro- and nano- tribological behavior of soybean oil-based polymers of different crosslinking densities," Tribol. Lett., submitted.

[15] Bhuyan, S., Sundararajan, S., Holden, L. S., Andjelkovic, D. and Larock, R., 2007, "Effect of crosslinking on the friction and wear behavior of soy-bean oil-based polymeric materials," Wear, 263, pp. 965-973.

[16] Check, J., Karuppiah, K. S. K. and Sundararajan, S., 2005, "Comparison of the effect of surface roughness on the micro/nanotribological behavior of ultra-high-molecularweight polyethylene (UHMWPE) in air and bovine serum solution," Journal of Biomedical Materials Research Part A, 74A(4), pp. 687-695.

[17] Bhushan, B., 1999 Principles and Application of Tribology, John Wiley & Sons, Inc., New York.

CHAPTER 9. CONCLUSIONS

A wide variety of naturally occurring polymers derived from renewable resources are available for material application. The beneficial aspect of utilizing polymers from renewable resources, when considering synthesis, processing disposal, biodegradability, and overall material life-cycle issues, suggests that this will continue to be an important and growing of interest. In this research, the tribological properties of biobased polymers have been evaluated as a function of several different processing parameters. In general, the tribomechanical properties of the biobased polymers can be tailored through appropriate synthesis thereby making it suitable for studying and discuss the possibility of their usefulness in structural applications. It was found that the addition of a suitable crosslinking agent, like divinyl benzene (DVB) to monofunctional styrene successfully reduces the nonuniformity of the crosslinking structure resulting in hard and rigid polymers produced by cationic copolymerization of the various natural oils. The mechanical properties of the resulting polymers are significantly improved which provided with an opportunity to investigate their tribological response as well The significant results of various research objectives are summarized below.

Effect of crosslinking on the friction and wear behavior of soybean oil-based polymeric materials

The tribological properties of novel soybean oil-based polymeric materials as a function of crosslinking density (10%, 15% and 20% of DVB concentration by weight) were evaluated. The coefficients of friction of DVB 10 and DVB 20 were 37% and 4% lower

respectively, than DVB 15. In sliding wear tests against a Si_3N_4 spherical probe, DVB 20 showed negligible wear whereas DVB 15 showed less adhesive wear depth than DVB 10. In sliding wear tests with a conical diamond probe, all samples exhibited abrasive wear. DVB 10 showed the highest wear depth followed by DVB 20 and DVB 15. The DVB 10 and DVB 15 samples exhibited delayed recovery of scratch grooves under intermediate loads. Thermosetting epoxy resin was used as a benchmark material in these studies and it was found that the wear properties of biobased materials were far superior. Based on the findings, these novel biobased materials show promise as replacements for conventional plastics as structural materials.

Comparasion of micro- and nano- tribological behavior of soybean oil-based polymers of different crosslinking densities

In this work wear behavior of soybean oil-based polymers of three different crosslinking densities were studied and compared at two different scales- microscale and nanoscale. It was observed that the trends displayed by the polymeric materials were similar both in microscale and nanoscale studies. The material with higher crosslinking displayed more resistance to wear. Crosslinking results in strong bonding amongst polymer network and reduces the mobility of molecular chain thereby making the molecule hard and wear resisting. Non-uniformity in wear behavior for the samples with high crosslinker concentrations was observed both in microscale and nanoscale regime. This non-uniformity is attributed to non-uniform crosslinking in the polymer network during synthesis. This irregularity in composition appears to be present at small scales on the surface. This non-uniformity in observed wear depths was found to be contact pressure dependent and invariant

of the Hertzian contact scale which disappears at contact pressures higher than a threshold for each of the samples.

Effect of crosslinking on the friction and wear behavior of tung oil-based polymeric materials

The tribological properties of novel tung oil-based polymeric materials as a function of crosslinking density (20%, 30% and 40% of crosslinking agent DVB concentration by weight) were evaluated. Nanoindentation tests have shown that the material with highest crosslinking density resulted in higher elastic modulus and hardness. The coefficients of friction of DVB 20 and DVB 30 against a spherical Si_3N_4 probe were lower than DVB 40. In sliding wear tests against the Si_3N_4, all samples showed negligible wear even after 500 cycles of sliding. An increase in crosslinking density resulted in better wear performance against the conical diamond probe. DVB 20 showed the highest wear depth of followed by DVB 30 and DVB 40. All samples exhibited abrasive wear as indicated by high magnification SEM images.

A study of the physical and tribological properties of biobased polymer-clay nanocomposites at different clay concentrations

Tung oil-based polymer resins can be reinforced with organoclay nanoplatelets, resulting in new, more viable applications of these polymers. The resulting nanocomposites show improved compressive material properties compared to pure polymers which provides with a thrust to study their friction and wear behavior as well. The tribological properties of

novel biobased nanocomposites from soybean oil and functionalized organoclay as a function of clay concentration (0%, 1% and 5% concentration by weight) were evaluated. The coefficient of friction of the sample with 1% (clay 1) clay concentration is lower than the ones with 0% (clay 0) and the 5% (clay 5). In sliding wear tests against a Si_3N_4 spherical probe, clay 0 showed the highest wear depth whereas the wear depth in clay 1 and clay 5 were less than clay 1. In sliding wear tests with a conical diamond probe, all samples exhibited abrasive wear. Clay 1 showed the lowest wear depth compared to clay 0 and clay 5. Thus, the addition of clay by 1% by weight resulted in a nanocomposite material with superior wear behavior than the ones with higher and lower clay concentrations. Based on these studies, it can be said that the VMMT in the polymer matrix play an important role in enhancing the wear behavior of the resulting nanocomposites.

Effect of filler composition and crosslinker concentration on the tribological behavior of spent germ particles and tung oil-based polymeric composites

The tribological properties of novel biobased polymer-composites from a tung oil-based resin and spent germ particles as a function of filler composition (40%, 50% and 60% by weight of spent germ) and as a function of crosslinker concentration (10%, 15% and 20% concentration by weight of divinyl benzene) were evaluated. The data from friction tests indicated that the coefficient of friction (COF) against a Si_3N_4 ball increases with filler composition. During the reciprocating wear tests, there was no evidence of damage on all samples against the Si_3N_4 ball indicating that these materials are resistance to wear under given loading conditions. On the other hand, wear against the sharp diamond probe was

predominantly abrasive in nature and data showed that an increase in filler composition had an adverse impact on abrasive wear. A similar trend was observed with macroscale wear tests implying that the spent germ as filler does not improve wear resistance. This is attributed to the fact that the spent germ has 10% unreactive crude corn oil which can sometimes act as a plasticizer in the matrix resulting in the formation of voids which in turn weakens the material strength. On the other hand, addition of divinyl benzene (DVB) as the crosslinker not only enhances the material strength but improves the tribological properties as well for a given filler composition. The COF and the average wear depth against diamond were observed to decrease with an increase in the crosslinker concentration. Microcracking of the matrix caused by surface fatigue was found to be the dominant mechanism of abrasive wear of polymer matrix composites caused by bulk solids.

The influence of crosslinking density on the tribological behavior of Ring-opening metathesis polymerized (ROMP) thermosetting polymers

The tribological properties of ring opening metathesis polymerization (ROMP) thermosetting polymeric materials as a function of crosslinking density (0%, 5%, 10%, 15% and 20% of crosslinking agent CL concentration by weight) were evaluated. The coefficients of friction of CL-5 and CL-10 against Si_3N_4 were lower than CL-0. In sliding wear tests against the Si_3N_4 spherical probe, CL-5, CL-10, CL-15 and CL-20 showed negligible wear whereas CL-0 showed wear which was observed by a change in roughness as well as by the formation of transfer film on the probe. In sliding wear tests with a conical diamond probe, all samples exhibited abrasive wear. CL-0 showed the highest wear depth. An addition of the

crosslinker by 1% reduces the wear depth. It was found that the materials with higher crosslinking density showed lower values of the average wear depth.

Archard's law states that the wear volume under plastic deformation is inversely proportional to the hardness of the materials. In these studies it was found that the hardness of the material increases with crosslinking density. A linear fit best describes the relationship between the two. Hence, the wear volume decreases with an increase in the crosslinking density. This was observed for the biobased polymeric materials as well as for the synthetic brand of polymers.

APPENDIX A. LABVIEW CODE FOR MONITORING AND CONTROL OF MICROTRIBOMETER

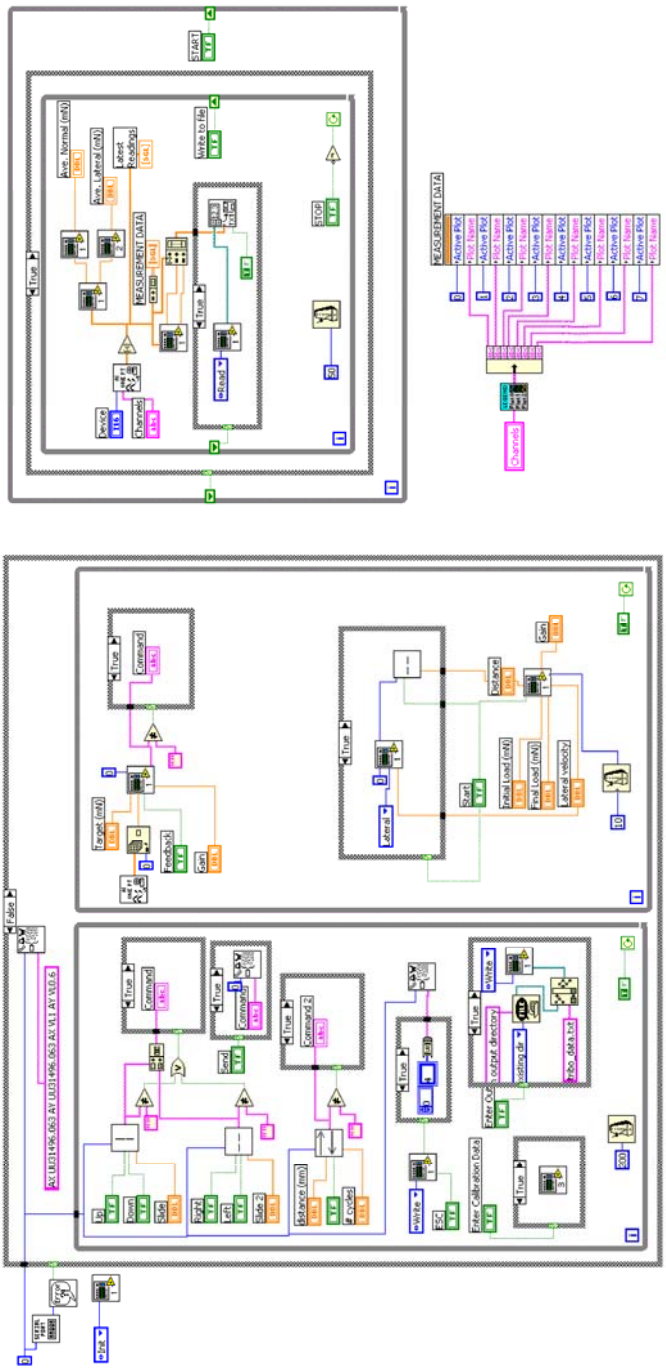

Figure 1. Main Program Diagram – module on the left controls stage movement, module on right controls data collection and display.

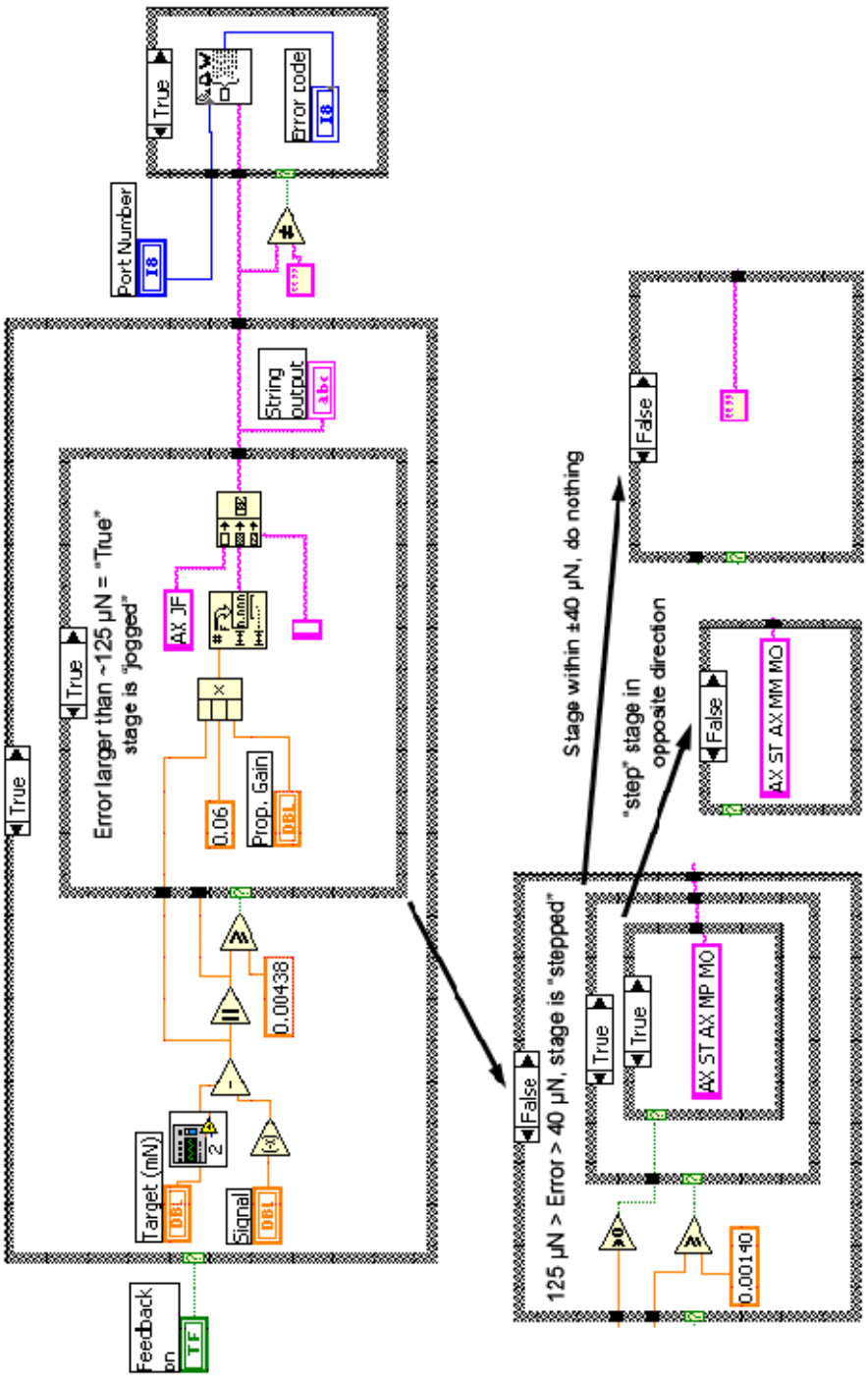

Figure 2. Proportional Feedback Diagram – Shows conditions under which stage is "jogged" at a given velocity, or "stepped". i.e one pulse is sent to the motor.

APPENDIX B. MATLAB CODE FOR FITTING A PARABOLA TO TIP SHAPE AND DETERMINATION OF TIP RADIUS

Program to read the DI image

```
function [im1a,im1b] = readimage(file)
fid = fopen(file,'rt');
for ii =1:110
        fgets(fid);
end;
test=fgets(fid);
soft=str2num(test(18:26));
for ii=114:544
        fgets(fid);
end
test=fgets(fid);
hard=str2num(test(49:58));
fclose(fid);
fid = fopen(file,'r','n');
fseek(fid,40960,'bof');
im1 = fread(fid,[256,512],'bit16');
im1a = (hard*soft)*((im1(:,1:256)-min(min(im1(:,1:256)))))/65536;
%im1b = im1(:,257:512);
Return
```

Program to locate the maximum points on x and y profile

```
function [p1,p2] = locate( xpts,ypts,imsize )
%This program takes the information about the tip across the x-axis and y-axis and finds the
max pts along the top of the tip
imsize1=imsize/256*1000;
h=size(xpts);
g=size(ypts);
h1=(1:h(1))*imsize1;
h2=(1:h(2))*imsize1;
g2=(1:g(2))*imsize1;
g1=(1:g(1))*imsize1;
yfit=max(xpts');
xfit=max(ypts);
p1=figure;
subplot(2,1,1); plot(h2,xpts')
subplot(2,1,2); plot(g2,xfit)
p2=figure;
subplot(2,1,1); plot(g1,ypts)
subplot(2,1,2); plot(h1,yfit)
[X1,RES1,fig1,Rc] = curve(yfit,imsize1);
[X2,RES2,fig2,Rc2] = curve(xfit,imsize1);
return;
```

Program for fitting a parabola

```
function [X,RES,ydata,f] = fitting(x0,ydata)
%Input the name of your file in the load function. The first column of the data file should be (xnot) values. The second col. should be y values. The function then utilizes a nonlinear least square fit to fit the function f.
for i=1:length(ydata)
        xdata(i)=i;
end
ydata=ydata;
f = inline('x(1)*(xdata).^2+x(2)*xdata+x(3)','x','xdata');
[x,resnorm]=lsqcurvefit(f,x0,xdata(:),ydata(:));
x0=x;
[x,resnorm] = lsqcurvefit(f,x0,xdata,ydata);
%The unknown values along with the residual value are passed out of the function
X=x;
RES=resnorm;
```

Program for best fit by iterative routine

```
function [X,RES,fig,Rc,xmax] = curve(ydata,imsize)
%This program utilizes fitting.m to find the lowest residual value and the best fit. It then plots the laboratory data against the best fit line and gives values for the radius of curvature and curvature in (nm).
y=ydata;
```

```
x0=[1,.2,325];
[X,RES,y,f] = fitting(x0,y);
n=0;
while (RES)>=1e-6
        x0=X;
        [X,RES,y,f] = fitting(x0,y);
        n=n+1;
        if n==30
        break
    end
end
X
RESIDUAL=RES;
%Post processing
X(1)=X(1)/imsize.^2;
X(2)=X(2)/imsize;
xmax=-X(2)/(2*X(1))
%calculate the radius of curvature
kappa=2*X(1)/((2*X(1)*xmax).^2+4*X(1)*xmax*X(2)+X(2).^2+1).^(3/2);
Rc=1/kappa
X(1)=X(1)*imsize.^2;
X(2)=X(2)*imsize;
%End post processing
```

```
for i=1:length(y)
        xdata(i)=i;
end
%Plotting laboratory data against best fit line
fig=figure; hold
plot(xdata*imsize,f(X,xdata))
plot(xdata*imsize,y,'o')
xlabel('nm')
ylabel('Height Data (nm)')
legend('NL least sq','data',sprintf('Radius of Curv. = %1.5f',Rc))
title('Find Radius of Curvature ')
return;
```

APPENDIX C. CODE FOR POST-PROCESSING OF MICROTRIBOMETER CYCLIC TEST DATA

###

Remove artifacts from cyclic data. Artifacts are from static friction at each change in direction.

Data file ("data.txt") must be in the format “load voltage" "friction voltage" "load force" "friction force" where these four elements are seperated by tabs

The data is first split into data points which contain either positive or negative values of friction and each set of data is processed separately.

The module "Remove Artifacts..." will calculate the mean and standard deviation of the next "x" data points. If the absolute value of the current data point is less than "mean + one standard deviation" it will be written to the new file. Otherwise it will be discarded.

The module "Capture Peak Values" will find local maxima of the friction force and write that line to a new file.

###

```
import string
```

```
#####  Definitions #####


def buildList(myStr):  #create a list of four elements from myStr
    strLen = len(myStr)
    first_tab = myStr.find("\t")
    myNum = myStr.count("\t")
    normVolt = myStr[:first_tab]
    sec_tab = myStr.find("\t",first_tab+1,strLen)
    latVolt = myStr[first_tab+1:sec_tab]
    thd_tab = myStr.find("\t", sec_tab+1,strLen)
    normForce = myStr[sec_tab+1:thd_tab]
    latForce = myStr[thd_tab+1:]
    myList = [normVolt, latVolt, normForce, latForce]
    return myList
def sum(myList): # calcu5ate the sum of a list
        x = 0
        for i in myList:
                x = x + i
        return x
def sumList(myList): # calculate the sum of the fifth member in a list of of numbers in string
format
        x = 0
        for i in myList:
```

```
            x = x + float(i[4])
        return x
def sqrList(myList): # calculate the squares of a list of numbers
        x = [pow(float(i[4]), 2) for i in myList]
        return x
def mean(myList):  # calcluate the mean of a list of numbers
        x = sumList(myList)/len(myList)
        return x
def stddev(myList):  # calculate the standard deviation of a list of numbers
        a = len(myList) * sum(sqrList(myList))
        b = (sumList(myList))**2
        x = ((a-b)/(len(myList)*(len(myList)-1)))**0.5
        return x
```

Split Data Into Positive & Negative Friction Values

```
input = open("data.txt", "r")
output_pos = open("data-pos.txt", "w")
output_neg = open("data-neg.txt", "w")
print "Separating data points containing positive and negative friction values."
count = 0
for line in input.readlines():
        count = count + 1
```

```
        if count % 5000 == 0:
                print ".",
        tempLst = buildList(line)
        if float(tempLst[3]) > 0:
                tempLst.insert(0,str(count))
                outStr = ",".join(tempLst)
                output_pos.write(outStr)
        elif float(tempLst[3]) < 0:
                tempLst.insert(0,str(count))
                outStr = ",".join(tempLst)
                output_neg.write(outStr)
input.close()
output_pos.close()
output_neg.close()
```

Remove Artifacts from Static Friction

```
input_pos = open("data-pos.txt", "r")
input_neg = open("data-neg.txt", "r")
output_pos = open("temp_data-pos.txt", "w")
output_neg = open("temp_data-neg.txt", "w")
i = 225  #choose # of pts to look ahead
myArr1 = []  #create and...
```

```
for x in range(i):  # initialize empty list
        myArr1.append(['0','0','0','0','0'])
print "\n"
print "Removing artifacts"
test_pt = 0
one_sigma = 0
count = 0
for line in input_pos.readlines():  #iterate over each line in file
        count = count + 1
        if count % 5000 == 0:
                print ".",
        for j in range(1,i):  #build list of last i-1 lines in file
                myArr1[i-j] = myArr1[i-j-1]
        myArr1[0] = line.split(",")  #add current line to front of list
        test_pt = float(myArr1[i-1][4])
        one_sigma = mean(myArr1)+stddev(myArr1)
        if count > i-1:
        if test_pt < one_sigma:  # if point is less than mean + sigma write it to new file
                outStr = ",".join(myArr1[i-1]) #create string of csv's out of list elements
                        output_pos.write(outStr)
for x in range(len(myArr1)):  # initialize list
        myArr1[x] = ['0','0','0','0','0']
test_pt = 0
```

```
one_sigma = 0
count = 0
for line in input_neg.readlines():  #iterate over each line in file
        count = count + 1
        if count % 5000 == 0:
                print ".",
        for j in range(1,i):  #build list of last i-1 lines in file
                myArr1[i-j] = myArr1[i-j-1]
        myArr1[0] = line.split(",")  #add current line to front of list
        test_pt = float(myArr1[i-1][4])
        one_sigma = mean(myArr1)-stddev(myArr1)
        if count > i-1:
        if test_pt > one_sigma:  # if point is greater than mean - sigma write it to new file
                outStr = ",".join(myArr1[i-1]) #create string of csv's out of list elements
                        output_neg.write(outStr)
input_pos.close()
input_neg.close()
output_pos.close()
output_neg.close()
```

Capture Peak Values

```
input_pos = open("temp_data-pos.txt", "r")
```

```
input_neg = open("temp_data-neg.txt", "r")
output_pos = open("final_data-pos.txt", "w")
output_neg = open("final_data-neg.txt", "w")
i = 50  #choose # of data pts to compare before and after data pt of interest
myArr2 = []  #create and...
for x in range(2*i+1):  # initialize empty list
        myArr2.append(["0","0","0","0","0"])
print "\n"
print "Calculating local peaks"
count = 0
for line in input_pos.readlines():  #iterate over each line in file
        count = count + 1
        if count % 5000 == 0:  # feedback on progress for end user
                print ".",
        for j in range(1,2*i+1):  #build list of last (2*i)th lines in file
                myArr2[2*i+1-j] = myArr2[2*i-j]
        myArr2[0] = line.split(",")  #add current line to front of list
        if float(myArr2[i][4]) == max([float(s[4]) for s in myArr2]): #check if ith lateral load
reading is largest
                outStrPos = ",".join(myArr2[i])  #create string of csv's out of list
                output_pos.write(outStrPos)
for x in range(len(myArr2)):  # initialize list
        myArr2[x] = ["0","0","0","0","0"]
```

```
count = 0
for line in input_neg.readlines():  #iterate over each line in file
        count = count + 1
        if count % 5000 == 0:  # feedback on progress for end user
                print ".",
        for j in range(1,2*i+1):  #build list of last (2*i)th lines in file
                myArr2[2*i+1-j] = myArr2[2*i-j]
        myArr2[0] = line.split(",")  #add current line to front of list
        if float(myArr2[i][4]) == min([float(s[4]) for s in myArr2]): #check if ith lateral load
reading is smallest
                myArr2[i][4] = str(abs(float(myArr2[i][4])))+"\n"  #make friction
measurement positive
                outStrNeg = ",".join(myArr2[i])  #create string of csv's out of list
                output_neg.write(outStrNeg)
input_pos.close()
input_neg.close()
output_pos.close()
output_neg.close()
print "\n" + "finished" + "\n"
```